DYNAMIC CHARACTERIZATION OF COHERENT SEMICONDUCTOR LASER ARRAYS

Nu Yu
B.S., Huazhong University, China, 1982
M.S., Oregon Graduate Center, Oregon, 1987

A dissertation submitted to the faculty
of the Oregon Graduate Institute
of Science and Technology
in partial fulfillment of the
requirements for the degree
Doctor of Philosophy
in
Electrical Engineering

August, 1990

The dissertation "Dynamic Characterization of Coherent Semiconductor Laser Arrays" by Nu Yu has been examined and approved by the following Examination Committee:

Richard K. DeFreez, Thesis Advisor
Associate Professor

J. Fred Holmes
Professor

Paul R. Davis
Professor

Herbert G. Winful
Associate Professor
University of Michigan

ACKNOWLEDGMENTS

I wish to express my deep appreciation to all of the people who have made this dissertation possible.

I am most grateful to my supervisors, Dr. Richard A. Elliott and Dr. Richard K. DeFreez, for their invaluable guidance and continuing encouragement as well as support throughout my graduate career.

I am very thankful to Dr. J. Fred Holmes, Dr. Paul R. Davis, and Dr. Herbert G. Winful for their participation on my thesis examination committee and their very careful examination of this thesis. I also would like to extend my thanks to Thomas L. Paoli, David F. Welch and Gary A. Evans for supplying laser arrays and device information. I would like to thank John Hunt for computer support. To my fellow graduate students Kathleen A. Hartnett, David J. Bossert, Jim Cser, Geoffrey A. Wilson, Shawe-Shiuan Wang, Rags Ranganathan, and Badih Rask go many thanks for their contributions and assistance.

Very special thanks go to my wife, Yuan Liu, for her patience and understanding throughout this project and the years of work leading up to it. I am greatly indebted to my parents for their love and encouragement.

This work was supported in part by the Innovative Science and Technology Office of the Strategic Defense Initiative, the National Aeronautics and Space Administration, the National Science Foundation, and the Air Force Office of Scientific Research.

To my daughter

Carlina Chunlin Yu

who is my inspiration

to succeed.

Table of Contents

ACKNOWLEDGEMENTS iii

DEDICATION iv

LIST OF FIGURES viii

LIST OF TABLES xii

ABSTRACT xiii

1. INTRODUCTION 1

2. DIODE LASER ARRAYS AND OPERATING CHARACTERISTICS 7

2.1 Review of Diode Laser Array Development 7

2.2 Coupled-Mode Formalism 12

2.3 Nonlinear Dynamic Model of Diode Laser Arrays 17

3. EXPERIMENTAL PROCEDURE 21

3.1 Spatio-Temporal Measurements of Phased Arrays 21

3.1.1 Streak Camera Operation 22

3.1.2 Spatio-Temporal Recording with Streak Camera 26

3.2 Spatio-Spectral Measurements of Laser Arrays 31

3.3 Optoelectronic Characterization of Diode Laser Arrays 33

3.3.1 Light-Current Characteristics 33

3.3.2 Carrier Lifetime 34

3.3.3 Optical Confinement Factor 35

3.3.4 Carrier-Induced Refractive-Index Change 36

3.3.5 Loss and Threshold Gain 38

3.3.6 Differential Gain 40

3.3.7 Linewidth Enhancement Factor 41

3.3.8 Emitter Coupling Coefficient 43

4. DYNAMIC CHARACTERISTICS OF GAIN-GUIDED ARRAYS 46

4.1 Ten-Stripe Multiple-Quantum-Well Array 46

4.1.1 Device Performance 48

4.1.2 Optical Spectra and Radiation Patterns 53

4.1.3 Picosecond Temporal Properties 59

4.2 Two-Stripe Multiple-Quantum-Well Array 67

4.2.1 Device Structure and Performance 67

4.2.2 Radiation Patterns and Optical Spectra 70

4.2.3 Picosecond Temporal Properties 75

5. DYNAMIC CHARACTERISTICS OF INDEX-GUIDED ARRAYS 87

5.1 Eight-Stripe Channeled-Substrate-Planar Arrays 87

5.1.1 Device Structure and Performance 89

5.1.2 Spectral Properties 95

5.1.3 Picosecond Temporal Properties 102

5.2 Ten-Stripe Array with Y-Coupling 112

5.2.1 Flared Guide Y-Coupled Laser Arrays 113

5.2.2 Spectral Properties 115

5.2.3 Temporal Properties 120

6. PHYSICAL MECHANISMS OF INSTABILITIES IN ARRAYS 127

6.1 Amplitude-Phase Coupling 127

6.2 Saturable Absorption 130

6.3 Feedback Effect 132

7. CONCLUSIONS 136

REFERENCES 139

APPENDIX A 154

APPENDIX B 161

APPENDIX C 166

APPENDIX D 181

VITA 185

List of Figures

3.1 Schematic diagram of a typical streak camera 23

3.2 Experimental setup of the streak camera recording system 28

3.3 The leading edge and first 5 ns of the current pulse used to drive a laser array 29

3.4 Experimental setup for spatio-spectral measurements 32

4.1 Schematic of a multiple stripe gain-guided laser array 47

4.2 The L-I characteristic of the ten-strip gain-guided laser array 49

4.3 Light output delay, wavelength shift and net gain dependence on current drive for the ten-stripe gain-guided array 51

4.4 Average optical spectrum of the ten-stripe gain-guided array 55

4.5 Spectrally integrated near-field pattern of the ten-stripe gain-guided array 57

4.6 Far-field pattern of the ten-stripe gain-guided array 58

4.7 Halftone representation of the time evolution of the near-field for the ten-stripe gain-guided array during pulsed operation 60

4.8 Single-pulse emission vs time from the seventh and eighth stripes in the ten-stripe gain-guided array 62

4.9 Average temporal evolution of 20 events for ten-stripe gain-guided array during pulsed operation 63

4.10 Average Fourier spectra for ten-stripe gain-guided laser array under pulsed operation 65

4.11 Time evolution of each of the emitters during CW operation of ten-stripe gain-guided array 66

4.12 Average Fourier spectra for ten-stripe gain-guided laser array under CW operation 68

4.13 Radiation patterns of two-stripe gain-guided laser array 71

4.14 Longitudinal mode spectra of the two-stripe gain-guided laser array under CW operation at $1.3I_{th}$ 74

4.15 Longitudinal mode spectra of the two-stripe gain-guided laser array under CW operation at $1.7I_{th}$ 76

4.16 The time evolution of the near-field pattern of the two-stripe gain-guided array under pulsed operation 77

4.17 Halftone representation of the time evolution of the near-field pattern for the two-stripe gain-guided array array during CW operation 78

4.18 The time evolution of the near-field pattern of the two-stripe gain-guided array under CW operation 80

4.19 The cross correlation between the first and second emitters of the two-stripe gain-guided array under CW operation 81

4.20 The power spectrum and the oscillation frequency of the two-stripe gain-guided array 82

4.21 The stability diagram in the plane of the coupling strength and

the normalized excess pump current 84

4.22 The stability diagram in the complex coupling strength plane 86

5.1 Schematic diagram of an eight-stripe CSP laser array 90

5.2 The L-I characteristic of the CSP laser array 91

5.3 The drive current plotted vs laser light output delay for the CSP laser array 93

5.4 Measured wavelength shift and net gain dependence on current for the CSP laser array 94

5.5 Spectrally resolved near-field patterns of the pulsed CSP laser array 98

5.6 Spectrally resolved near-field patterns of the CW CSP array 100

5.7 Lateral far-field pattern of the CSP laser array 101

5.8 Halftone representation of the time evolution of the near-field intensity of the CSP laser array during pulsed operation 103

5.9 Quantitative representation of time evolution of each of the emitters of the CSP laser array during pulsed operation 104

5.10 Average Fourier spectra for a pulsed CSP array 106

5.11 Time evolution of each of the emitters during CW operation of the CSP laser array 107

5.12 Halftone representations of the time evolution of far-field patterns for a pulsed CSP laser array 109

5.13 Streak traces of a far-field pattern for a 20 pulse average of the

CSP laser array 110

5.14 Average Fourier spectra of measured far-field time evolution for a pulsed CSP laser array 111

5.15 Schematic diagram of waveguide pattern of flared Y-coupled laser array 114

5.16 Near-field pattern of the Y-coupled laser array 116

5.17 Low-resolution spatio-spectral properties of a CW Y-coupled laser array 118

5.18 High-resolution spectral properties of the dominant mode of Emitter 1 of the CW Y-coupled laser array 119

5.19 The time evolution of the near field during CW operation of the Y-coupled laser array 121

5.20 The time evolution of the near field of the pulsed Y-coupled laser array 122

5.21 Average temporal evolution of the near field of the Y-coupled laser array 123

5.22 Average power spectra for the CW Y-coupled laser array 125

List of Tables

4.1 Ten-stripe gain-guided laser array parameters 54

4.2 Two-stripe gain-guided laser array parameters 69

5.1 CSP laser array parameters 96

ABSTRACT

DYNAMIC CHARACTERIZATION OF COHERENT SEMICONDUCTOR LASER ARRAYS

Nu Yu, Ph.D.

Oregon Graduate Institute, 1990

Supervising Professors: Richard A. Elliott

Richard K. DeFreez

Although there has been over one decade of extensive research on various high-power semiconductor laser arrays, not much is known about the temporal, spectral and spatial stability of array operation and there is only a limited amount of experimental data available for studies of array nonlinear dynamics which is of both practical importance and theoretical interest. In this dissertation, the experimental characterization of the spatio-spectral and spatio-temporal properties under both continuous-wave and pulsed operating conditions is reported for various AlGaAs monolithic one-dimensional coherent arrays of semiconductor diode lasers with different structures such as (1) ten-stripe gain-guided, (2) twin-stripe gain-guided, (3) eight-stripe channeled-substrate-planar, and (4) ten-stripe Y-coupled arrays. Streak camera observation of the time evolution of the near- and far-field radiation patterns reveals that these arrays are

unstable in the picosecond to nanosecond domain with complex dynamic behavior. Furthermore, a series of experiments have also been performed to systematically determine the values, for the first time, of such array device operating parameters as resonator dimensions, group refractive index, optical confinement factor, lasing wavelength, longitudinal mode spacing, mirror loss, internal loss, carrier lifetime, photon lifetime, threshold carrier density, transparency carrier density, threshold gain, differential gain, the linewidth enhancement factor, and emitter-to-emitter coupling coefficient. The experiments carried out to measure spatio-temporal and spatio-spectral properties as well as a variety of operating parameters demonstrate the capability for study of the nonlinear dynamics in diode laser arrays. The results provide the necessary experimental basis and important information for modeling the dynamic behavior of coherent semiconductor laser arrays and designing devices with optimum characteristics for various applications.

Chapter 1
INTRODUCTION

During the last decade there has been an ever-increasing demand for semiconductor diode lasers that could emit higher and higher output powers, under either continuous-wave (CW) or high-duty-cycle conditions, and spatially coherent output beams allowing for fine focusing and other optical processing. Examination of possible applications reveals the need for two main categories of diode laser components. One is the diffraction limited, single frequency laser with outputs from a few hundreds of milliwatts to 1 watt for both long-haul optical fiber and space inter-satellite communications at high data rates[1-8], compact optical disks[9], optical recording[10], high-speed printing, data distribution systems[11], etc. The other requires high power (tens to hundreds of watts) and high efficiency for diode laser radar ranging[12], direct doubling of diode radiation into the blue[13], pumping solid-state lasers[14] for industrial, military and medical applications, etc. For reliable operation at such high powers, three main ingredients are necessary: a large emitting area, high efficiency, and longevity at high emitting-power densities.

Even though techniques such as expanding the lasing spot, antireflection coating the output facet and forming nonabsorbing mirrors can be used to fabricating laser diodes that can reliably emit 20 to 50 mW or more[15-18], there are inherent limits to the power obtainable from a single-element (narrow width ≤ 8

μm) diode laser. Above a certain power, no matter what its construction, the tiny device will be destroyed by catastrophic facet damage or excessive thermal dissipation within it. Recently, under both CW and high-duty-cycle drive conditions the upper limit of the power level that a single-element diode laser can be counted on to emit for a long time while maintaining fundamental-transverse-mode operation appears to be about 200 mW[13,19-25]. Although semiconductor lasers with wide stripe or broad-area contacts are capable of generating high-power optical output in the 1 to 6 W range[26-28], they operate in several higher-order lateral modes or in several relatively independent filaments in contrast to narrow-stripe fundamental transverse mode laser, so that the emitted light exhibits little or no spatial coherence. Hence, the far-field radiation patterns of wide-stripe lasers are generally broad and fluctuate with time or drive current.

To achieve high-power optical output with low-divergence beam, therefore, it becomes necessary to develop monolithic arrays of mutually coupled spatially coherent semiconductor lasers, which are generally referred to as phase-locked diode laser arrays by utilizing ideas from microwave phased-antenna arrays. The term monolithic implies that all means of making the diode coherent are integrated on the diode laser wafer. In one-dimensional (1-D) laser arrays or linear laser arrays, a number of diode lasers are fabricated on the same substrate. When the array is powered through a common electrical contact, each element's optical modes spread out through the active and cladding layers, overlapping with the optical modes from its neighbors and interacting with them. Individual lasers of the array couple with each other, and establishes a definite phase relation between elements. As a result all the lasers of the array may act together as

a single powerful coherent source. Since for semiconductor lasers, the failure rate is directly related to the optical flux density, an array provides significantly greater reliability at a given output power than a single-stripe device. 1-D laser diode laser arrays can be grouped into two categories, single and multiple emitter arrays. The single emitter arrays have a single broad light emitting region, whereas the multiple emitter arrays have multiples of such regions spaced monolithically along a bar of laser material. To date the highest CW output power levels demonstrated have been 8 W for the single emitter arrays (200-μm aperture width)[29] and 76 W for the multiple emitter arrays (thirty ten-stripe arrays spaced in a 1-cm bar, 3000-μm total aperture width)[30].

Three basic types of surface-emitting semiconductor lasers — the vertical cavity[31,32], the 45° deflecting mirror[33-35], and grating coupled surface emitter[36,37] have made the fabrication of monolithic two-dimensional (2-D) arrays of semiconductor lasers possible. Such arrays offer the promise of very high powers with a large-area aperture producing a narrow beam divergences with unity aspect ratio, using either on-chip or external means of optical coupling between emitters. The high performance of 2-D surface-emitting arrays with circular beam divergences of about 0.01°, 30%-50% power-conversion efficiency, diffraction-limited beam quality, and output powers of many watts could be achieved in the near future[38].

However, stable, diffraction-limited single-lobe operation to high optical power levels remains a major challenge in diode laser array development. Typically, array devices tend to have rather broad and irregular multiple-lobed far-field patterns which result when individual array elements operate out-of-

phase[39,40]. A further problem with these arrays is the strong temporal spiking in the emission of the individual emitters which was first experimentally observed by Elliott *et al*[41]. Under some conditions the arrays exhibit regular sustained self-pulsation while under others they develop irregular pulsations. Recent experiments show that Y-guide arrays exhibit far-field beam steering[42] and have regular sustained self-pulsations during both CW[43] and pulsed[44] operations. Even more recently, it has been shown that 2-D grating-surface-emitting (GSE) arrays can also exhibit periods of sustained self-pulsation interleaved with periods of quiescent or chaotic behavior[45]. Observations of the picosecond temporal behavior in one hundred element GSE ring laser arrays have revealed a similar variety of nonlinear dynamic regimes[46]. The occurrence of temporally unstable emission will limit data-transmission rates in optical communication application of phase arrays. An understanding of the dynamic characteristics of phase-locked arrays is therefore important for eliminating or controlling the causes of instability in array devices for such applications.

The initial experimental observation of array dynamic behavior[41-44] mentioned above has stimulated several theoretical studies on nonlinear dynamics of semiconductor laser arrays[47-55]. A recent theory analyses the diode laser array as an important example of the complicated dynamics of coupled nonlinear oscillators and predicts that the output of individual array emitters is dynamically unstable and can exhibit large amplitude chaotic pulsations[47]. In the unstable regime semiconductor laser arrays exhibit time-varying behaviors which may be periodic, quasi-periodic, or chaotic[48]. However, there is a limited amount of data available, particularly concerning device operating parameters, for theoretical

modeling of the physical processes responsible for the observed dynamical behavior. Experimental results will be very valuable to these theoretical studies. In addition, from the physical viewpoint the possibility of using laser arrays to provide a nearly ideal setting for studying chaos, squeezed states, and optical bistability is also particularly attractive.

The factors discussed above provide a strong motivation to seriously study the temporal, spectral and spatial stability of array operation. The work presented in this dissertation focuses on the experimental characterization of spatio-spectral and spatio-temporal properties of various coherent semiconductor laser arrays under both CW and pulsed operating conditions. Through the direct observation of the time evolution of the near- and far-field radiation patterns with streak cameras, it is experimentally demonstrated that these arrays are unstable in the picosecond to nanosecond domain with complex dynamic behavior such as periodicity, quasi-periodicity and chaos. Furthermore, a series of experiments have also been carried out to systematically determine the values, for the first time, for such array device operating parameters as resonator dimensions, group refractive index, optical confinement factor, lasing wavelength, longitudinal mode spacing, mirror loss, internal photon loss, carrier lifetime, photon lifetime, threshold carrier density, transparency carrier density, threshold gain, differential gain, the linewidth enhancement factor, and the emitter-to-emitter complex coupling coefficient. These results provide the necessary experimental basis and important information for the evaluation of the dynamic behavior of coherent semiconductor laser arrays and designing devices with optimum characteristics for various applications. It should be stressed that this dissertation

addresses only monolithic 1-D coherent arrays of semiconductor diode lasers with aluminum gallium arsenide (AlGaAs) materials. Hybrid devices (e.g., injection locking or external cavity control) and 2-D GSE laser arrays are beyond the scope of this dissertation.

The organization of the dissertation is as follows. Chapter 2 provides background information on semiconductor laser arrays and their basic modal and dynamical mechanism. Chapter 3 describes the experimental techniques employed in the measurement of spatio-temporal and spatio-spectral properties as well as a variety of operating parameters important for modeling laser array behavior. Detailed experimental results of dynamic characteristics of gain-guided arrays and index-guided arrays are presented in Chapters 4 and 5, respectively. In Chapter 6, some mechanisms that may cause or enhance the instability in diode laser arrays are discussed. Finally, conclusions and suggestions for future work are given in Chapter 7.

Chapter 2

DIODE LASER ARRAYS AND OPERATING CHARACTERISTICS

Many developmental efforts on phase-locked semiconductor laser arrays continue toward the eventual goal of obtaining high-power, compact and efficient, fundamental-mode diode laser sources[56-58]. To identify optimal structures, different arrays, including gain-guided, index-guided, anti-guided arrays, and so on, have been developed. This chapter provides background information on semiconductor laser arrays as well as their basic modal and dynamical mechanism for reference throughout this thesis work. Section 2.1 reviews the development and status of semiconductor laser arrays. The coupled-mode formalism of phased array laser operation is given in Section 2.2. The final section of the chapter presents a nonlinear dynamic model to understand the physical mechanism underlying the dynamics of diode laser arrays.

2.1 Review of Diode Laser Array Development

As early as 1970, semiconductor laser arrays were investigated when Ripper and Paoli experimentally studied the optical coupling of adjacent dual-stripe-geometry junction lasers[59]. Several years later phase-locked arrays operating under low-duty-cycle condition at room temperature or CW condition at low temperature were reported[60-62]. The first CW array devices fabricated from a

multiple quantum well laser structure in 1982 by Scifres *et al.* were demonstrated to be capable of operation at power levels of 600 mW CW at room temperature[63]. Since that time higher output powers, higher efficiency, and greater reliability laser arrays fabricated from the AlGaAs material system have been extensively studied and commercialized. For example, in 1983 at Xerox Palo Alto Research Center (PARC) a 40-element array delivered a total CW power of 2.6 W[64]. Phase-locked arrays of gain-guided diode lasers with reliable CW power up to 3 W[65] are available from Spectra Diode Labs (SDL). Even higher CW output power levels have recently been achieved. 8 W of single facet CW output has been obtained from a 200 μm aperture quantum well array[66]. Output power levels of 76 W CW and 55 W CW have also been obtained from 1-cm-wide monolithic arrays with total active aperture widths of 3 mm and 2mm at heatsink temperatures of 0° C and 23° C, respectively[30]. SDL recently announced an output power level in excess of 200 W with a power conversion efficiency of 40% from a 1-cm monolithic AlGaAs laser array for a pulse width of 200 μs (quasi-CW operation)[67]. These devices are powerful, yet they have poor beam quality.

Linear laser-array structures can be classified into two groups: gain-guided arrays and index guided arrays. The difference between the two types is that the mode profile along the junction plane is determined by gain guiding for the former and by weak index guiding for the latter. In most gain-guided arrays, the current is confined to a group of parallel contact stripes via high-resistivity proton-implanted regions[68] or Schottky-barrier defined stripes[69]. The optical modes are controlled laterally by the injected carrier profile and optical coupling between lasers occurs when the evanescent fields of adjacent devices substantially

overlap. In contrast to gain-guided arrays, index-guided arrays have the remarkable feature that they can operate at a single-longitudinal mode even at very high powers. Since the realization in late 1982 of the first room-temperature CW-operating array of index-guided lasers[70], many efforts in this area have concentrated on index-guided array structures[70-79], and also ridge index guides have been employed in grating-surface-emitting laser arrays at David Sarnoff Research Center[36]. There are four main types of index-guided phase-locked arrays. The first type is a ridge waveguide structure, a configuration that is generally obtained by chemical etching grooves into a planar double heterostructure or large-optical-cavity structure, and provides mode confinement mainly due to the variations in cladding-layer thickness[62,73,74,77]. Next is a Zn-diffused device[70], obtained by Zn diffusion into a planar double heterostructure with a channeled top surface. The dopant reaching the active layer locally lowers the index of refraction such that each nondiffused area represents the high-index region of a lateral dielectric waveguide (i.e., an anti-guide). Two other index-guided array types take advantage of crystal-growth characteristics of metal-organic vapor-phase epitaxy (MOVPE)[80], also known as metal-organic chemical vapor deposition (MOCVD), and liquid-phase epitaxy (LPE)[81] over channeled substrates. MOCVD replicates the substrate channels, creating a constant-thickness active layer with periodic bends[82], which control the lateral modes[83]. LPE over a sawtooth substrate grating partially dissolves the peaks of the grating and fills in the channels, creating an array of channeled-substrate planar devices[71,72,78,79].

At present an often-encountered problem in the performance of a laser array is poor beam quality since controlled fundamental-array-mode operation to high

power is still a challenge. The problem is twofold: (1) fundamental-mode selection is difficult since an array has several array modes, and (2) even when one succeeds in selecting the fundamental mode, the far field pattern either broadens with increasing drive current above threshold or is three to four times broader than the diffraction limit. The nature of the far field depends critically on the phase relationships between neighboring emitters, and single-lobe and twin-lobe far fields are generally related to in-phase and out-of-phase operations, respectively[84,85]. The relative phase between adjacent emitters, however, is generally determined by the lateral variation of the optical gain and the refractive index. The array interelement regions are usually lossy; thus, operation of array modes with field nulls between elements is preferred. These are the high-order modes of the array, and the resulting multilobed condition is out-of-phase operation. Furthermore, the operation of multiple array modes closely spaced in wavelength produces the far-field lobes two to three times wider than the diffraction limit. To maintain a single diffraction limited Gaussian beam from a monolithic array of lasers, three elements are necessary: (1) the phases of individual emitters need to be in-phase and stable with increasing output power; (2) the emitters need to be configured to maximize the power in a dominant lobe, typically the radiation lobe emitting normal to the facet; and (3) the coherence has to be maintained across the array of emitters. Several approaches have been demonstrated for achieving fundamental array-mode operation that leads to single-lobe far fields by making either positive-index-guided[71,74,86-88] or negative-index-guided (antiguided)[89,90] array structures.

Positive-index-guided structures that favor fundamental-mode operation

have different types: (1) net gain between the elements[73,74,78]; (2) a chirped laser array[72,91]; (3) diffraction-coupled arrays[92]; and (4) Y-junction arrays[86,87]. The net-gain-between-elements approach provides enhanced gain in the regions between the lasing elements so that array modes with most of the field between the elements are favored to lase (i.e., the fundamental mode). This approach, however, appears rather inefficient with high thresholds and low-differential quantum efficiencies. A chirped-array is a laser array with variable emitter dimensions or a variable spacing between emitters. The main drawback of this approach is that the emitting area is relatively small compared to the total array dimension, thus defeating the main purpose for making arrays: the achievement of a large emitting area. When the array elements are interrupted longitudinally, mode-mixing regions are created, which allow for strong diffraction coupling[92]. This is also a means of providing regions of high gain, which will generally favor in-phase operations. Finally, the Y-junction structure relies on the fact that the in-phase mode of a two-stripe section is efficiently coupled into a one-stripe section, while the out-of-phase mode does not couple but is lost in a radiative mode. These approaches are successful in providing fundamental-mode operation, but the eventual goal, high power in a single diffraction-limited beam, is still elusive. The apparent reasons are that in evanescently coupled devices, gain spatial hole burning invariably causes beam broadening with increasing drive current above threshold[93], whereas in Y-junction-coupled devices, difficulty for all array elements to self-lock[94] produces beams three to four times the width of the diffraction limit.

The most promising approach to achieve stable, diffraction-limited beams to

high powers is the use of arrays of closely spaced leaky waveguides (antiguides)[89,90]. As opposed to standard positive-index guides, light is confined in the low-index regions of the array. Each antiguide leaks radiation outwardly, which causes much stronger interelement coupling than in evanescent-wave-coupled or Y-junction-coupled devices. One can make arrays with both strong optical-mode confinement (i.e., immune to gain spatial hole burning) and strong interelement coupling. Between channels one introduces passive waveguides that have a dual role: creation of high-index regions between elements and suppression of lasing in these high-index regions. Thus, lasing can occur only in the low-index regions, the antiguide cores. Optimized arrays of antiguides should easily provide 0.5 to 1 W in an in-phase diffraction-limited-beam pattern.

Development of phased-array diode lasers is still in its adolescency. Much more work needs to be done before a reliable high-power coherent device can be producted. As is enunciated in this dissertation, the instability in semiconductor laser arrays is also a great challenge. With increased understanding it should be possible to optimize diode laser arrays so that they might radiate high power in a stable single narrow-divergence beam.

2.2 Coupled-Mode Formalism

The operation of a phase-locked laser array of identical emitters with weak coupling between them has been studied using coupled-mode analysis[39,40]. The normal modes of a phased array, generally referred to as array modes or supermodes because of their mathematical representation as a superposition of the individual emitter modes, oscillate at different wavelengths with different near-

field and far-field patterns. Coupled-mode analysis is very useful for a qualitative analysis of device behavior since it can provide analytic forms of the near- and far-fields associated with the array modes. However, these early analyses included only the effects of passive systems of coupled waveguides, i.e., the gain and loss considerations of array modes were not analyzed. In a more recent approach[95] the modes of a composite-array cavity are determined through a self-consistent solution of the paraxial wave equation that incorporates lateral variations of both the optical gain and the refractive index while the concept of coupling between emitters is not invoked. The modified coupled-mode analysis that is given here is based on the work of Butler *et al.*[96], which includes both the passive and active nature of the waveguide in the problem. By modeling an active structure, both wavelength splitting and the "gain splitting" of the individual array modes can be calculated.

Consider a laser array that consists of N parallel waveguides. Each individual laser waveguide, when isolated from its neighbors, supports a single TE spatial mode described by its electric field

$$E^m(x,y,z) = u^m(x)v^m(y)e^{-\gamma^m z}, \qquad m=1,2,...,N \ , \tag{2.2.1}$$

where the superscript pertains to the mth waveguide and γ^m is the complex propagation constant. The field of the single element satisfies the time-independent wave equation known as the Helmholtz equation

$$\nabla^2 E^m(x,y,z) + k_0^2 \epsilon^m(x,y) E^m(x,y,z) = 0 \ , \tag{2.2.2}$$

where k_0 is the free space propagation constant, and $\epsilon^m(x,y)$ the dielectric function that describes the mth waveguide.

The total electric field of the array may be described as the superposition of the field of the N individual elements

$$E(x,y,z) = \sum_{m=1}^{N} A_m(z)E^m(x,y,z) , \tag{2.2.3}$$

where $A_m(z)$ is a complex coefficient that determines the amplitude and phase of each of the individual emitters in the allowed modes of the array. The z dependence of $A_m(z)$ is due to the interaction, or coupling, among the array elements. $A_m(z)$ has only a weak z dependence.

The total electric field of the array also satisfies the Helmholtz equation

$$\nabla^2 E(x,y,z) + k_0^2 \epsilon(x,y)E(x,y,z) = 0 , \tag{2.2.4}$$

where $\epsilon(x,y)$ is the array dielectric function.

Substituting the assumed field solution (2.2.3) into (2.2.4) and using (2.2.1) and (2.2.2), we get

$$\sum_{m=1}^{N}\left[2\frac{\partial A_m}{\partial z}\left(\frac{\partial u^m}{\partial x}v^m + u^m\frac{\partial v^m}{\partial y} - \gamma u^m v^m\right) + k_0^2(\epsilon-\epsilon^m)A_m u^m v^m\right] = 0 , \tag{2.2.5}$$

where the second-order term $\partial^2 A_m/\partial z^2$ has been neglected, and all the array elements have been assumed to be identical, i.e.,

$$\gamma^1 = \gamma^2 = \cdots = \gamma^N = \gamma .$$

Multiplying (2.2.5) by $(u^n)^*(v^n)^*$ and integrating over x and y, using the following orthogonal condition:

$$\int_{-\infty}^{\infty}\int_{-\infty}^{\infty} u^m v^m (u^n)^*(v^n)^* dxdy = \begin{cases} 0 & m \neq n \\ \iint |u^n v^n|^2 dxdy \neq 0 & m = n \end{cases}$$

we obtain the following set of coupling equations

$$\sum_{n=1}^{N} \kappa_{mn} A_m = \frac{\partial A_m}{\partial z} , \tag{2.2.6}$$

where

$$\kappa_{mn} = \frac{k_0^2}{2\gamma} \frac{\int_{-\infty}^{\infty}\int_{-\infty}^{\infty} u^m v^m (\epsilon - \epsilon^m)(u^n)^*(v^n)^* dxdy}{\int_{-\infty}^{\infty}\int_{-\infty}^{\infty} | u^m v^m |^2 dxdy} \tag{2.2.7}$$

are the emitter-to-emitter coupling coefficients. The array modes of a group of coupled laser waveguides can be obtained by solving the set of simultaneous equations given by (2.2.6). Because A_m is a slowly varying function of z under weak coupling, it is convenient to put

$$A_m(z) = a_m e^{-\delta\gamma\, z} . \tag{2.2.8}$$

Note: 1) for zero coupling, $\delta\gamma = 0$; and 2) $\delta\gamma$ is element independent. Substitution of (2.2.8) into (2.2.6) gives

$$\sum_{n=1}^{N} \kappa_{mn} a_m = -\delta\gamma\ a_m . \tag{2.2.9}$$

Equation (2.2.9) is the well known eigenvalue equation

$$\begin{bmatrix} \kappa_{11} & \kappa_{12} & \cdot & \kappa_{1N} \\ \kappa_{21} & \kappa_{22} & \cdot & \kappa_{2N} \\ \cdot & \cdot & \cdot & \cdot \\ \kappa_{N1} & \kappa_{N2} & \cdot & \kappa_{NN} \end{bmatrix} \begin{bmatrix} a_1 \\ a_2 \\ \cdot \\ a_N \end{bmatrix} = \xi \begin{bmatrix} a_1 \\ a_2 \\ \cdot \\ a_N \end{bmatrix} , \tag{2.2.10}$$

where $\xi = -\delta\gamma$ is the eigenvalue. Generally, Equation (2.2.10) cannot be solved in closed form. However, when only nearest neighbor coupling is considered, and

when the array elements are assumed identical and uniformly spaced, we have the orthonormality condition of the modes

$$\kappa_{mn} = \begin{cases} 0 & m \neq n \pm 1 \\ \kappa & m = n \pm 1 \end{cases}$$

and

$$\begin{bmatrix} 0 & \kappa & 0 & \cdot & 0 \\ \kappa & 0 & \kappa & \cdot & 0 \\ 0 & \kappa & 0 & \cdot & 0 \\ \cdot & \cdot & \cdot & \cdot & \cdot \\ 0 & 0 & 0 & \cdot & 0 \end{bmatrix} \begin{bmatrix} a_1 \\ a_2 \\ a_3 \\ \cdot \\ a_N \end{bmatrix} = \xi \begin{bmatrix} a_1 \\ a_2 \\ a_3 \\ \cdot \\ a_N \end{bmatrix} . \tag{2.2.11}$$

The corresponding secular eigenvalue equation is

$$\begin{vmatrix} -\xi & \kappa & 0 & \cdot & 0 \\ \kappa & -\xi & \kappa & \cdot & 0 \\ 0 & \kappa & -\xi & \cdot & 0 \\ \cdot & \cdot & \cdot & \cdot & \cdot \\ 0 & 0 & 0 & \cdot & -\xi \end{vmatrix} = 0 . \tag{2.2.12}$$

This equation can be readily solved and the resultant eigenvalues are

$$\xi_l = 2\kappa\cos\left(\frac{l\pi}{N+1}\right), \qquad l = 1,2,\ldots,N . \tag{2.2.13}$$

Substitution of (2.2.13) into (2.2.11) and solution for a_m, the eigenvectors, gives

$$a_m^l = \sin\left(m\frac{l\pi}{N+1}\right), \qquad l = 1,2,\ldots,N . \tag{2.2.14}$$

Thus, the resulting lth array mode is given by

$$E_l(x,y,z) = \sum_{m=1}^{N} \sin\left(m\frac{l\pi}{N+1}\right) u^m(x) v^m(y) e^{-(\gamma+\delta\gamma_l)z} , \tag{2.2.15}$$

where $\delta\gamma_l$ is obtained from Equation (2.2.13)

$$\delta\gamma_l = -2\kappa\cos\left(\frac{l\pi}{N+1}\right) .$$

Hence, the array modes have propagation constants

$$\gamma_l = \gamma - i2\kappa\cos\theta_l , \tag{2.2.16}$$

with

$$\theta_l = \frac{l\pi}{N+1}, \qquad l = 1,2,...,N .$$

The value $\gamma = -g/2 + i\beta$ where g is the modal gain and β is the real propagation constant of the single laser element. The complex coupling coefficient is written as $\kappa = \kappa_r + i\kappa_i$ where κ_r and κ_i represent the real and imaginary components of the coupling coefficient. Equation (2.2.16) is then separated into two equations:

$$\beta_l = \beta - 2\kappa_r\cos\theta_l , \tag{2.2.17}$$

$$g_l = g - 4\kappa_i\cos\theta . \tag{2.2.18}$$

The complex coupling coefficient can then be determined from the wavelength splitting and the "gain splitting" of the array modes. The experimental determination of the complex coupling coefficient will be discussed in Section 3.3.8.

2.3 Nonlinear Dynamic Model of Diode Laser Arrays

The dynamic characteristics of semiconductor lasers are generally studied with a unified approach provided by a set of rate equations. A full description of

the lasing action rests on the dynamical interplay among the field variable, carrier density variable and the semiconductor material variable that defines the polarization. However, the polarization relaxation time (typically $\sim$100 fs) governed by the intraband scattering processes is much shorter than the carrier and photon lifetimes[97]. It is therefore reasonable to assume that the polarization decay rate is "fast" and replace the polarization variable by its equilibrium values. This is commonly referred to as "adiabatic elimination of fast variables". Once the polarization variable is eliminated adiabatically in the description of semiconductor lasers, the problem is considerably simplified.

The problem of synchronization of coupled oscillators is fundamental to many areas of science[98]. When synchronization is successful the several oscillators act as one, with a unique frequency and with well-defined phase relationships between the oscillators. When synchronization fails, the behavior of the oscillators is marvelously complex and displays a rich dynamical structure: beat oscillations, quasi-periodic motions and chaotic dynamics. From the viewpoint of contemporary nonlinear dynamics theory the phase-locked semiconductor laser arrays can be seen, at least in the weak to moderate coupling regimes, as an interesting physical system with coupled nonlinear oscillators[99,100].

Recently, a nonlinear dynamic model of single mode semiconductor laser arrays has been presented by Winful and Wang[47,48]. Time-dependent coupled mode theory is used to investigate the dynamic behavior of the arrays, and the analysis is based on semiclassical laser theory modified to include terms that describe evanescent wave coupling between adjacent elements of the array. An array of N coupled lasers is considered. When isolated from its neighbors, each

laser supports a single transverse and longitudinal mode assumed the same for all the lasers. The temporal evolution of the electric field E_j and of the carrier density N_j in the jth laser element of the array is described by nonlinear differential equations[48]

$$\frac{dE_j}{dt} = \frac{1}{2}\left[G_N(N_j - N_{th}) - \frac{1}{\tau_p}\right](1 - i\alpha)E_j + i\kappa(E_{j+1} + E_{j-1}), \quad (2.3.1)$$

$$\frac{dN_j}{dt} = \frac{J}{ed} - \frac{N_j}{\tau_s} - G_N(N_j - N_{th})E_j^2 . \quad (2.3.2)$$

Here the field amplitude is normalized such that E_j^2 gives the photon density in the jth element. The other parameters are the differential gain $G_N = \partial G/\partial N$, the coupling coefficient κ, the threshold carrier density N_{th}, the linewidth enhancement factor α, the photon lifetime τ_p, the carrier lifetime τ_s, the injection current density J, the width d of the active region and the electronic charge e. Equation (2.3.1) can also be separated into parts corresponding to the amplitude A and phase ϕ of the electric field using $E = A\exp(-i\phi)$. It should be noted that the above equations are completely deterministic and do not involve any noise sources such as spontaneous emission into the lasing mode.

The main findings of this dynamic model are that the laser arrays are unstable over a wide range of coupling strengths, and exhibits sustained pulsations, in the field amplitude, phase and the carrier density, which may be periodic, quasi-periodic, or chaotic. The origin of the instability is the amplitude/phase coupling that occurs in semiconductor lasers and is described by the linewidth enhancement factor α[101]. An amplitude fluctuation in one laser leads to a carrier density fluctuation and a phase fluctuation in that same laser

through α. A change in relative phase leads to an amplitude change in a neighboring laser and an accompanying change in its carrier density. Also, the coupling strength between elements is the major parameter to determine the stability of the arrays because it is important to the time needed to send a signal from one element to its neighbors for controlling the type of oscillation of the outputs[50].

Chapter 3
EXPERIMENTAL PROCEDURE

The performance of the diode laser arrays may be characterized according to their dynamic, spectral, spatial, optical and electrical features[102]. This chapter presents experimental techniques with the emphasis on the measurements of temporal and spectral properties as well as a variety of operating parameters important for modeling laser array behavior.

3.1 Spatio-Temporal Measurements of Phased Arrays

Conventional techniques[103] used to study and measure picosecond optical phenomena include nonlinear correlation methods and ultrafast photodetectors in conjunction with oscilloscopes. However, correlation method data provides only indirect information on the pulse shape and width and, although sampling oscilloscope/photodetector combinations are capable of time resolution of tens of picoseconds, the time response of single event oscilloscopes is limited to hundreds of picoseconds. At present, ultrafast streak cameras have distinct advantages over conventional techniques. In contrast to other techniques, a streak camera can directly measure optical temporal profiles with good sensitivity and with a time resolution as short as a few hundreds of femtoseconds for a single optical event. While nonlinear autocorrelation techniques usually averaged over many

pulses generally have superior time resolution, streak cameras produce linear, real-time measurement without the need for deconvolution or curve fitting. They also have the capability of two-dimensional analysis such as time-resolved spatial measurements and time-resolved spectroscopy of a single event. Streak cameras also cover a wide spectral range, from near infrared to ultraviolet, and even into the X-ray region[104]. They have the disadvantage, though, that it is very difficult to obtain a wide time-window for long time-series data.

3.1.1 Streak Camera Operation

The heart of the streak camera is the electron-optical streak tube. The operation of the streak tube is depicted schematically in Figure 3.1. The incident optical signal first enters through a slit of the input optics and the slit image of the incident light is formed on a photocathode plane of the streak tube by the relay lens system. The photocathode converts the light to photoelectrons which are then rapidly accelerated with a mesh at high potential and sharply focused on a microchannel plate with a focusing electrode providing an electrostatic lensing field. A pair of deflection plates are present in the deflecting field. At the moment when the electron beam is passing through the deflecting field, a high-speed linear ramp voltage is applied to the deflection plates to sweep the electron beam from top to bottom across the microchannel plate. The microchannel plate increases the number of electrons, with the gain depending on the voltage placed across it. A phosphor screen converts the electron image to light again and is then read out with a silicon intensified target (SIT) vidicon camera through the output relay lens. The intensity of the slit image on the phosphor is proportional

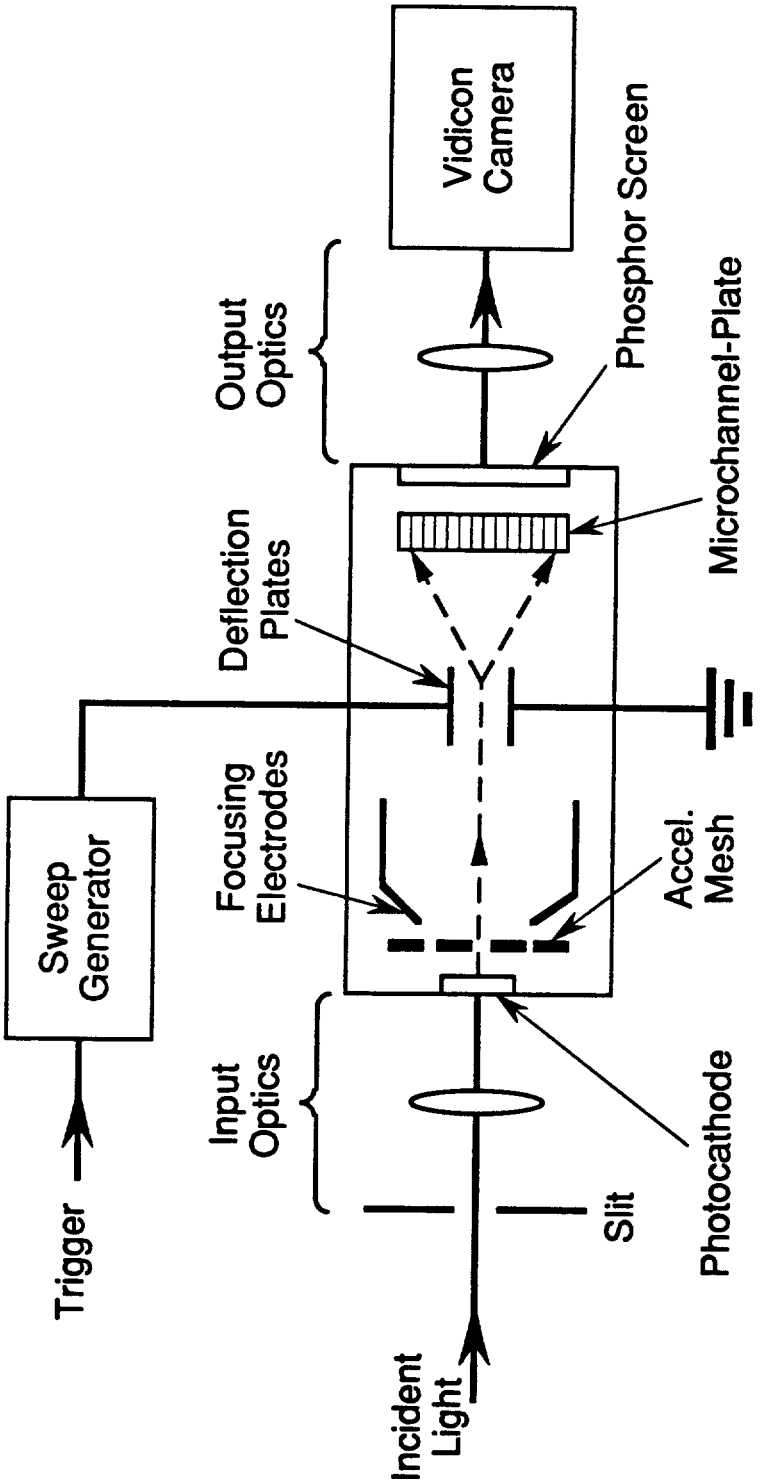

Figure 3.1 Schematic diagram of a typical streak camera.

to the intensity of the incident optical signal and thus the streak observed with the vidicon represents a time-intensity profile of the optical signal. The displacement along the streak image is directly related to time, while the image intensity is proportional to the optical signal intensity.

The temporal resolution of a streak camera is determined by several factors. The first is commonly called the technical time resolution t_T and is determined by the streak speed v_s at which electrons are swept across the microchannel plate (typically 1.5-50 mm/ns), and the dynamic spatial resolution L of the image converter tube (typically 5-25 line pairs/mm)[103,105]:

$$t_T = \frac{1}{L\, v_s}. \tag{3.1.1}$$

With streak speeds approaching that of light and a spatial resolution of about 7 lp/mm, the technical time limit is in the subpicosecond range. In this thesis work, the Hamamatsu N895 and N2367 streak tubes are employed. The Hamamatsu N895 streak tube has a dynamic spatial resolution of ~7 lp/mm so its technical resolution is ~10 ps. The Hamamatsu N2367 streak tube equipped with a M1952 high-speed streak unit can obtain a technical resolution of ~2 ps. In general, the spatial resolution is determined by the electrostatic lensing characteristics of the image converter tube. During the streak, the dynamic spatial resolution is somewhat poorer than in the static mode. Additional degradation of the technical time resolution may be caused by saturation effects in the streak system and limitations due to the spatial resolution of the intensifier and/or recording medium.

A second limiting factor is that due to photoelectron time dispersion t_d.

This effect, which is also called "chromatic time dispersion" arises because photoelectrons are emitted from the photocathode with a distribution of velocities. The effect is small when the incident optical signal has a wavelength near the photocathode red cutoff but becomes progressively more severe with shorter incident wavelengths. The distribution in initial photoelectron energy and velocity gives rise to a distribution in the transit times of the photoelectrons through the streak tube. This cause a broadening in the streak trace and a loss in temporal resolution. The electron time spread is given by the following relation[103,105]:

$$t_d = \frac{\Delta v}{\mu E} \tag{3.1.2}$$

where Δv is the half-width of the distribution of initial photoelectron velocities, μ is the electron charge/mass ratio, and E is the electric field in the photocathode. The spread in photoelectron transit times can be reduced significantly by incorporating a high-potential mesh electrode placed in close proximity to the photocathode to produce an extraction field for the photoelectrons. When this field approaches 10 kV/cm, t_d is reduced to subpicosecond values. The more rapidly the electrons are accelerated to high velocity, the faster they forget their initial velocity distribution. The initial photoelectron velocity distribution is a function of both photocathode type and incident wavelength, but typically $\Delta v \sim 2\times10^7$ cm/s^3. With the mesh mounted at a distance of 0.5 mm from the photocathode and biased 2 kV positive with respect to the photocathode, the Hamamatsu M1952 high speed streak unit can produce a net extraction field of 20 kV/cm, so typical photoelectron transit-time spreading is <2 ps.

If one assumes that the functional form of the various contributions to the time dispersion are Gaussian, then the instrumental time resolution t_{instr} is given by[105, 106]

$$t_{instr} = \sqrt{t_T + t_d}. \tag{3.1.3}$$

Instrumental time resolutions of currently available streak tubes are in the range of 0.7-2 ps. Designs are currently under development which would extend the limit to tens of femtoseconds[107].

Several important instrumental parameters (streak speed, optical delay required, and jitter) are directly related to the streak camera deflection system. Typically, a 1-10 kV voltage ramp is applied to the deflection plates, the rise time determining the streak speed. In practice, the fastest rise time ($\sim$1 ns) is limited by the intrinsic capacitance and induction of the deflection system. Because there is an inherent switch delay in the start of the ramp with respect to the incoming trigger signal, it is necessary to delay the arrival of the optical pulse with respect to the trigger, typical delay times being tens of nanoseconds, even at the fastest deflection speeds. In addition to optical delay, the ramp switch introduces jitter in the start of the streak. Tigger jitter can range from a picosecond to a nanosecond, depending upon the type of switch used.

3.1.2 Spatio-Temporal Recording with Streak Camera

The first application of a streak camera to the measurement of the dynamics of multiple emitter phase-locked injection laser arrays was reported in 1984[108]. Since then advances in equipment and analysis have made possible the simultane-

ous observation of the time evolution of the intensity profile of each of the individual emitters in the array. This was accomplished by adding video frame grabbing capability to the streak camera system thereby making full use of the intensity information available on each of the individual emitters in the array[109].

The measurements of the temporal evolution of the laser array optical output discussed in this thesis were made under both pulsed and CW conditions. The lasers were operated at various drive currents above lasing threshold. In each case the near- or far-field of the laser was imaged on the streak camera optical input plane with a 20×, 0.4 NA microscope objective.

The experimental setup with a Hamamatsu C979 streak camera used to measure the time evolution of the *pulsed* light intensity from the laser array is shown schematically in Figure 3.2. The laser array was driven by an Avtech AVO-2-C avalanche transistor pulser operating at a duty cycle of $\sim 10^{-5}\%$ with $\sim$50 ns wide square-wave pulses. Current through the laser diode was monitored on a Tektronix 7104/7A29/7B15 1-GHz oscilloscope by placing a high frequency (3.5 GHz) oscilloscope probe across the resistor. Figure 3.3 shows the leading edge of a typical pulse with a risetime of 1.8 ns. The current pulser and the streak camera were triggered synchronously by a video frame pulse extracted from the free-running video output of the vidicon by a Colorado Video Inc 302-2 video sync-stripper. The duty cycle was controlled with a Tektronix DD501 digital delay unit ("event delay" in Figure 3.2) by controlling the number of video frames between pulses. A Stanford Research System DG535 digital delay generator was used to adjust the time delay, making it possible to observe approximately 5 ns of the time-evolution of the laser output anywhere within the 50 ns

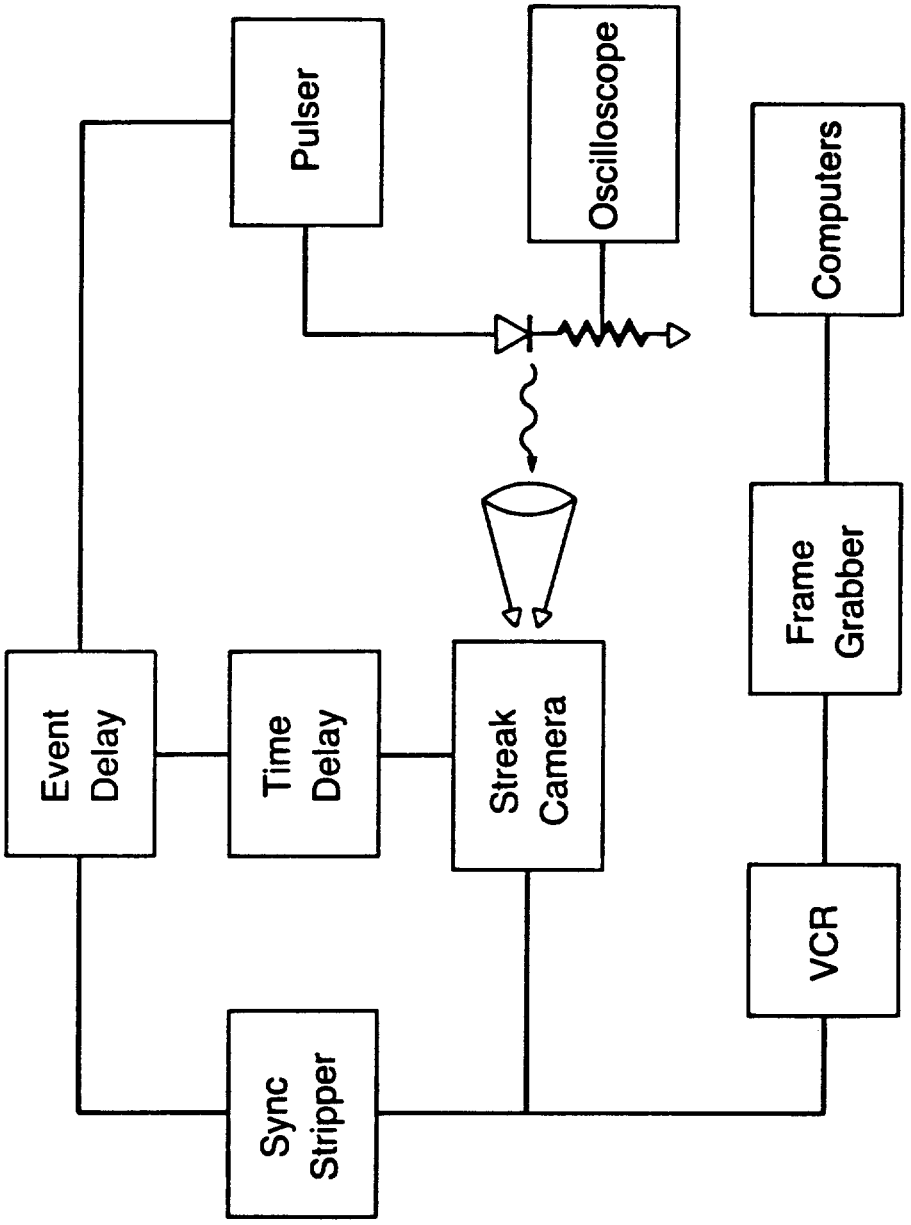

Figure 3.2 Experimental setup of the streak camera recording system.

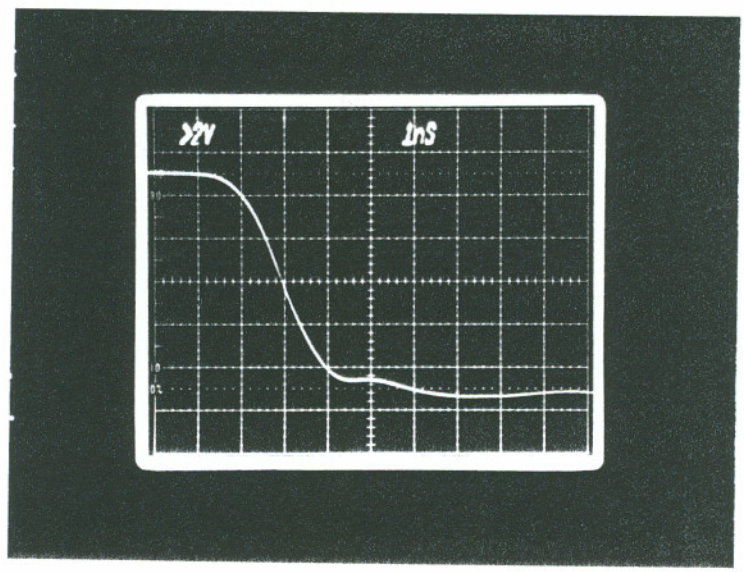

Figure 3.3 The leading edge and first 5 ns of the current pulse used to drive a laser array.

pulse.

For CW operation, the setup was almost the same, except the current pulser was replaced with a CW constant current source and the time delay device was removed. The time evolution of the CW light intensity was measured with a Hamamatsu C1587 streak camera equipped with a M1952 high-speed streak unit. The photocathode of the streak camera was gated on for a duration of a few hundred nanoseconds surrounding the laser optical pulse and a streak sweep of approximately 6 ns duration was initiated near the center of the gate.

In both cases, the streak events were recorded in video fields separated by one second time intervals and stored with a Panasonic AG-6200 video cassette recorder (VCR) which had been adjusted to achieve maximum storage bandwidth. The images stored in the VCR were digitized with a Robot 650 video frame grabber connected to an Apple IIe computer and then transferred to a MicroVAX II computer for data analysis. The data processing began on the MicroVAX with the FORTRAN program f.norm.jitter.f for pulsed time-intensity data to find the triggering delay for each of the fields. For CW time-intensity data the FORTRAN program cw.norm.f was used for normalization of the data. A complete listing of the code for f.norm.jitter.f and cw.norm.f may be found in Appendix A. The data processing also involved creating array files using the FORTRAN program mkarray.b.f (see Appendix B). A FORTRAN program, named analyser.F (see Appendix C), was modified after the work of Hartnett[109] for the analysis including: (1) the time-intensity profile (i.e., time-series) for each emitter of the array; (2) the average time-intensity profile for each emitter of the array; (3) discrete Fourier transforms (DFT) for each emitter of the array; (4)

auto- and cross-correlations among the individual emitters; and (5) averages of both the discrete Fourier transform and correlation results for the time-series data set. Appendix D contains a source listing of shell scripts plot.prof and plot.stat for a representative sample of the programs written to control the graphic display of the time-intensity profiles, the discrete Fourier transform and correlation results. The images were also reproduced by half-tone generation[110] on a laser printer connected to the MicroVAX.

3.2 Spatio-Spectral Measurements of Laser Arrays

The time averaged spectra of the laser arrays were measured during both CW and pulsed operation for various drive current conditions with a SPEX 1269 1.26m spectrometer employing a 600 line/mm grating used in the first, second and third diffraction orders. Figure 3.4 shows a schematic diagram of the measurement setup for the experiments described here. The spectrally resolved near-field pattern of the laser was obtained by imaging its output facet on the 5-μm-wide entrance slit of the spectrometer using a 10× microscope objective lens. The output of the spectrometer was displayed on a TV monitor using a SONY XC-57 miniature charge coupled device (CCD) video camera. As shown in the figure, the CCD output was conditioned to achieve the maximum dynamic range possible, and stored on videotape with the VCR for subsequent digitization. In our experiments, the measurement of the spectrally resolved near-field pattern was done on entire array. The spatial intensity distribution of the individual modes could then be obtained by averaging over windows placed in the stored spectral data. Fabry-Perot resonances were also observed in the below- and

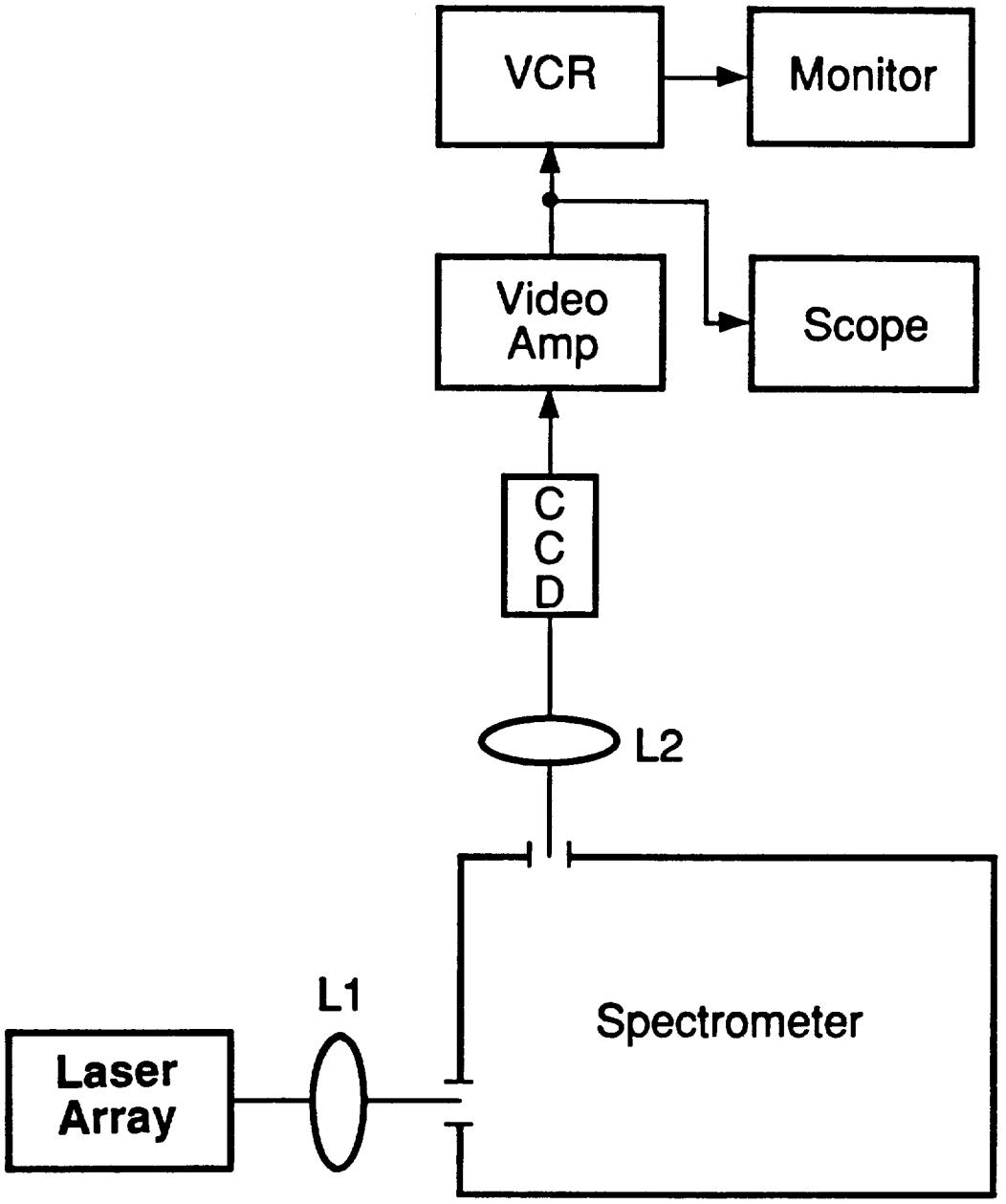

Figure 3.4 Experimental setup for spatio-spectral measurements of the diode laser array.

near-threshold (spontaneous emission) spectra for an individual stripe of the arrays in order to measure the wavelength shift and the net gain which will be discussed in Sections 3.3.4 and 3.3.6.

3.3 Optoelectronic Characterization of Diode Laser Arrays

As mentioned in Chapter 2, the developed dynamic model[47,48] of single longitudinal mode phase-locked semiconductor laser arrays depends on various device parameters. At present, only limited experimental data are available for theoretical modeling and analysis of semiconductor laser arrays. It is therefore necessary to develop techniques to experimentally determine relevant characteristics and parameters of these arrays. In this section, systematic measurements are described for obtaining laser array parameters such as the carrier lifetime, photon lifetime, carrier-induced index change, threshold gain, differential gain and the line-width enhancement factor as well as emitter-to-emitter coupling coefficient.

3.3.1 Light-Current Characteristics

The light-current (L-I) curve is the most commonly measured diode laser characteristic, which shows what optical powers the laser puts out at what drive current applied to the laser. This curve is a key characteristic for judging the efficiency of a diode laser and also used to determine the laser's operating point and threshold current. The CW light output power was measured collecting the light from entire array with a 1 cm-diameter Si-pin detector mounted in front of the laser array using a calibrated neutral density filter, while the average output

of the pulsed light was measured with a Tektronix J16 digital photometer. The slope efficiency of a diode laser can be derived from the L-I curve, most commonly expressed in units of mW/mA.

3.3.2 Carrier Lifetime

The carrier lifetime is an important parameter in the modeling of semiconductor lasers. Analyses of the delay between the beginning of the excitation pulse and the onset of lasing have been carried out[111,112]. These analyses justify the use of the delay as a method of measuring the spontaneous carrier lifetime, even when this lifetime is not the same for all carriers. The lifetime thus measured is the average lifetime of all carriers at threshold population inversion level[111]. A generalized expression for the time delay has also been derived for the case when both radiative and nonradiative recombination are present and for the case in which a dc bias is applied to the laser[112].

A widely used method proposed by Konnerth and Lanza[113] is to extract the carrier lifetime from the experimentally measured time delay between the input current pulse and the output light pulse without prebias. The delay is attributed to the time it takes the injected carrier population N to build up to a threshold value N_{th} necessary to achieve lasing action. Assuming a constant lifetime recombination, the measured delay T_d at a current I is given by[114]

$$T_d = T_0 + \tau_s \ln\left(\frac{I}{I - I_{th}}\right), \tag{3.3.1}$$

where T_0 is an arbitrary fixed delay caused by various cable lengths in the exper-

imental set up, I_{th} is the threshold current, and τ_s is the carrier lifetime at threshold. Thus, a plot of T_d vs $\ln[I/(I-I_{th})]$ is a straight line with a slope τ_s. In our measurements, the laser output pulse of an array was detected with a fast PIN photodiode and the delay time was measured using a Tektronix 7104/7A29/7B15 1-GHz oscilloscope.

For uniform carrier density in the active region, the threshold carrier density N_{th} has the following relationship with the threshold current I_{th} and the carrier lifetime τ_s[115]

$$I_{th} = \frac{qV}{\tau_s} N_{th} \ , \tag{3.3.2}$$

where q is the electron charge and V is the volume of the active region. The dimensions of the active region were measured with a scanning electron micrograph (SEM) to determine the active volume. Once the threshold current and the carrier lifetime were known, the threshold carrier density was determined using Equation (3.3.2).

3.3.3 Optical Confinement Factor

The optical confinement factor Γ is defined as the fraction of the mode energy contained in the active region and depends strongly on the laser structure. In semiconductor laser arrays, the lateral dimension of the array elements is much larger than their vertical or transverse dimension. Thus, what is of most concern is the transverse mode confinement, while the lateral confinement can be considered unity. Using a Gaussian beam approximation for the transverse field $\phi(x)$, the optical confinement factor Γ is given by

$$\Gamma = \frac{\int_{-d/2}^{d/2} |\phi(x)|^2 dx}{\int_{-\infty}^{\infty} |\phi(x)|^2 dx} = \frac{4}{\omega_0\sqrt{2\pi}} \int_0^{d/2} \exp\left(-\frac{2x^2}{\omega_0^2}\right) dx \ , \qquad (3.3.3)$$

where d is the active layer thickness, and ω_0 is the Gaussian beam waist, defined as the $1/e^2$ intensity width. In the far-field region the beam divergence half angle θ is given by[116]

$$\theta = \frac{\lambda}{\pi\omega_0} \ , \qquad (3.3.4)$$

where λ is the laser wavelength. To determine θ, the far-field pattern was recorded with a CCD camera at different distances from the laser facet. The laser was mounted on a microtranslation stage such that the distance could be accurately changed in steps of 1 mm. The output of the CCD camera was recorded with a VCR and then digitized by a video frame grabber. The data were transferred to a MicroVAX computer where they were fitted with a Gaussian function using a nonlinear least-squares fit (Marquardt's method)[117]. The resulting spot sizes were plotted against distances from the array. At large distances these data fell on a straight line with a slope which gaves the beam divergence angle θ. The spot size at the laser end facet was thus determined according to Equation (3.3.4), and the confinement factor Γ was calculated using Equation (3.3.3).

3.3.4 Carrier-Induced Refractive-Index Change

The carrier induced change of the refractive index in semiconductor injec-

tion lasers plays an important role in determining device characteristics. A convenient way of determining the refractive index variations is to look at the movements of individual longitudinal modes in the spontaneous emission spectrum as a function of drive current. The refractive index change, δn, of the active layer may be related to the wavelength shift $\delta\lambda$ of the mode by the expression[118,119]

$$\Gamma \frac{\delta n}{n_g} = \frac{\delta \lambda}{\lambda} , \tag{3.3.5}$$

where Γ is the optical confinement factor, n_e is the effective index of refraction and n_g is the group index defined as $n_g = n_e - \lambda \, dn_e/d\lambda$. This group index can be calculated from the longitudinal mode spacing $\Delta\lambda$ for a cavity length L

$$n_g = \frac{\lambda^2}{2L\Delta\lambda} . \tag{3.3.6}$$

Thus the observation of the movement of a longitudinal mode gives a measurement of the refractive-index change as a function of current. Experimentally, the light output of the array under CW operation was directed into a spectrometer whose output was captured with a CCD camera, displayed on a TV monitor, and recorded with a VCR. Fabry-Perot resonances were observable in the below- and near-threshold (spontaneous emission) spectra of the laser array. Traces of the spectra for an individual emitter were taken at subsequent current intervals such that the same longitudinal mode from one trace to the next could be unambiguously identified. Cross correlations between two consecutive traces were calculated to find the corresponding mode shifts. Below threshold, the mode wavelength shifts down as the drive current is increased, in contrast to the shift to longer wavelength above threshold. At low current levels the wavelength shift

due to carrier density increase dominates the shift. However, at threshold the carrier level is "clamped", and above threshold only the thermal contribution, due to nonradiative recombination and ohmic heating remains. Therefore, the shift should be corrected for the wavelength variation due to the increase of temperature with current using a linear heating correction factor deduced from the measured wavelength shift above threshold[120,121]. The measured wavelength shift of a longitudinal mode due to injected carrier density as a function of current, i.e., $d\lambda/dI$, gives the slope which yields a value of dn/dN in terms of the carrier density N calculated as a function of current from the measurement of the carrier lifetime τ_s through Equation (3.3.2).

3.3.5 Loss and Threshold Gain

The internal optical loss coefficient in a semiconductor laser, α_i, can be related to the external differential quantum efficiency η_d as[115]

$$\eta_d = \eta_i \frac{\alpha_m}{\alpha_m + \alpha_i} , \tag{3.3.7}$$

where α_m is the mirror facet loss per unit length, and η_i is the internal differential quantum efficiency indicating what fraction of injected carrier is converted into photons. The mirror facet loss is given by

$$\alpha_m = \frac{1}{2L} \ln\left(\frac{1}{R_1 R_2}\right) , \tag{3.3.8}$$

where R_1 and R_2 are the facet reflectivities at the two ends and L is the length of the laser. The value of η_i is quite difficult to determine experimentally. It

has been shown that the differential quantum efficiency η_d is directly proportional to the slope dP_{out}/dI of the light-current (L-I) curve, i.e.[115],

$$\eta_d = \eta_i \frac{q}{\zeta h\nu} \frac{dP_{out}}{dI} , \tag{3.3.9}$$

where $h\nu$ is the photon energy and ζ is the factor to account for the portion of the power emitted by the front facet which is defined as[122]

$$\zeta = \frac{(1-R_1)\sqrt{R_2}}{(\sqrt{R_1} + \sqrt{R_2})(1 - \sqrt{R_1 R_2})} . \tag{3.3.10}$$

Thus, combining Equations (3.3.7) and (3.3.9), η_i cancels out, and the internal loss α_i is given by

$$\alpha_i = \alpha_m \left[\frac{\zeta h\nu}{q} \frac{1}{dP_{out}/dI} - 1 \right] . \tag{3.3.11}$$

In practice, laser output power saturates for large values of drive current I and the slope dP_{out}/dI will change. However, before the power saturation mechanisms set in, the slope is reasonably constant and can be used to determine η_d.

At lasing threshold, the gain g_{th} in the active region is equal to the total loss, $\alpha_t = \alpha_m + \alpha_i$, in the laser

$$\Gamma g_{th} = \alpha_t , \tag{3.3.12}$$

where Γ is the optical confinement factor of the active region. After finding the total loss α_t, the photon lifetime can also be determined according to the following relation

$$\frac{1}{\tau_p} = \frac{c}{n_g} \alpha_t , \tag{3.3.13}$$

where c is the velocity of light in vacuum.

3.3.6 Differential Gain

The gain is an important quantity in predicting and understanding the performance of semiconductor lasers. Usually, the optical modal gain is determined from the Fabry-Perot spontaneous emission spectra of the laser. If we denote the intensity of the laser emission at one of the maxima of the Fabry-Perot resonances by $P_{\max}$ and the intensity at a neighboring minima by $P_{\min}$, then, as shown by Hakki and Paoli, the net gain experienced by the guided light at a wavelength is given by[123]

$$G = \frac{1}{L}\ln\left(\frac{r^{1/2}-1}{r^{1/2}+1}\right), \tag{3.3.14}$$

where $r = P_{\max}/P_{\min}$ is the intensity modulation depth. Here $G = \Gamma g - \alpha_t$, α_t being the total loss per unit length in the cavity including facet loss, and g the optical modal gain per unit length which has been multiplied by the confinement factor Γ to take into account that portion of the propagation mode within the active layer. In our experiments, the spontaneous emission spectra of the device were taken at a number of drive currents. For each current a set of modal gain values were calculated using Equation (3.3.14) for an individual emitter and later plotted as a function of wavelength. The dependence of gain on current for a particular wavelength was then determined from these gain spectra. As the current was increased, the gain at the lasing wavelength increased linearly up to the lasing threshold. A straight line drawn through the data points fits the equation

$$\Gamma g - \alpha_t = \frac{dG}{dI}(I - I_{th}) \ . \tag{3.3.15}$$

Using the values α_t, Γ and the carrier density N calculated as a function of current from the measurements of the carrier lifetime τ_s, the modal gain may be expressed using this phenomenological model as

$$g = a(N - N_0) \ , \tag{3.3.16}$$

where $a = dg/dN$ is the differential gain, and N_0 is the injected carrier density at which the gain is equal to zero.

3.3.7 Linewidth Enhancement Factor

The linewidth enhancement factor α, also called the antiguiding parameter, is a fundamental parameter of the laser active material and has paramount importance in semiconductor lasers. It is used to describe the coupling between the real and imaginary parts of the carrier-dependent susceptibility in the active medium. Many properties that are unique to semiconductor lasers can be traced back to the nonzero value of this parameter. The linewidth enhancement factor α is defined as the ratio between the carrier-induced variations of the real and imaginary parts (i.e., the refractive index n and the modal gain g) of the propagation constant of the optical field[101,124,125] i.e.,

$$\alpha = -2k_0 \frac{dn/dN}{dg/dN} \ , \tag{3.3.17}$$

where k_0 is the free-space wave vector and N is the electron concentration. The values of dn/dN and dg/dN depend on the values of N_{th}, Γ and L. This dependence, however, is removed in the determination of α since N_{th}, Γ and L cancel

in Equation (3.3.17). We assume an optical propagation in the positive coordinate direction with a time factor $i\omega t$. This means that a positive gain corresponds to a positive value of the imaginary part of the permittivity. Since dn/dN is found to be negative[119, 126-128], the sign in the definition (3.3.17) is chosen such that the value of α is positive at semiconductor laser wavelengths.

In a GaAs/(AlGa)As (GaAs active layer) laser, the gain dependence on injection carrier density dg/dN is almost linear and that of the refractive index dn/dN is slightly sublinear[128]; hence, the direct ratio of dn/dN and dg/dN can be used for calculation of α with only a small error. However, in lasers with a (AlGa)As active layer, dg/dN is negligible at low injection due to the bandgap shrinkage[129], which shifts the absorption edge to the lower side of energy and prevents the increase of the gain change with increasing N, and the resultant dn/dN is presumed to be nonlinear. This makes the direct ratio useless for (AlGa)As lasers at low injection levels. Therefore, following the definition of α, dn/dN and dg/dN near threshold will be used as this provides more accurate values of α since dn/dN and dg/dN are linear near threshold for both GaAs/(AlGa)As and (AlGa)As lasers[128-130].

In practice, the propagating optical field in a semiconductor laser penetrates into the cladding regions surrounding the active layer. It is therefore appropriate to use the effective index n_e instead of n in Equation (3.3.17). As described in Sections 3.3.4 and 3.3.6 both dn/dN and dg/dN can be obtained from the changes in the Fabry-Perot mode wavelength shift and the depth of modulation in spontaneous emission spectra as current for individual emitters is varied below threshold. The value of α depends on device structures and ranges between 0.5

and 8 for GaAlAs lasers[124,130]. The magnitude of α decreases with the decrease of active layer thickness and cavity length[130] since the carrier concentration and the lasing photon energy become higher[124].

3.3.8 Emitter Coupling Coefficient

The coupling coefficient is a useful parameter in indicating how factors such as guide separation and index discontinuity affect the semiconductor laser stripe interaction. As discussed in Section 2.2, the coupling coefficient can be determined from both wavelength splitting in a longitudinal mode and the "gain splitting" of the array modes. From coupled-mode analysis it is known that an array of N emitters, each being single moded, can support simultaneously N array modes formed as a result of the optical coupling between the emitters. When both the passive and active nature of the waveguide are considered, the propagation constant becomes complex. According to Equations (2.2.17) and (2.2.18), its real and imaginary parts depend on the real propagation constant and the modal gain, respectively.

From Equation (2.2.17), the lth and the $(l+1)$th modes with the wavelengths of λ_l and λ_{l+1}, respectively, have real propagation constants

$$\beta_l = \beta - 2\kappa_r \cos\theta_l \ , \tag{3.3.18}$$

$$\beta_{l+1} = \beta - 2\kappa_r \cos\theta_{l+1} \ . \tag{3.3.19}$$

By subtracting Equation (3.3.19) from Equation (3.3.18), we have a difference of the propagation constants as

$$\beta_{l+1}-\beta_l = -2\kappa_r(\cos\theta_{l+1}-\cos\theta_l) . \tag{3.3.20}$$

Since $\beta_l = 2n_e\pi/\lambda_l$ with the effective index n_e, Equation (3.3.20) gives the real component κ_r of the complex coupling coefficient, i.e.,

$$\kappa_r = \frac{n_e\pi}{\cos\theta_{l+1}-\cos\theta_l}\left(\frac{1}{\lambda_l}-\frac{1}{\lambda_{l+1}}\right) . \tag{3.3.21}$$

For $\kappa_r > 0$, there is $\lambda_{l+1} < \lambda_l$ which indicates that higher order array modes operate at shorter wavelengths than the fundamental or lowest order array mode. Such wavelength splittings can be directly obtained from spectral measurements.

Again, from Equation (2.2.18), the lth and the $(l+1)$th modes have the modal gain

$$g_l = g - 4\kappa_i\cos\theta_l , \tag{3.3.22}$$

$$g_{l+1} = g - 4\kappa_i\cos\theta_{l+1} . \tag{3.3.23}$$

respectively. Their difference directly leads to the imaginary component of the complex coefficient as

$$\kappa_i = \frac{1}{4(\cos\theta_{l+1}-\cos\theta_l)}(g_l-g_{l+1}) . \tag{3.3.24}$$

The fundamental array mode is favored due to larger gain for $\kappa_i < 0$, while the highest order mode lases for $\kappa_i > 0$. The gain splitting may be evaluated from the mode suppression ratio (MSR) as follows.

If P_l represents the photon population for lth array mode oscillating at the frequency ω_l, the array mode rate equation is

$$\frac{dP_l}{dt} = (G_l-\gamma_l)P_l + R_{sp}(\omega_l) , \tag{3.3.25}$$

where $G_l = G(\omega_l)$ is the mode gain and γ_l is mode loss. In conventional Fabry-Perot semiconductor lasers, γ_l is frequency-independent and $\gamma_l = \gamma = \tau^{-1}$ for all modes. The last term R_{sp} in the equation above takes into account the rate at which spontaneously emitted photons are added to the intracavity photon population. R_{sp} can be obtained using the gain spectrum related to the spontaneous-emission spectrum[97]

$$R_{sp}(\omega_l) = n_{sp}(\omega_l) G_m \ , \tag{3.3.26}$$

where n_{sp} is the population-inversion factor. Assuming non-interaction of array modes at a given current, the steady-state solution of the array mode rate equation is obtained by setting the time derivative to zero and the photon number is given by

$$P_l = \frac{n_{sp} G_l}{\gamma - G_l} \ . \tag{3.3.26}$$

For two array modes, the mode suppression ratio is approximated by

$$\frac{P_1}{P_2} \approx \frac{G_1(\gamma - G_2)}{G_2(\gamma - G_1)} \ . \tag{3.3.27}$$

Thus the gain splitting may be evaluated from the mode suppression ratio measurements. We should note that the coupling coefficient depends on the drive current because the gain spectrum and the mode suppression ratio change with the power level.

Chapter 4

DYNAMIC CHARACTERISTICS OF GAIN-GUIDED ARRAYS

In gain-guided stripe-geometry laser arrays, the current is confined to a group of parallel stripe contacts via high-resistivity proton-implanted regions[68] or Schottky-barrier defined stripes[69]. The injected carriers control the optical modes through a spatially inhomogeneous gain profile and optical coupling between array elements occurs when the evanescent fields of adjacent devices substantially overlap. Index antiguiding arising from the carrier induced refractive-index changes plays an important role in affecting the far-field distributions of stripe-geometry lasers[95,131,132] and the dynamic behavior of semiconductor laser arrays[48]. This Chapter presents experimental measurements of the radiation field, the mode spectrum, the time evolution of light emission, and device operating parameters for ten- and twin-stripe multiple-quantum-well gain-guided diode laser arrays.

4.1 Ten-Stripe Multiple-Quantum-Well Array

Multiple quantum well (MQW) lasers are known to have several superior lasing properties such as low threshold current density[133] and high output powers[134] relative to conventional double-heterostructure lasers. The ten-stripe MQW laser array reported in this study is shown schematically in Figure 4.1 and

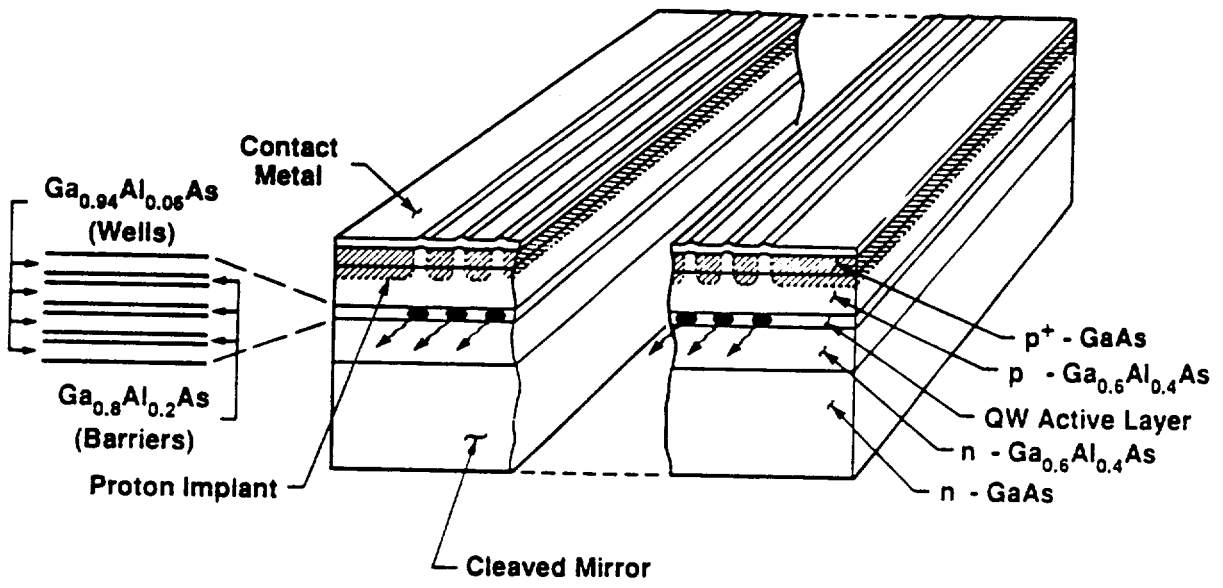

Figure 4.1 Schematic of a multiple stripe gain-guided laser array.

is typical of several we have investigated. The laser array stripe pattern was delineated by a proton implantation technique[81] through a photoresist mask on a metal-oxide-chemical-vapor deposited (MOCVD) grown multiple-quantum-well laser wafer[66,135]. Shallow proton implantation serves to destroy the conductivity of the unmasked areas. Optical coupling results from evanescent wave overlap between the adjacent closely spaced emitters. The structure consists of a GaAs substrate, an n cladding layer 1.4 μm thick, an undoped modified[133] quantum well active layer with a total thickness of 0.095 μm composed of four 140 Å-thick $Ga_{0.94}Al_{0.06}As$ wells separated by three 100 Å-thick $Ga_{0.8}Al_{0.2}As$ barriers, a p-type cladding layer 1.3 μm thick, and a 0.64 μm-thick p^+-GaAs cap layer. The laser was cleaved to a cavity length of 240 μm and its facets were not coated. The laser chip was mounted p side down on a copper heat sink with indium solder. The device used in this study consists of 10 gain-guided, 6-μm-wide stripe semiconductor lasers which are spaced on 10-μm centers.

4.1.1 Device Performance

The array was tested under both pulsed and CW operating conditions. Shown in Figure 4.2 are the CW (solid line) and pulsed (dashed line) light output power versus current characteristics of the device operating at room temperature. For pulsed measurements, a pulse width of 47 ns and a repetition rate of 250 Hz were used. The pulsed threshold was 225 mA and the slope efficiency was 0.43 mW/mA from the front facet. Under CW operation, the threshold current level was 230 mA and the slope efficiency was 0.41 mW/mA. As illustrated in Figure 4.2, the CW and pulsed curves differ little, thus indicating good heatsinking of

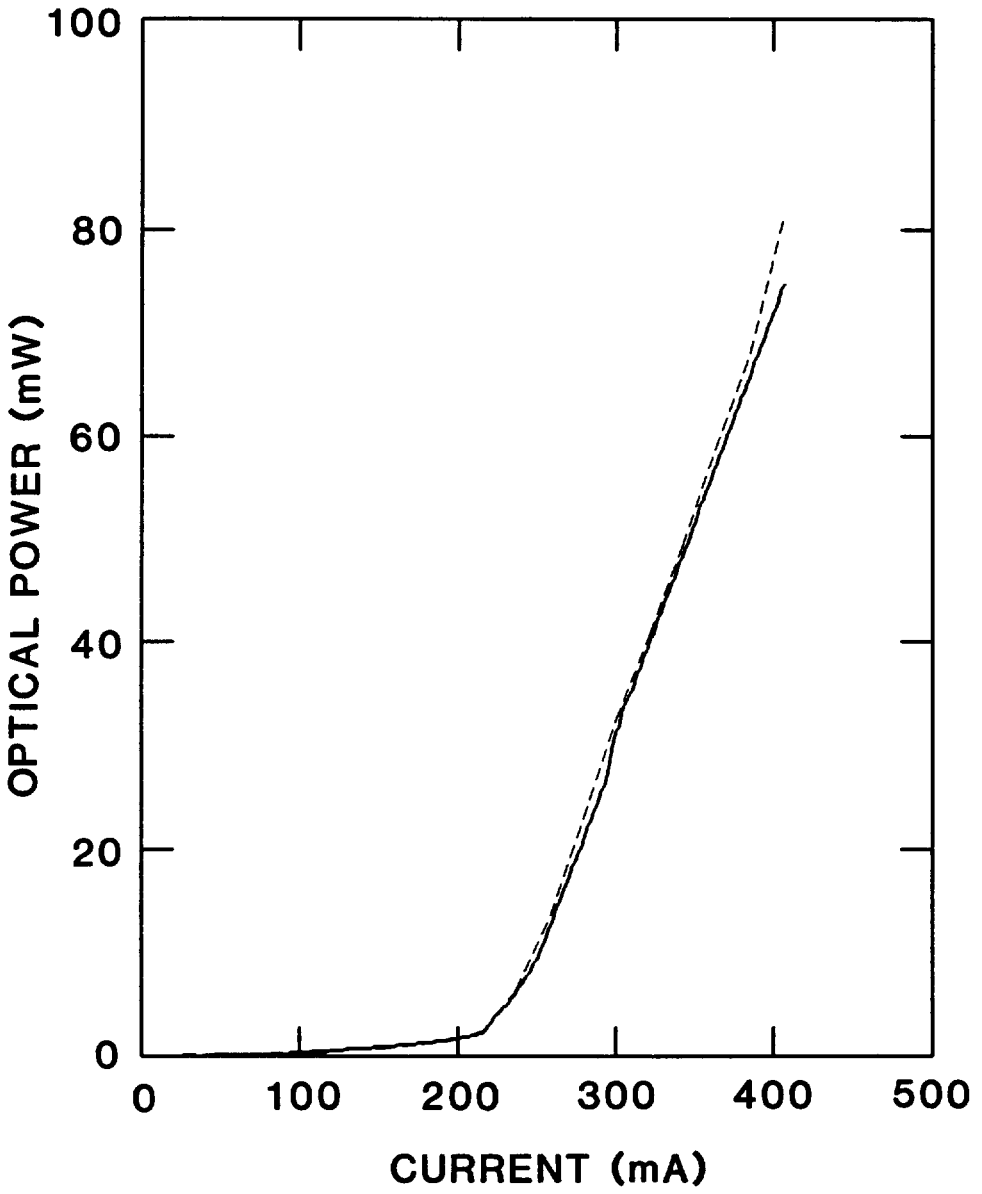

Figure 4.2 The *L-I* characteristic of the ten-strip gain-guided laser array in CW (solid line) and pulsed (dashed line) operation.

the device. The pulsed characteristic is only approximately linear, and has a slight positive curvature, corresponding to an increase in differential efficiency with increasing output power. Conceivably, such an effect occurs as a result of improved lateral optical confinement, improved lateral charge confinement, or increasing injected charge collection efficiency perpendicular to the p-n junction, with increasing pumping current and output power. The CW L-I curve has an obvious kink in the current range of 290-310 mA as shown in Figure 4.2. The appearance of the kink is associated with a change in the optical mode (mode movement, mode transition, or appearance of high-order modes) along the junction plane.

For uncoated facets, the facet loss $\alpha_m = -L^{-1}\ln R$ was obtained to be 50 cm^{-1} by taking $R = 0.3$ due to Fresnel reflectivity at a facet interface with an internal effective modal refractive index of approximately 3.4. From Equation (3.3.11), the internal loss α_i was calculated to be 37 cm^{-1} using the L-I curve slope efficiency of 0.41 mW/mA and the lasing wavelength $\lambda = 8650$ Å. Then the total loss $\alpha_t = \alpha_m + \alpha_i$ in the laser is 87 cm^{-1}. With the technique described in Section 3.3.3, the beam divergence angle in the transverse direction was measured to be 25° so that the spot size at the output facet was determined to be 0.59 μm. Using Equation (3.3.3), the optical confinement factor Γ was estimated to be 0.13 from the nominal active thickness of 0.095 μm and the beam spot size at the output facet. Equation (3.3.12) gives the threshold gain $g_{th} = 669$ cm^{-1} which is smaller than that in SQW lasers ($g_{th} \geq 10^3$ cm^{-1})[136]. Figure 4.3(a) shows $\ln(I/I - I_{th})$ as a function of the measured time delay. The observed linear variation suggests that it is appropriate to use Equation (3.3.1) to

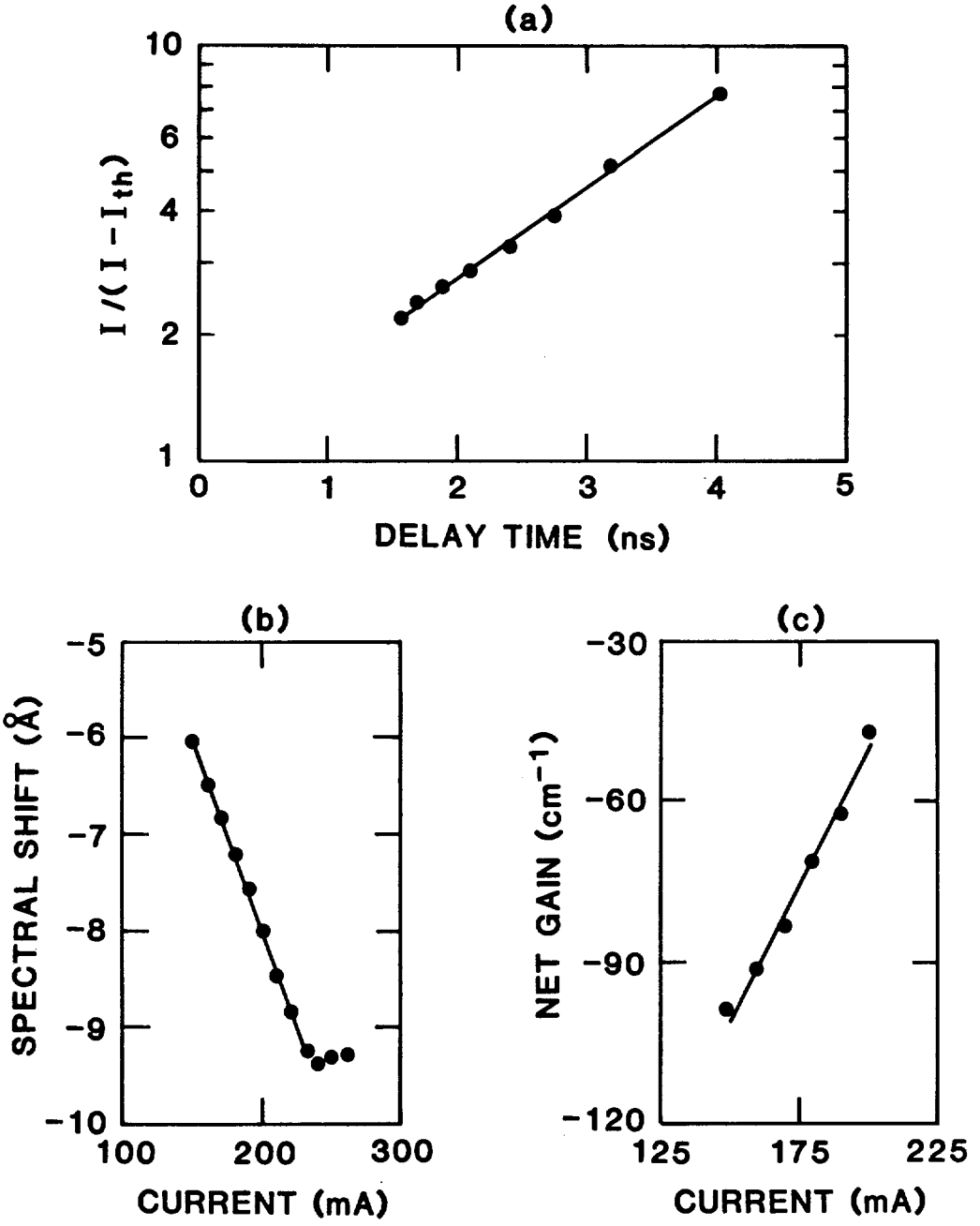

Figure 4.3 (a) The drive current plotted vs laser light output delay; (b) Plot of measured wavelength shift as a function of drive current; (c) The net gain dependence on current drive at a wavelength of 8650Å for the ten-stripe gain-guided laser array.

calculate the carrier lifetime, and it is found to be 2 ns. For a group index n_g = 4.1 that was calculated from the measured longitudinal mode spacing $\Delta\lambda$ = 3.8 Å with Equation (3.3.6), the photon lifetime τ_p = 1.6 ps from Equation (3.3.13).

The wavelength shift and the net gain of the Fabry-Perot resonances for the array were measured as a function of injected current below threshold following the experimental procedure given in Section 3.3. Figure 4.3(b) shows the measured wavelength shift for a longitudinal mode due to injected carrier density vs current. Below threshold the mode wavelength shifts down as the drive current is increased. At threshold the wavelength shift is "clamped", and above threshold the shift moves toward the longer wavelength due to temperature rise. Thus, the shift shown in Figure 4.3(b) has been corrected for the wavelength variation due to the increase in temperature with current using a linear heating correction factor of 3.3×10^{-2} Å/mA deduced from the measured wavelength shift above threshold[120,121]. From Equation (3.3.5), the slope -0.04 Å/mA of the line yields a value of -1.6×10^{-20} cm^3 for the carrier-induced index change dn/dN in terms of the carrier density N calculated as a function of current from the measurement of the carrier lifetime τ_s using Equation (3.3.2). With spontaneous emission spectra taken at currents from 150 mA to 200 mA at intervals of 10 mA, the net gain for unit length was evaluated using Equation (3.3.14) from the modulation depth of these spectra and plotted as a function of current at the lasing wavelength of 8650 Å in Figure 4.3(c). The gain varies almost linearly with current and the slope dG/dI is 1.03 cm^{-1}/mA. Using the values α_t = 87 cm^{-1}, Γ = 0.13, and the carrier density N calculated as a function of

current from the measurements of the carrier lifetime τ_s, one can obtain the differential gain $dg/dN = 8.7\times10^{-16}\,\mathrm{cm}^2$ and the carrier density $N_0 = 1.3\times10^{18}\,\mathrm{cm}^{-3}$. As compared to that in conventional double-heterostructure lasers, the absolute values of both dg/dN and dn/dN are enhanced owing to the large density of states at band edge in the MQW structure[137,138]. However, the enhancement in dg/dN is much more marked than that in dn/dN[139]. Using the values of dn/dN and dg/dN at the lasing wavelength, the linewidth enhancement factor α was calculated to be 2.7. This is about half of the value for conventional gain-guided lasers.

All the parameter values measured for the ten-stripe MQW gain-guided array are summerized in Table 4.1.

4.1.2 Optical Spectra and Radiation Patterns

The spectral characteristics of the lasing emission from the ten-stripe array has been investigated. The spectrum of the optical emission from the laser was obtained with a 1.26 m spectrometer. As discussed in Section 2.2, a phase-locked diode laser array is expected to simultaneously operate in different array modes which have different lasing wavelengths and different spatial intensity patterns. Experimental identification of array modes in an diode laser array has been previously reported[41,132]. In the present study, several array modes have been observed. Figure 4.4 shows the spectrum of the optical emission when the device was continuously operating at $1.7\,I_{th}$. There are three longitudinal modes separated by 3.8 Å, which agrees with the expected Fabry-Perot resonance mode spacing of the laser cavity. Each longitudinal mode has a well defined fine

Table 4.1 Parameter Values of a Ten-Stripe Gain-Guided Laser Array

Parameter	Symbol	Value	Unit
Active layer thickness	d	0.095	μm
Cavity length	L	240	μm
Stripe width	w	6	μm
Emitter spacing	Λ	10	μm
Active volume	V	1.4×10^{-9}	cm^3
Group index	n_g	4.1	
Confinement factor	Γ	0.13	
Lasing wavelength	λ	8650	Å
Longitudinal mode spacing	$\Delta\lambda$	3.8	Å
Facet loss	α_m	50	cm^{-1}
Internal loss	α_i	37	cm^{-1}
Carrier lifetime	τ_s	2	ns
Photon lifetime	τ_p	1.6	ps
Carrier density to reach zero gain	N_0	1.3×10^{18}	cm^{-3}
Threshold carrier density	N_{th}	2.1×10^{18}	cm^{-3}
Gain at threshold	g_{th}	669	cm^{-1}
Gain derivative	dg/dN	8.7×10^{-16}	cm^2
Index derivative	dn/dN	-1.6×10^{-20}	cm^3
Line-width enhancement factor	α	2.7	

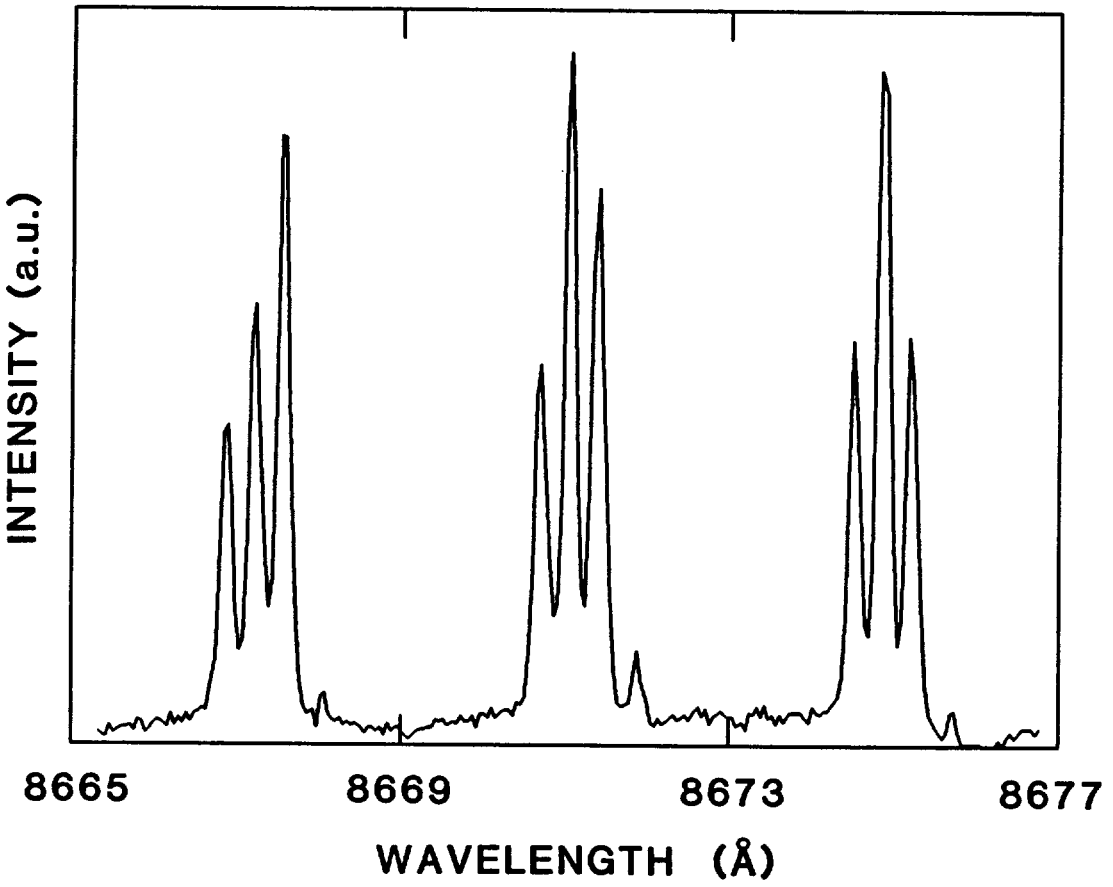

Figure 4.4 Average optical spectrum of the ten-stripe gain-guided laser array during continuously operation at 1.7 times threshold.

structure consisting of three major closely spaced peaks separated by ~0.3 Å from each other. This fine structure corresponds to the simultaneously excited array modes, with the first order array mode having the longest wavelength.

Shown in Figure 4.5(a) is the spectrally integrated near-field pattern of the array driven by a current pulse of $1.7\,I_{th}$. The near-field measurement was obtained by imaging the output array facet on the object plane of the streak camera's input optics with a 20 X, 0.4 NA microscope objective while the streak camera operated in focus mode. The near-field intensity distribution parallel to the junction plane is shown in Figure 4.5(b). Distinct light spots are evident and are almost confined to the ten regions correlated to the stripe structure. Since there existed simultaneously several array modes, the spatial profile is the superposition of the spatial distributions of those array modes. The outer emitters have much lower intensity than those in the center. This is typical behavior for all of the gain-guided laser arrays we have studied, and is due to lower active region charge density because of current spreading at the array edges.

Far-field radiation patterns were observed by directing the light output of the array onto the CCD camera. The far-field pattern of the array displayed three dominant lobes when operated in CW or pulsed mode. Figure 4.6 shows the pulsed far-field pattern for the drive current of $1.7\,I_{th}$. Figure 4.6(a) is the halftone representation of the far field pattern and Figure 4.6(b) is the corresponding intensity distribution digitized from the profile of the far field parallel to the junction plane. The central lobe has a beam full width at half-maximum (FWHM) of 2° and is accompanied by two side lobes each has a FWHM of about 2°. The two side lobes are symmetrically located at ~5.3° from

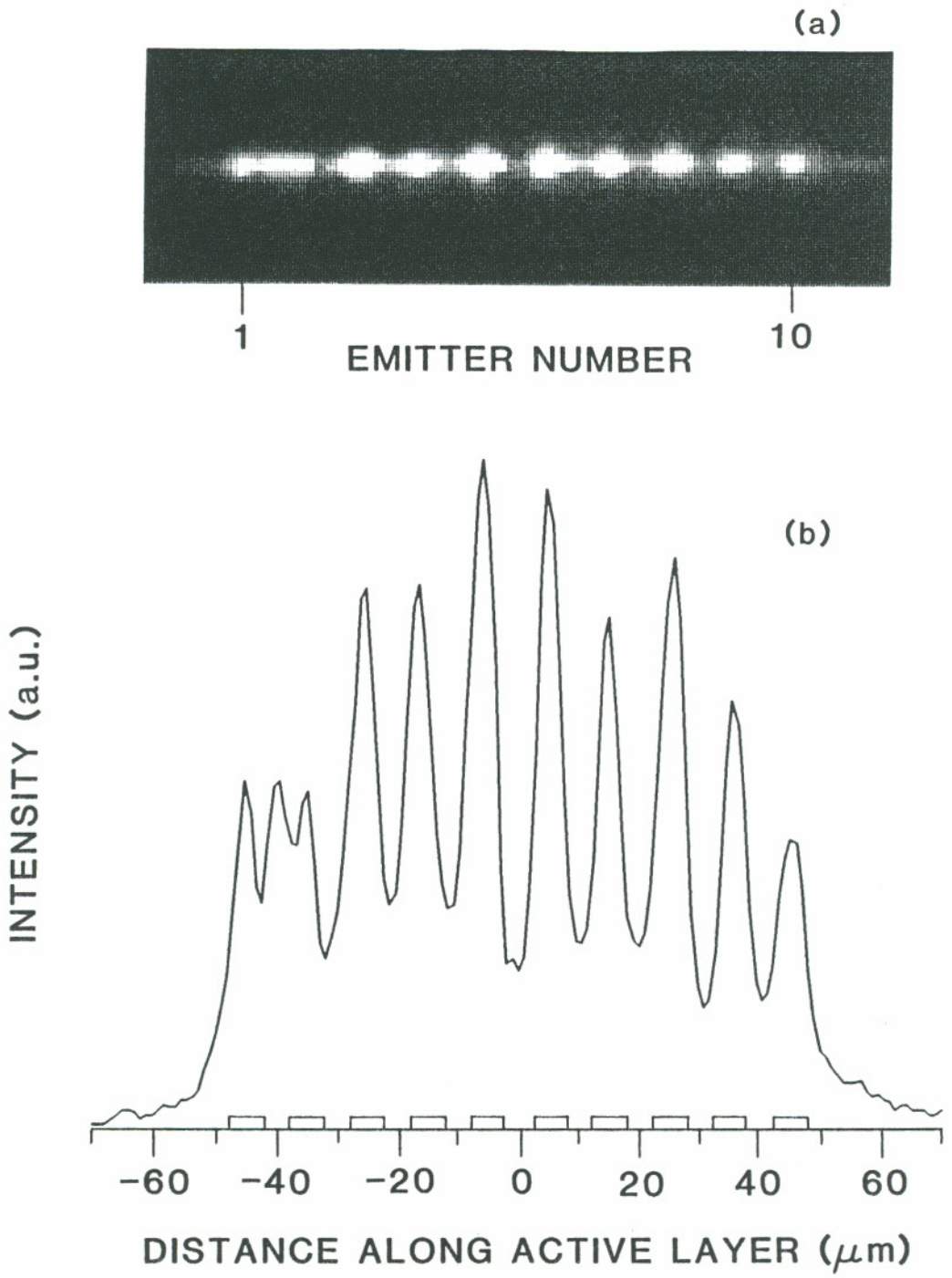

Figure 4.5 (a) The spectrally integrated near-field pattern and (b) the intensity distribution parallel to the junction plan of the ten-stripe laser array during pulsed operation at 1.7 times threshold.

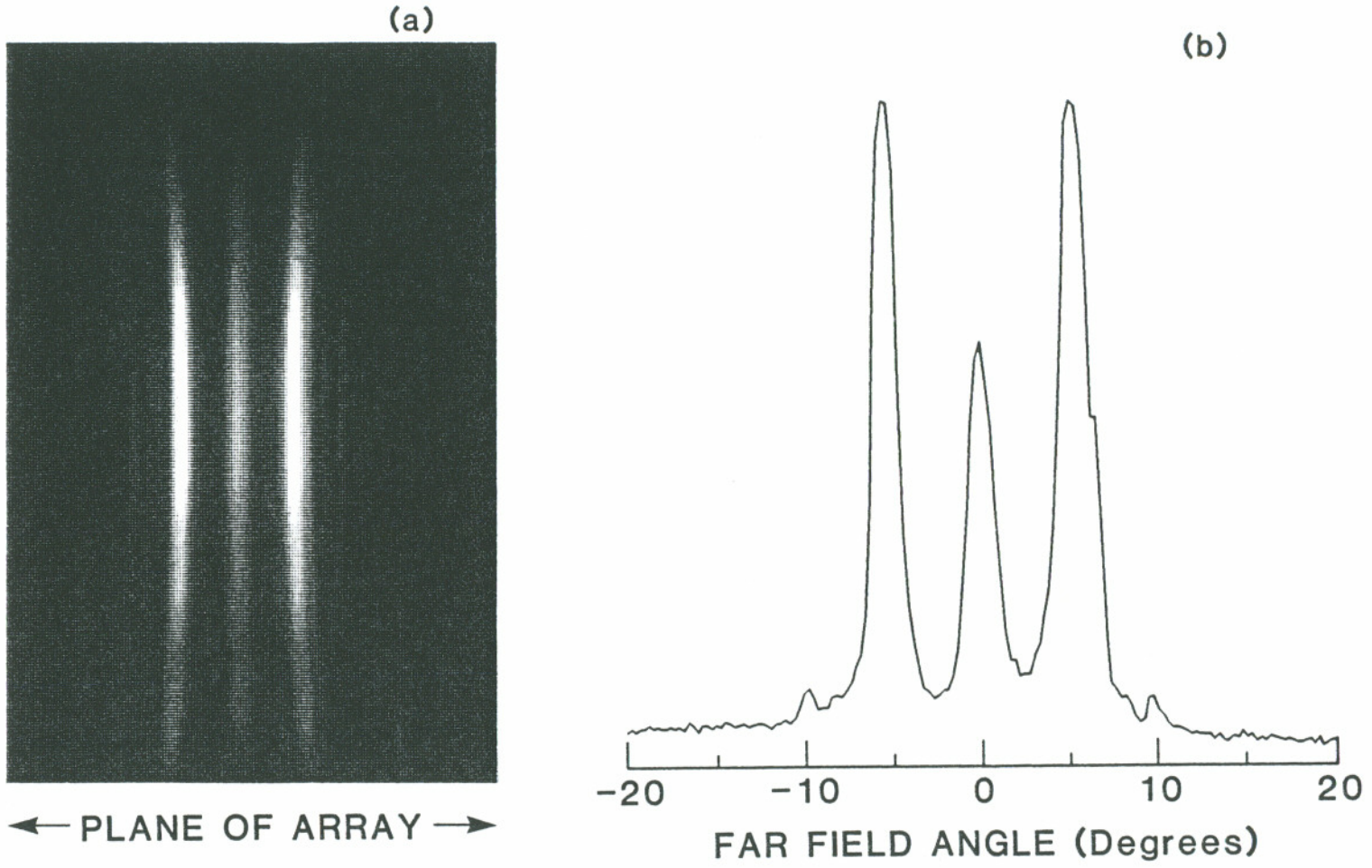

Figure 4.6 (a) The far-field pattern and (b) the intensity distribution parallel to the junction plan of the ten-stripe laser array during pulsed operation at 1.7 times threshold.

the central lobe. This angular separation of 5.3° is quite close to the 5° angle that predicted for an array of emitters periodically spaced on 10-μm centers by simple diffraction calculation[140] according to $\tan\theta = \lambda_0/\Lambda$, where θ is the lobe separation angle in degrees, λ is the laser wavelength and Λ is the emitter spacing. This three-lobed far field is consistent with in-phase operation of individual emitters with antiguiding[132]. Also note that there exist two small diffraction lobes located at angles of $\pm 9.8°$ from the center lobe, respectively, corresponding to higher diffraction orders, i.e., $\tan^{-1}(2\lambda_0/\Lambda) = 9.8°$,

4.1.3 Picosecond Temporal Properties

The time evolution of the light emission from the ten emitter MQW gain-guided laser array was measured with streak cameras in the picosecond to nanosecond time domain. The experimental arrangement for streak-camera measurements has been described in detail in Chapter 3. Figure 4.7 presents the halftone reproduction of the time evolution of the near field pattern for the ten emitter MQW gain-guided array under pulsed operation with two different drive current levels. Figure 4.7(a) corresponds to the light emitted by the array operating with a current pulse of 1.3 I_{th} from zero bias and Figure 4.7(b) corresponds to a current pulse of 1.7 I_{th}. In both cases, the current pulse width = 46 ns, and duty cycle = 5.5×10^{-5} %. The vertical scale for these halftones is time in ns, beginning with zero at the top and increasing to 5.3 ns at the bottom of the frame. The data sampling time is 22 ps. At $I = 1.3\ I_{th}$, the optical response of the array is apparently not uniform across the emitters especially at the beginning of the pulse. As shown in Figure 4.7(a), the first two emitters at

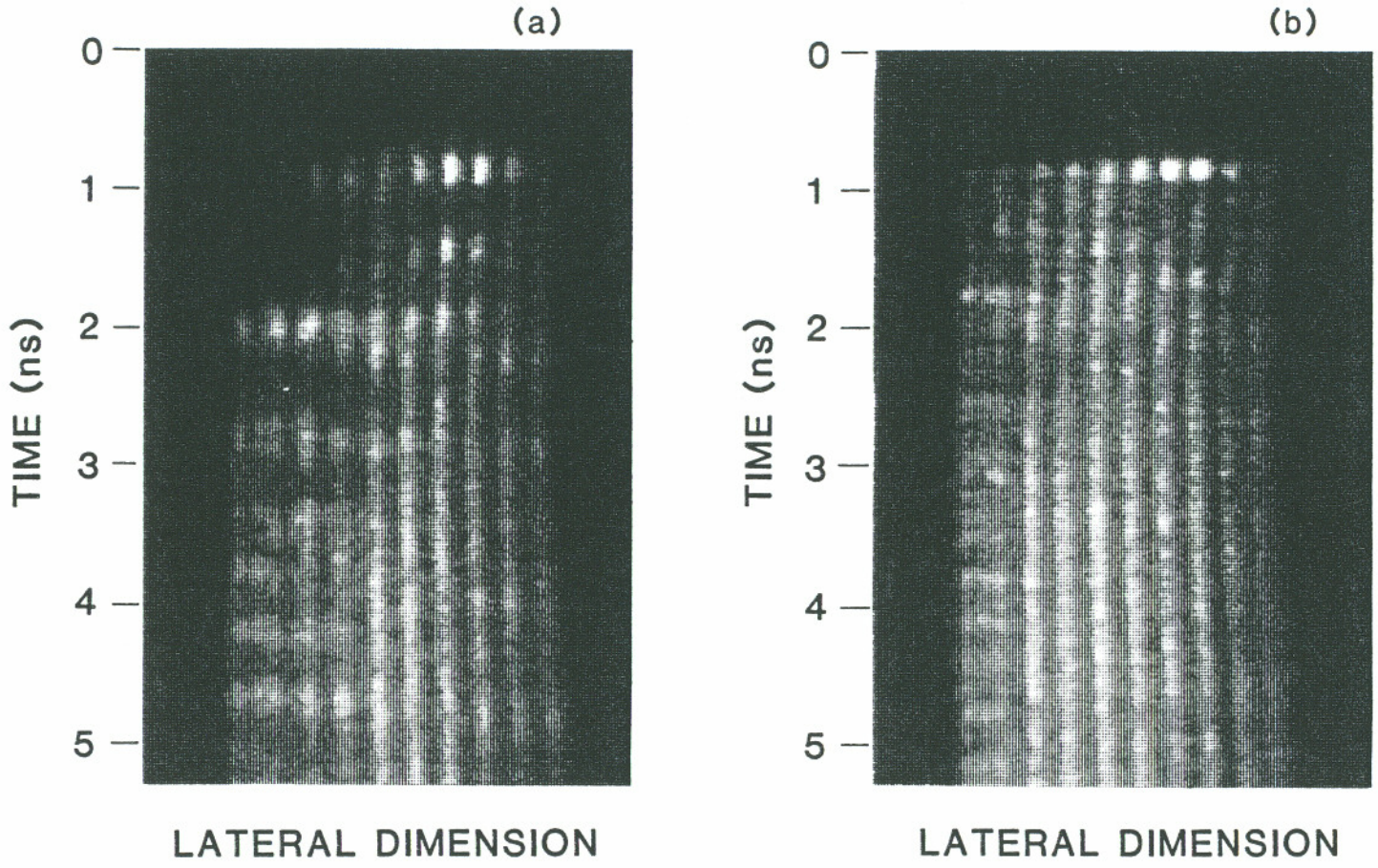

Figure 4.7 Halftone representation of the time evolution of the near-field intensity for the ten-stripe gain-guided laser array during pulsed operation at (a) 1.3 times threshold, and (b) at 1.7 times threshold.

left start to lase about 1 ns later than the rest of the emitters in this particular sample. This may be caused by the asymmetrical coupling or by any other unintended device asymmetry such that two left emitters have lower carrier concentration especially at low injection. Hence these two emitters need a little longer delay time to build up carrier density from the initial value to above the threshold inversion level. When $I = 1.7\ I_{th}$, the carrier concentration is high enough for all emitters to lase, they begin emitting almost simultaneously as shown in Figure 4.7(b). Single-pulse emission versus time from the seventh and eighth stripes in the same array is displayed in Figure 4.8. The data were taken under the same operation conditions as for Figure 4.7(a). Both emitters show strong relaxation oscillations (highly nonlinear oscillations)[141] during the first 2 ns with a frequency of about 1.7 GHz. Such ringing effects result from the interaction of the optical field and the inverted carrier population, and has been well studied for single emitter diode lasers[97,142,143] and for multi-stripe diode laser arrays[47] on the basis of the rate equations. There are also considerable erratic high frequency fluctuations with much lower amplitude than the relaxation oscillation which persist through out the time window. Although these figures show only the first 5 ns, fluctuations were observed through the entire pulse duration.

The intensities emitted from each stripe of the array averaged over 20 pulses are displayed in Figure 4.9 for $1.3\ I_{th}$ and $1.7\ I_{th}$, respectively. The average was computed numerically by summation and normalization of the intensity profiles comprising 20 events. Comparing Figure 4.8 with 4.9, we see that the erratic fluctuations are averaged out while the relaxation oscillations add constructively. This indicates that the fluctuations have random phase relationships from pulse

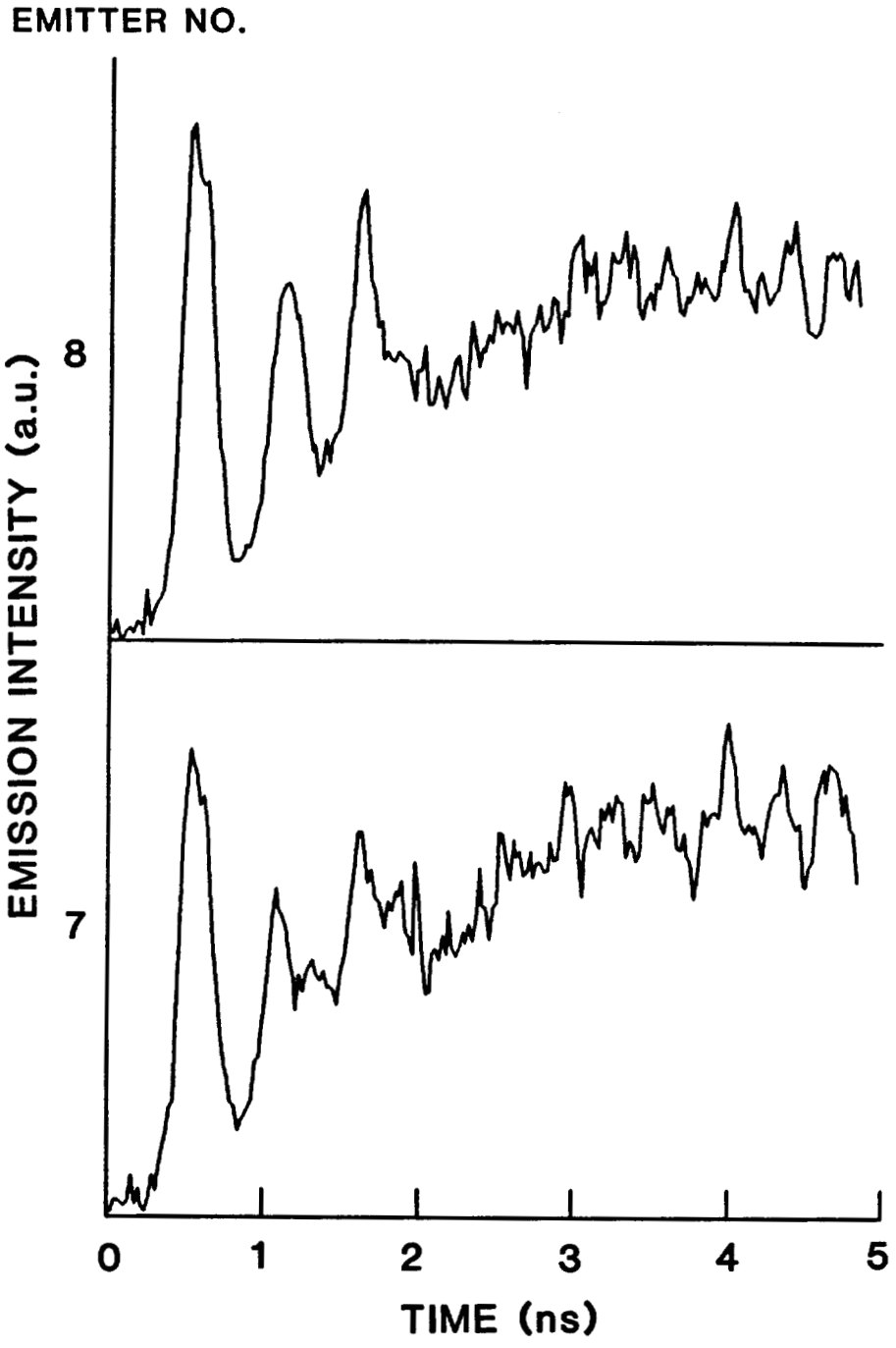

Figure 4.8 Single-pulse emission vs time from the seventh and eighth stripes in the ten-stripe laser array during pulsed operation at 1.3 times threshold.

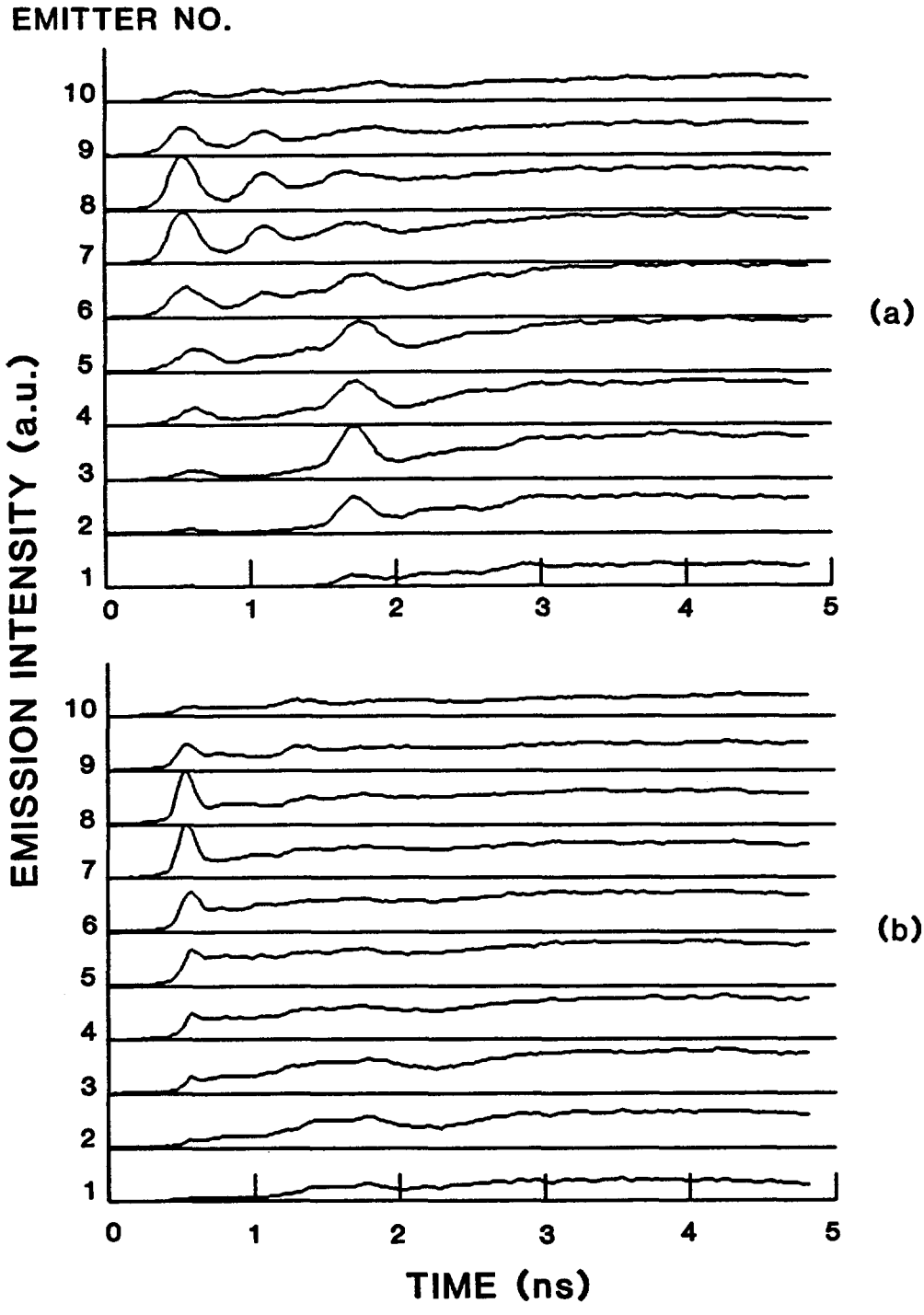

Figure 4.9 Average temporal evolution of 20 events such as those shown in Figure 4.7 for ten-stripe laser array during pulsed operation at (a) 1.3 times threshold, and (b) at 1.7 times threshold.

to pulse. Same behavior for MQW gain-guided arrays was first reported by Elliott and DeFreez[41] in 1985. Each emitter shows about three relaxation oscillation peaks over the first 2 ns when the array was operated at $I=1.3\ I_{th}$. The intensity distribution across the array at each of the three relaxation oscillation peaks does not correspond to any pure array mode. Referring Figure 4.4 it suggests that three array mode are running concurrently. When $I=1.7\ I_{th}$, as shown in Figure 4.9(b), the relaxation oscillation dies out quickly within the first 1 ns, leaving only the first strong oscillating peak visible for most of the emitters.

The frequency characteristics of the time series were studied by Fourier analysis. Using a discrete Fourier transform (DFT) algorithm, Fourier spectra were calculated for each emitter, and then averaged over 20 consecutive frames[109]. The normalized frequency spectra of the array under pulsed $1.3\,I_{th}$ operation are displayed in Figure 4.10. For most emitters, the spectrum exhibits multiple peaks corresponding to the relaxation oscillation frequency and its harmonics. The average relaxation oscillation frequency is approximately 1.7 GHz at pulsed current of $1.3\,I_{th}$, while approximately 2.6 GHz at $1.7\,I_{th}$. It can be seen that the peaks are quite broad. This may be due to the fact that the array was operating simultaneously with several array modes, and each array mode having a different relaxation oscillation frequency corresponding to its gain.

The intensity fluctuations in the array were also observed under CW operation. Figure 4.11 shows the time evolution of light output from the emitters of the same device during CW operation. The data shown was recorded after the laser array had been operating for several minutes at a CW drive current of approximately 1.3 times threshold. From the figure, it is clear that output inten-

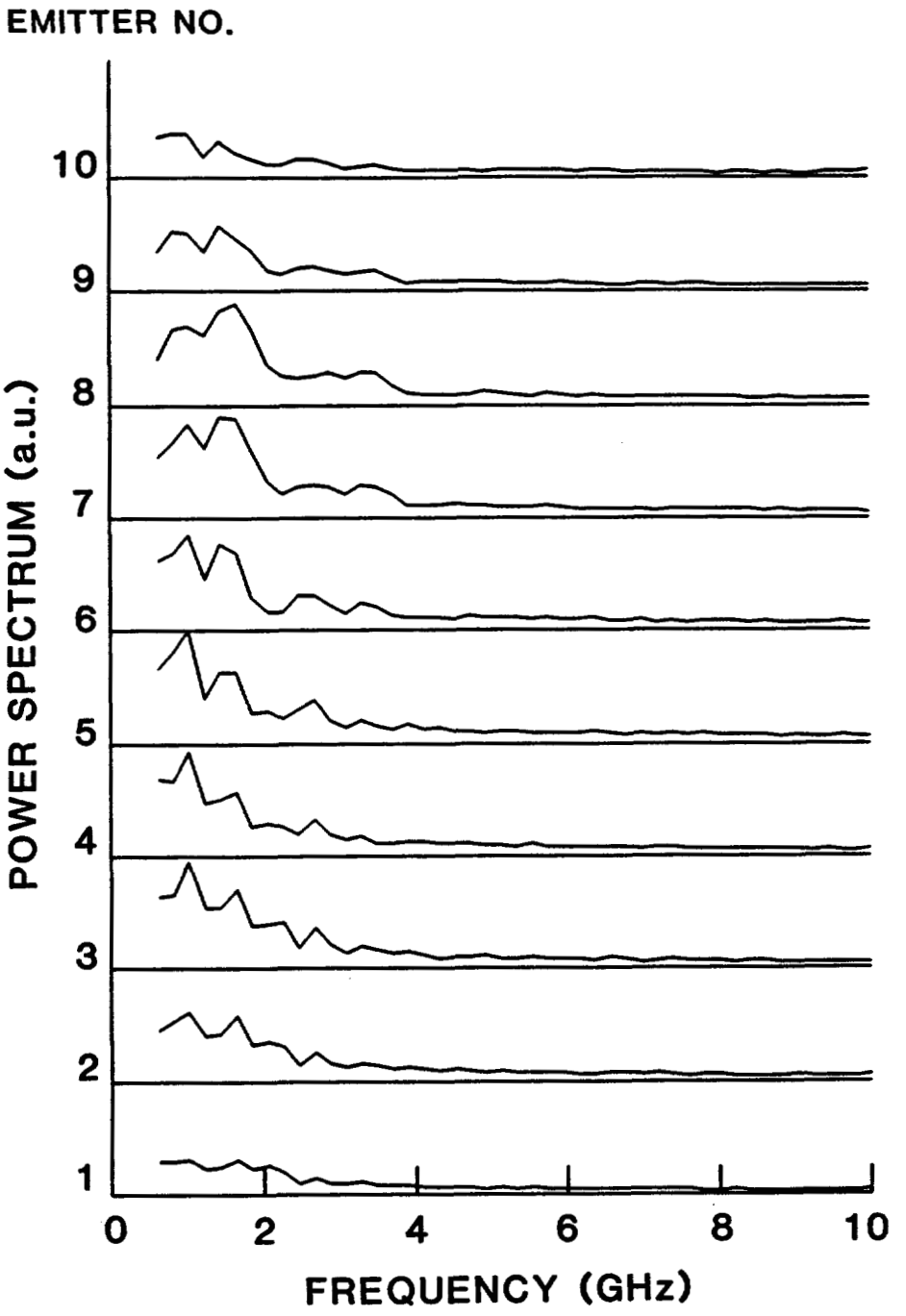

Figure 4.10 Average Fourier spectra for ten-stripe gain-guided laser array under pulsed 1.3 times threshold operation.

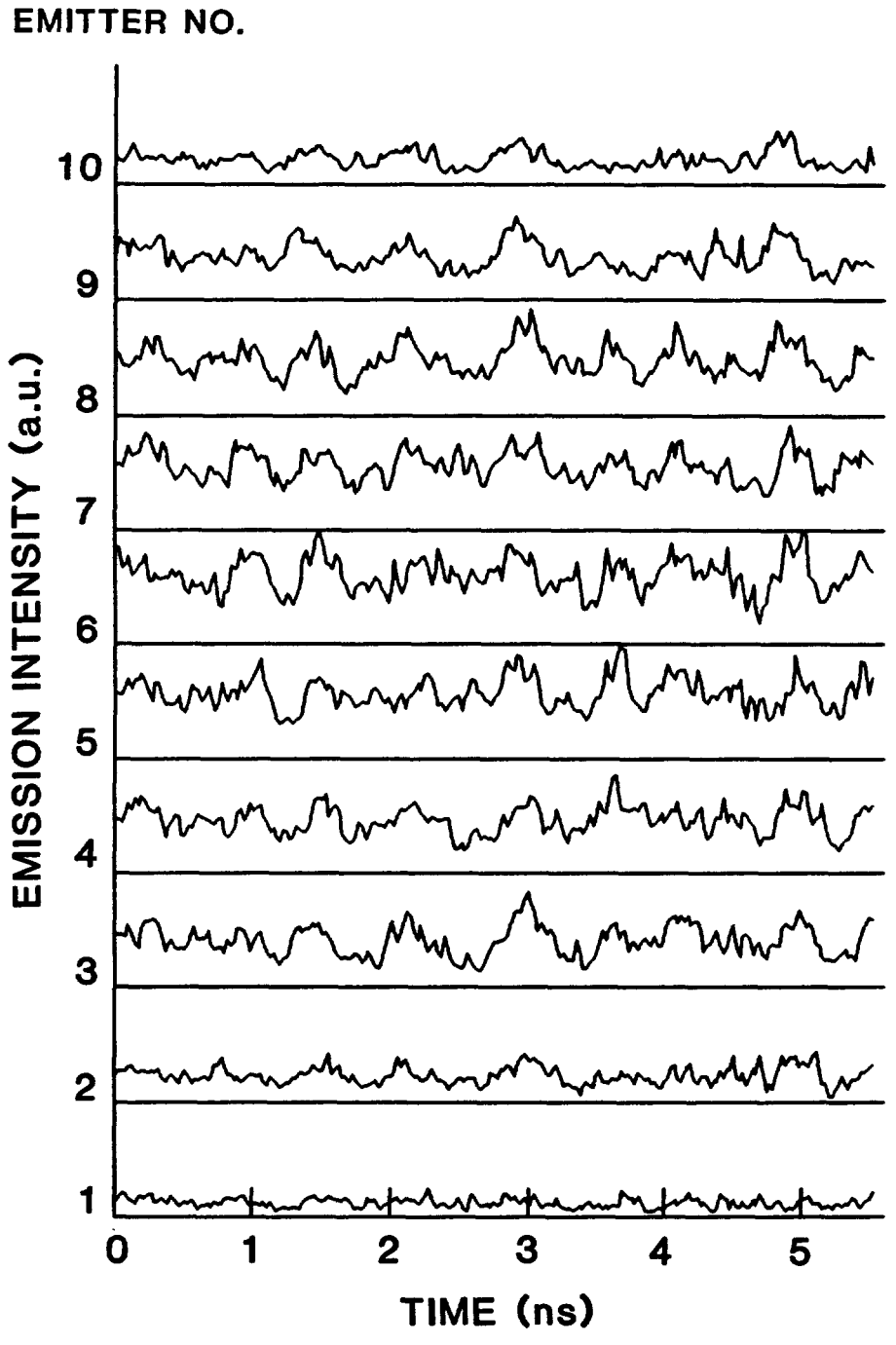

Figure 4.11 Time evolution of each of the emitters during CW operation of ten-stripe laser array at 1.3 times threshold.

sity is highly erratic. Figure 4.12 is average Fourier spectra for this device under CW 1.3 times threshold operation and shows very broad power spectra. This chaotic or noisy behavior is typical of the device at various drive currents.

4.2 Two-Stripe Multiple-Quantum-Well Array

As the simplest laser array, the two-stripe device provides valuable insights into the operation of larger laser arrays. In this section, experimental observations of the operation of a two-stripe MQW array are presented. These are compared to those of the ten-stripe MQW array discussed in Section 4.1.

4.2.1 Device Structure and Performance

The two-stripe array studied has a similar structure to the device described in Section 4.1. It is fabricated from a wafer with an AlGaAs multiple quantum well structure and consists of 2 gain-guided 4-μm-wide stripes with a center-to-center spacing of 12-μm and a cavity length of 240 μm. The quantum well active layer is composed of four $Ga_{0.93}Al_{0.07}As$ wells of 160 Å-thick separated by three 100 Å-thick $Ga_{0.8}Al_{0.2}As$ barrier layers, with a total thickness of 0.14 μm, and is enclosed between n- and p-type cladding layers. The laser chip was bonded p side up to a copper heat sink.

The operating parameters of this device were measured in a manner similar to that of the ten-stripe MQW array following the procedure presented in Chapter 3. All the parameter values measured for the two-stripe MQW gain-guided array are listed in Table 4.2. In summary, the array had a pulsed thres-

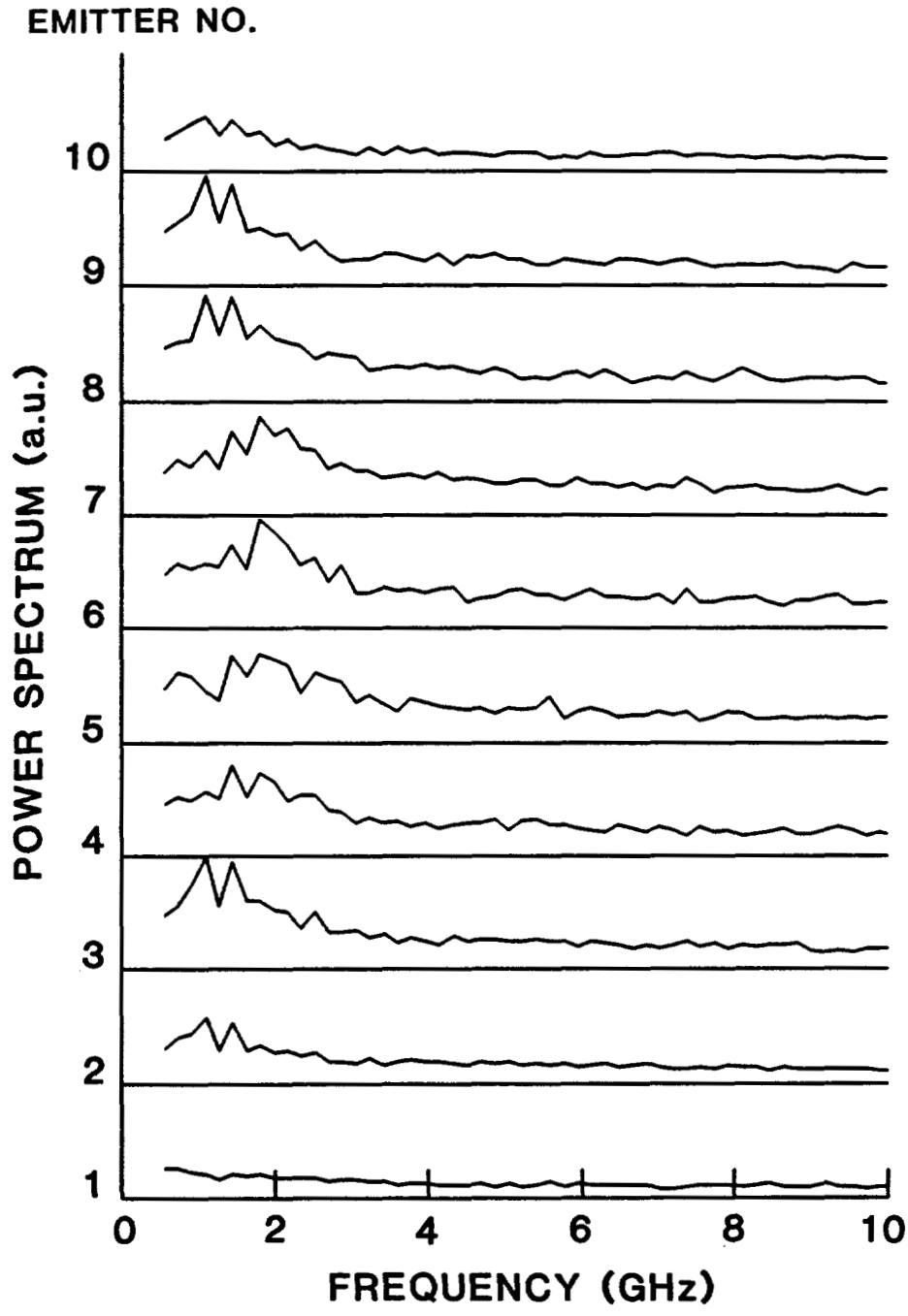

Figure 4.12 Average Fourier spectra for ten-stripe gain-guided laser array under CW operation.

Table 4.2 Parameter Values of a Two-Stripe Gain-Guided Laser Array

Parameter	Symbol	Value	Unit
Active layer thickness	d	0.14	μm
Cavity length	L	240	μm
Stripe width	w	4	μm
Emitter spacing	Λ	12	μm
Active volume	V	4.5×10^{-10}	cm^3
Group index	n_g	4.1	
Confinement factor	Γ	0.15	
Lasing wavelength	λ	8175	Å
Longitudinal mode spacing	$\Delta\lambda$	3.4	Å
Facet loss	α_m	50	cm^{-1}
Internal loss	α_i	40	cm^{-1}
Carrier lifetime	τ_s	2.4	ns
Photon lifetime	τ_p	1.5	ps
Threshold carrier density	N_{th}	3.0×10^{18}	cm^{-3}
Gain at threshold	g_{th}	600	cm^{-1}
Gain derivative	dg/dN	3.8×10^{-16}	cm^2
Index derivative	dn/dN	-1.9×10^{-20}	cm^3
Line-width enhancement factor	α	7.5	
Complex coupling coefficient	η	$0.3-0.4i$	

hold of 70 mA with slope efficiency 0.42 mW/mA from the front facet. Under CW operation, the threshold current level rose to 90 mA. The carrier lifetime τ_s was found to be 2.4 ns. At lasing wavelength of 8175 Å, the total loss α_t in the laser was estimated to be 90 cm^{-1} including the facet loss α_m of 50 cm^{-1} for uncoated facets and the internal loss α_i of 40 cm^{-1}. The optical confinement factor Γ was measured to be 0.15. Then, according to Equation (3.3.12) the threshold gain g_{th} was 600 cm^{-1}. From the measured longitudinal mode spacing $\Delta\lambda$ of 3.4 Å the group index n_g was calculated to be 4.1, and the determined photon lifetime τ_p was 1.5 ps. The carrier-induced index change dn/dN and the differential gain dg/dN were -1.9×10^{-20} cm^3 and 3.8×10^{-16} cm^2, respectively. The linewidth enhancement factor α was calculated to be 7.5. Using the technique discussed in Section 3.3.8, the complex coupling coefficient was obtained to be $\eta = 0.3 - 0.4i$ for 1.7 times threshold drive current.

4.2.2 Radiation Patterns and Optical Spectra

The near- and far-field radiation patterns of the two-stripe laser array are shown in Figure 4.13, with $I = 1.3\,I_{th}$. The near-field, Figure 4.13(a), has two dominant lobes corresponding to the two emitters, with a smaller peak in the middle. For this device, in which the stripe region is defined by proton bombardment, guiding along the junction is primarily provided by a gain mechanism. However, it should be kept in mind that the stripe-geometry gain-guided device is not purely gain guided. This is because the lateral variation of the carrier density is responsible not only for gain guiding but also for index antiguiding governed by the parameter α as defined by Equation 3.3.17. In the context of

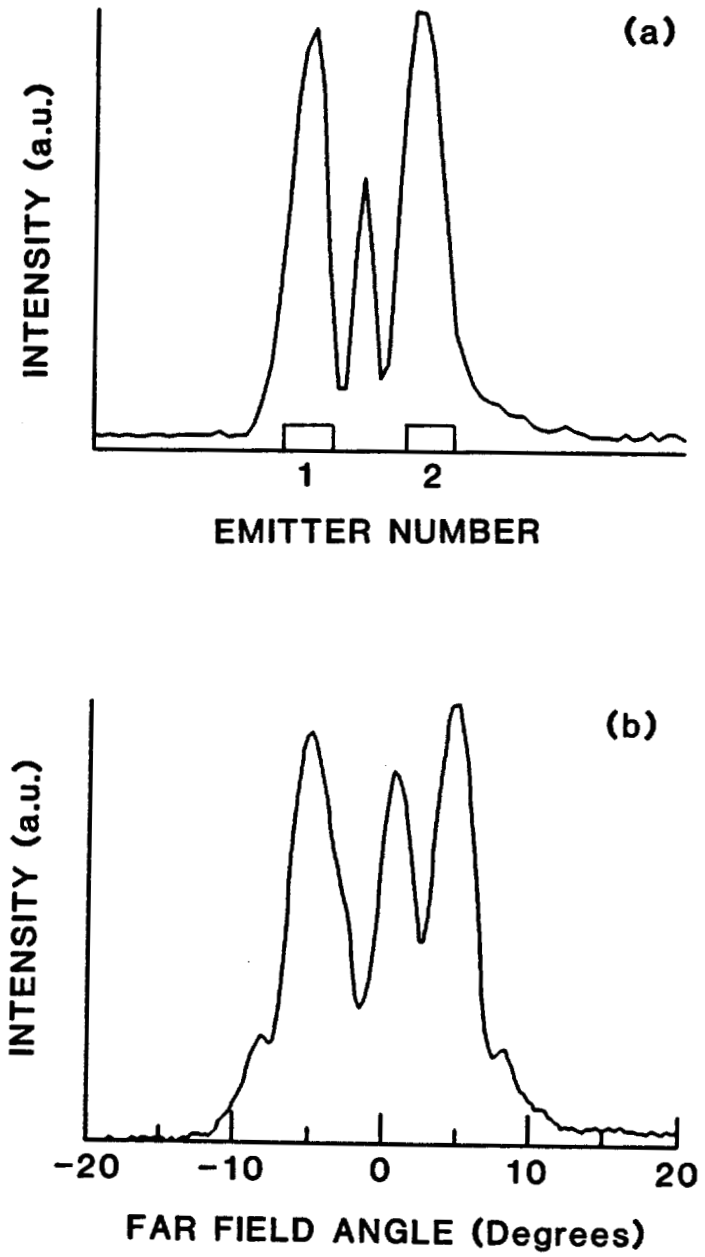

Figure 4.13 The radiation patterns of two-stripe gain-guided laser array at 1.3 times threshold. (a) The near field. (b) The far field.

gain-guided lasers, the α factor is usually referred to as the antiguiding parameter. The lateral variation of the carrier density arising from carrier injection gives rise to an index profile that is out of phase with the gain profile, i.e., the gain peaks at the emitter center while the index peaks in between the emitters. Consequently, the optical gain tries to confine the mode under emitters while the refractive index tents to focus it in between the emitters. These two opposing mechanisms interfere and give rise to additional near-field peak between the emitters. Another feature is that this near-field has an asymmetric intensity profile in which emitter 2 is stronger than emitter 1. The presence of such an asymmetric array mode may result from a slight asymmetry in the composition of the waveguides.

Figure 4.13(b) shows the far-field pattern corresponding to the near-field in Figure 4.13(a). The far-field has three lobes with two strong side peaks, similar to the far-field pattern of the ten-stripe array. Since the twin-stripe array was operating with single lateral mode, the physical mechanism responsible for the observed three-lobed far-field may be the tilting of the near-field phase fronts due to interference between the two opposing guiding mechanisms: Gain guiding tries to focus the mode inside the emitter region while carrier-induced antiguiding tents to defocus it. Actually, since neither the term "gain guiding" nor "antiguiding" provide a fully adequate description, a more appropriate name may be "carrier guiding."[124] The characteristic feature of carrier guiding is that the phase front of propagating wave is curved[144], and the beam waist appears to be located behind the facet[145]. Physically, the origin of a curved wavefront in gain-guided devices can be traced back to the carrier-induced index change, and

the α factor plays an important role. It is well known that such phase aberrations will reduce the intensity maximum in the center of the far field pattern for a single emitter[140]. In the presence of increasing antiguiding, the radiation pattern for a single emitter is broadened, flattened, and then becomes double peaked with a relative minimum in the direction normal to the laser mirror. The radiation pattern of an array can be viewed as the convolution of the pattern for a single emitter with aperture function of the array. Thus, the three-lobed far-field can be produced by convolving a double-peaked, single-emitter distribution with the far-field intensity distribution of the array mode in which the individual emitters are in-phase. This strongly supports that the single operating array mode is the first-order array mode. One last feature of interest is the slightly skewed central lobe shown in Figure 4.13(b). Were the phase fronts under each stripe symmetrical and all the emitters exactly in phase, the observed far-field pattern would be symmetrically peaked at 0°. At the opposite extreme, a 180° phase shift between adjacent emitters with symmetrical phase fronts would produce two symmetrically located identical radiation lobes. The result shown in Figure 4.13(b) indicates some intermediate phase delay and probably an asymmetrical phase front under each stripe caused by the asymmetric stripe pattern.

The longitudinal mode spectra of the device during CW operation at $1.3\,I_{th}$ are shown in Figure 4.14. The array displayed multilongitudinal mode operation. Both emitters show the same multiple longitudinal modes with a mode separation of $\sim$3.4 Å, and the same mode envelope which is approximately centered at 8175 Å. This simultaneous operation of both emitters at the same optical frequency is a indication that they are well phase-locked to each other. The locking

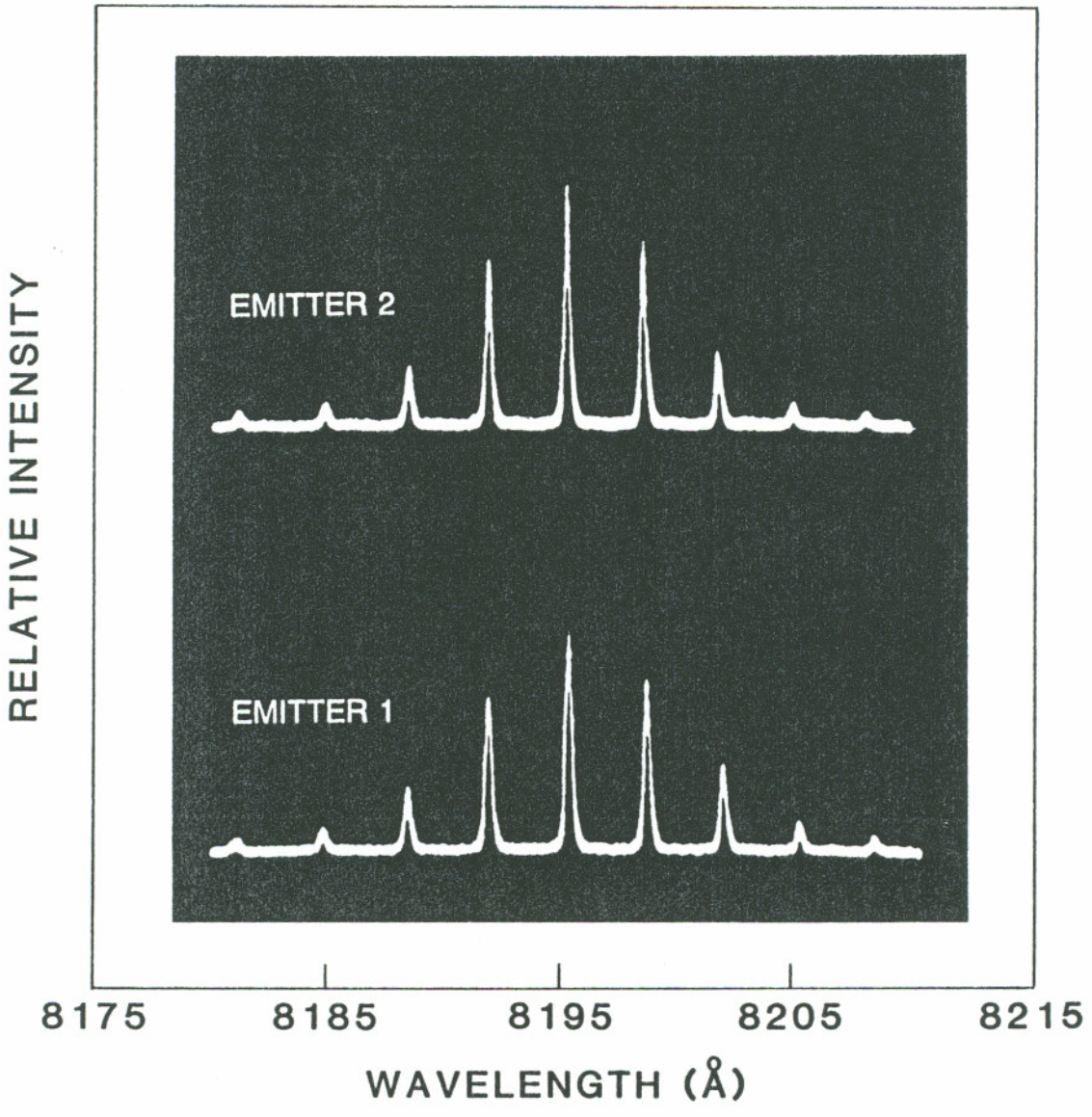

Figure 4.14 The longitudinal mode spectra of the two-stripe gain-guided laser array during CW operation at 1.3 times threshold.

occurs as a result of the stimulated emission induced by either field in the other cavity and the mutual interaction of the fields in the lossy region between the stripes. As illustrated in Figure 4.14, each longitudinal mode is single peaked, suggesting that only one array mode was excited at this current level. According to the near- and far-field patterns discussed above, this array mode was identified as the first-order array mode. When the drive current increased up to 1.7 I_{th}, as shown in Figure 4.15, an additional set of very weak peaks started to appear in the spectra, which indicates the existence of the second-order array mode with a separation of 1.7 Å from the fundamental array mode.

4.2.3 Picosecond Temporal Properties

The transient response of the two-stripe MQW gain-guided array when it is driven by a current pulse also features strong relaxation oscillations at the beginning of its optical emission. Figure 4.16 illustrates the time evolution of the near field pattern of this device responding to a single pulse of 1.3 I_{th}. It is clear from the figure that both emitters oscillate simultaneously and the ringing lasts through out the first 5 ns. The relaxation oscillation frequency was found to be 1.4 GHz.

Under CW operation, the array exhibited self-pulsation behavior. Figure 4.17 presents the halftone representation of the time evolution of the near-field pattern of the array during CW operation at 1.3 and 1.7 times threshold drive current levels. The array exhibited sustained self-pulsation behavior which is very different form the time dependence of the CW light output of the ten-stripe gain-guided array that had noisy characteristics.

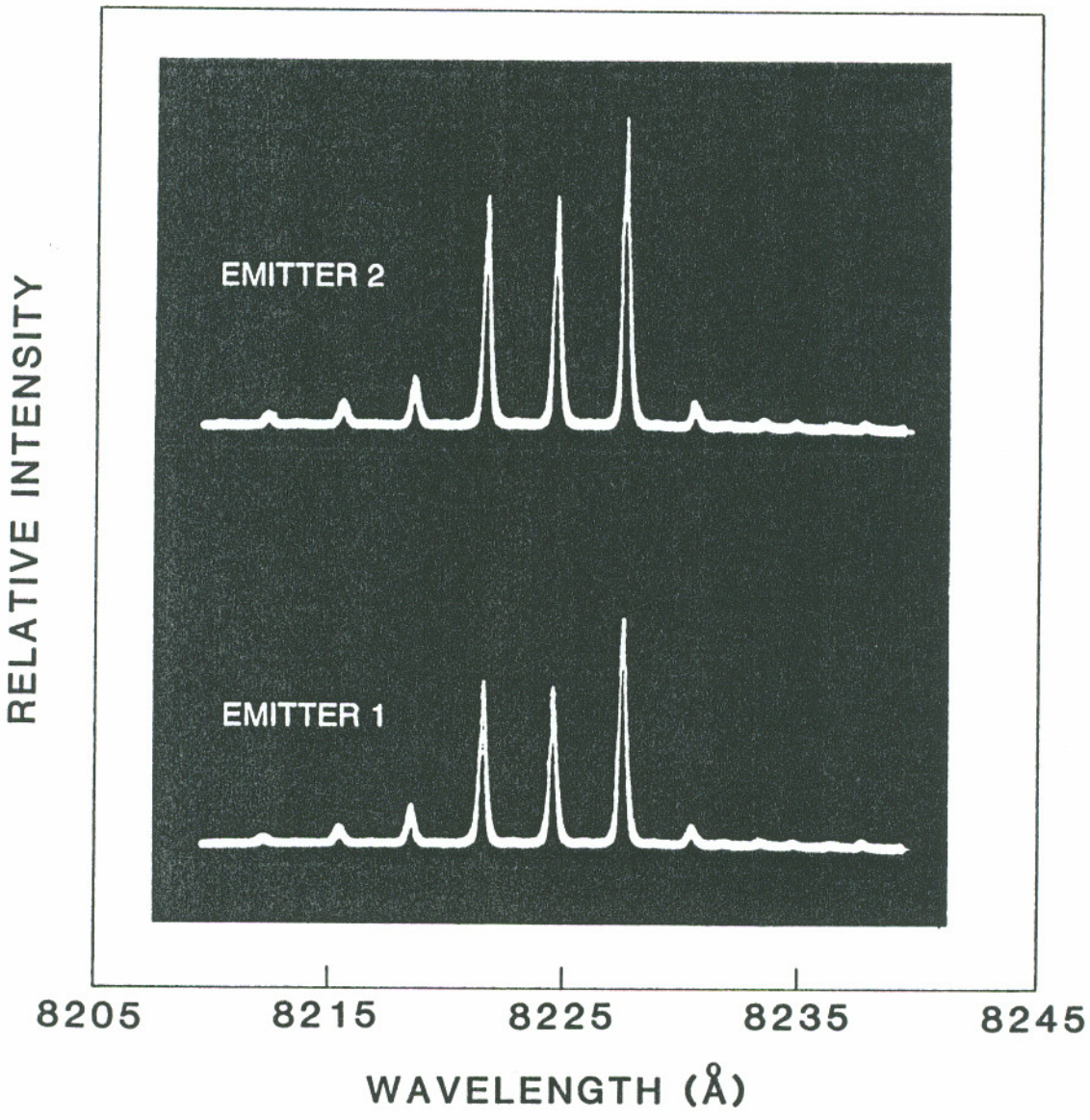

Figure 4.15 The longitudinal mode spectra of the two-stripe gain-guided laser array during CW operation at 1.7 times threshold.

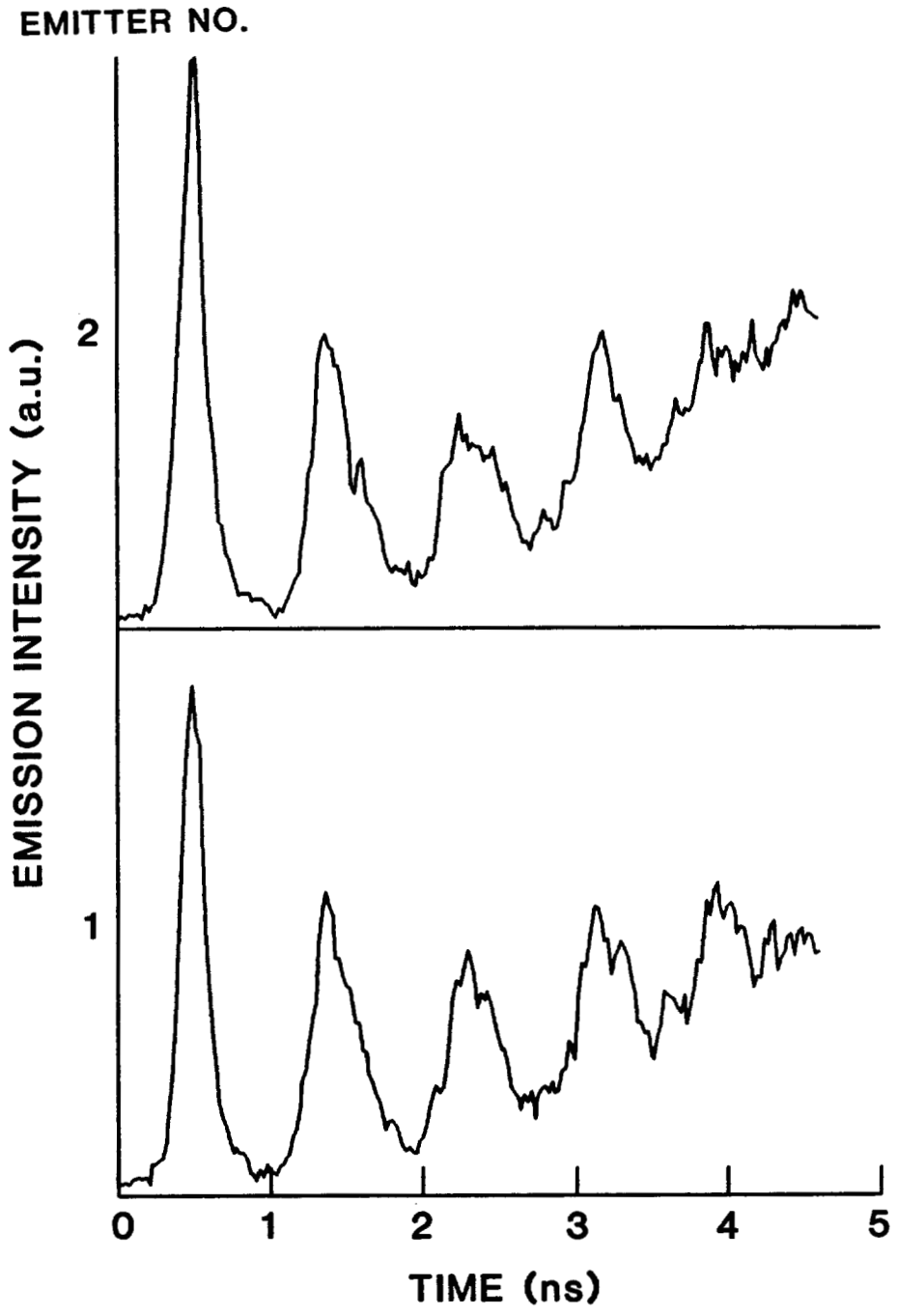

Figure 4.16 The time evolution of the near-field pattern of the two-stripe gain-guided laser array at 1.3 times threshold pulsed operation.

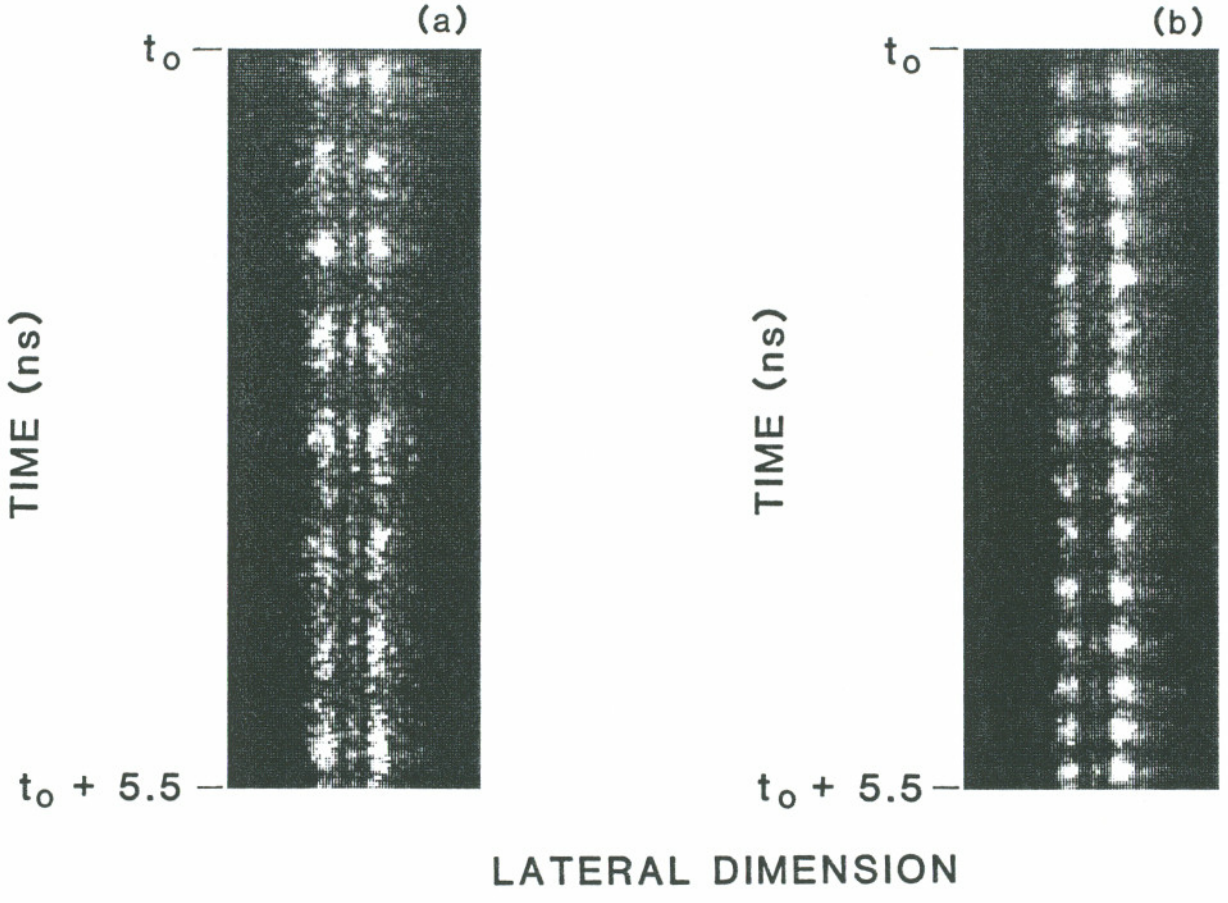

Figure 4.17 Halftone representations of the time evolution of the near-field pattern for the two-stripe gain-guided laser array under CW operation at (a) 1.3 times threshold, and (b) 1.7 times threshold.

Figure 4.18 shows the observed optical output intensities from the two emitters as a function of time. The data were taken when the device was continuously operated at $I = 1.3\ I_{th}$. Undamped, regular spiking is quite pronounced, and the self-pulsations in the output from both emitters are seen to be well synchronized with each other by referring to Figure 4.19 which shows the calculated auto-correlation of the first emitter and the cross-correlation[109] between the first and the second emitters.

Figure 4.20(a) is the power spectrum calculated for the pulsations of Emitter 2 shown in Figure 4.18. It displays a major peak centered at around 1.5 GHz with broadband background. As shown in Figure 4.20(b), the oscillation frequency increased with increasing drive currents, fitting the known relationship between the semiconductor relaxation oscillation frequency and the current overdrive[146].

This pulsation behavior may be used to test the nonlinear dynamic model described in Section 2.3. The model shows that laser arrays are unstable over large regions of coupling constants and injection currents. For two-stripe laser, closed-form expressions for the stability boundaries have been obtained[48]. The Routh-Hurwitz criterion[147] is used to determine the regions in which the steady-state solutions are stable when discrimination in favor of neither of two array modes is assumed, i.e., the coupling coefficient is real for $\eta_I \to 0$. For in-phase operation, the array is stable if

$$\eta > \frac{\alpha p}{1 + 2p}, \tag{4.1}$$

while for the out-of-phase operation it requires

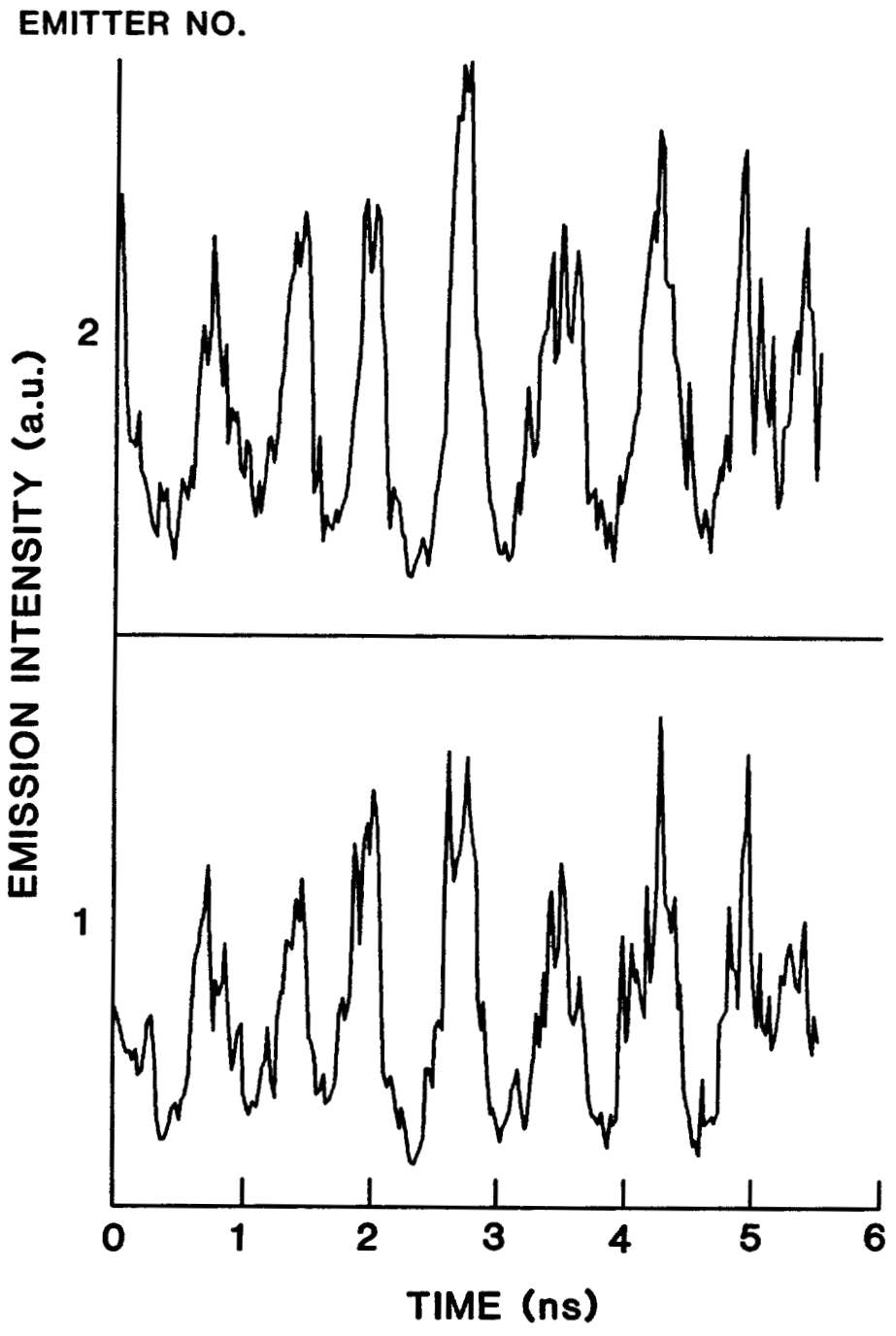

Figure 4.18 The time evolution of the near-field pattern of the two-stripe gain-guided laser array under CW operation at 1.3 times threshold.

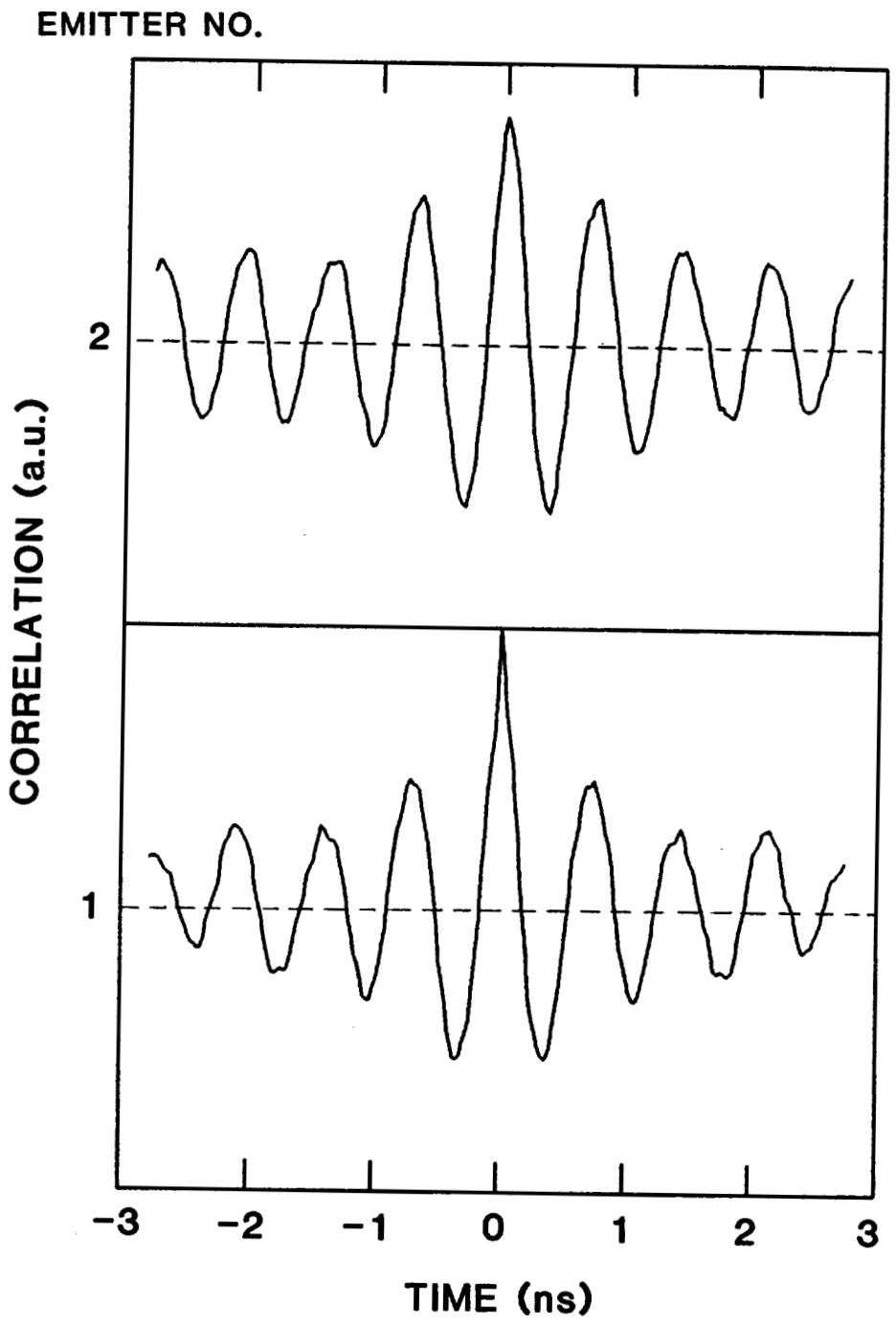

Figure 4.19 The auto-correlation of the first emitter and the cross correlation between the first and second emitters of the two-stripe gain-guided laser array under CW operation at 1.3 times threshold.

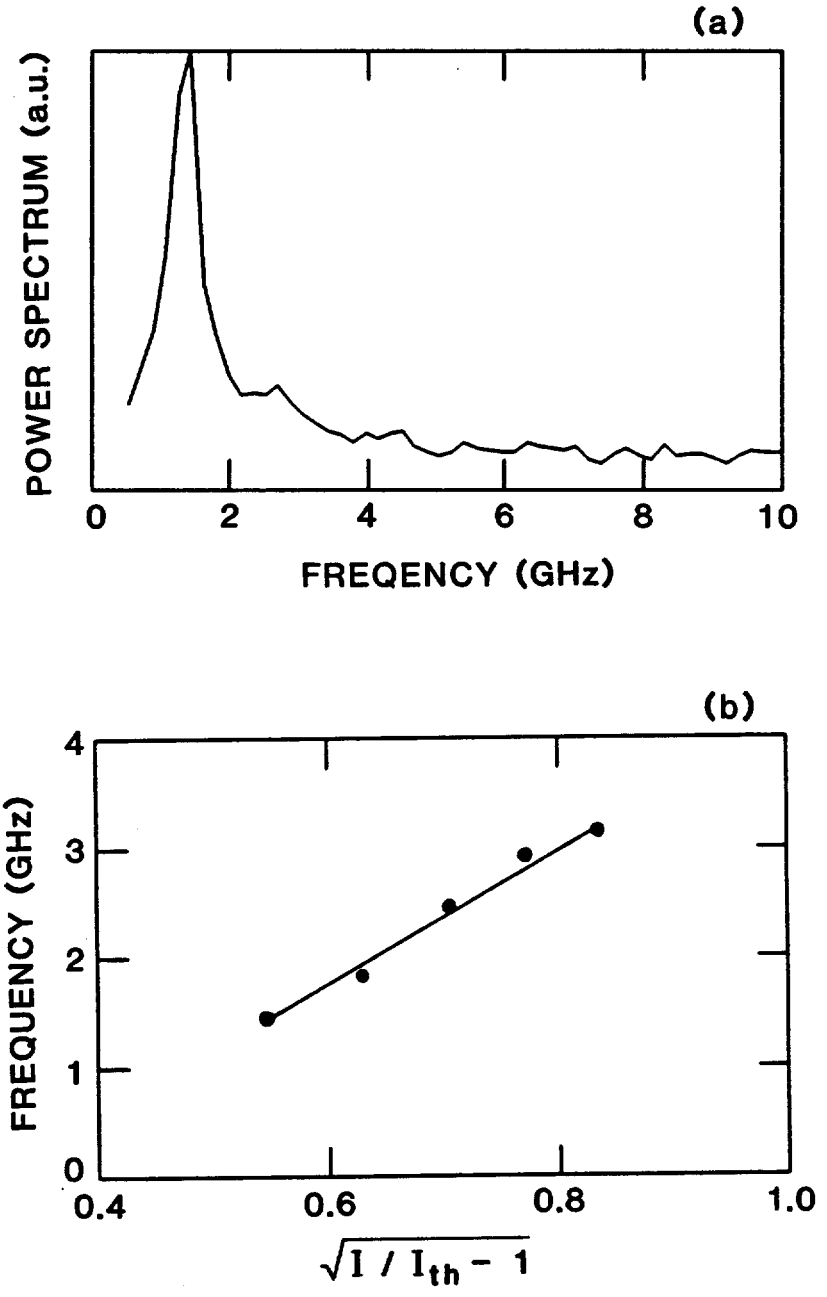

Figure 4.20 (a) The power spectrum for the pulsations of Emitter 2 shown in Figure 4.14(b). (b) The oscillation frequency increased with increasing drive currents.

$$\eta < \frac{(1 + 2p)\tau_p}{2\alpha\tau_s}, \tag{4.2}$$

where the coupling strength is given by $\eta = \kappa v_g \tau_p$, the normalized excess pump current is $p = (1/2)G_N N_0 \tau_p (I/I_{th} - 1)$, and all of the other parameters included here have been defined in Chapter 2.

Figure 4.21 shows the stability diagram which is calculated using our experimental values of those parameters listed in table 4.2 for the two-stripe laser. The region between the two lines is the instability domain. It is thus clear that the phase-locked array is unstable over a wide region in the plane of the variables η and I/I_{th}. In the unstable regime a laser array exhibits sustained oscillations which may be periodic, quasi-periodic, or chaotic[48]. Stability is assured only for very small values of η in which case the two emitters are essentially independent, or for very large values of η, in which case the emitters are so tightly coupled that they act as one. Another key parameter is the α factor which affects the stability boundaries. As indicated by Equation (4.1) and (4.2), the instability domain is reduced with decreasing α values. The operation state of the two-stripe laser under the experimental condition corresponding to Figure 4.18 has been estimated and indicated in Figure 4.21 by the star which falls in the unstable regime near the in-phase stability boundary. In general, when η is large, the pulsation frequency has simply the rate of energy transfer between the stripes[48] with a typic value of tens of gigahertz. However, the observed pulsation frequency of the two-stripe laser is only a few gigahertz which is not at the proper frequency with respect to the real coupling coefficient. This indicates the oscillations are due to some mechanisms such as saturable absorption.

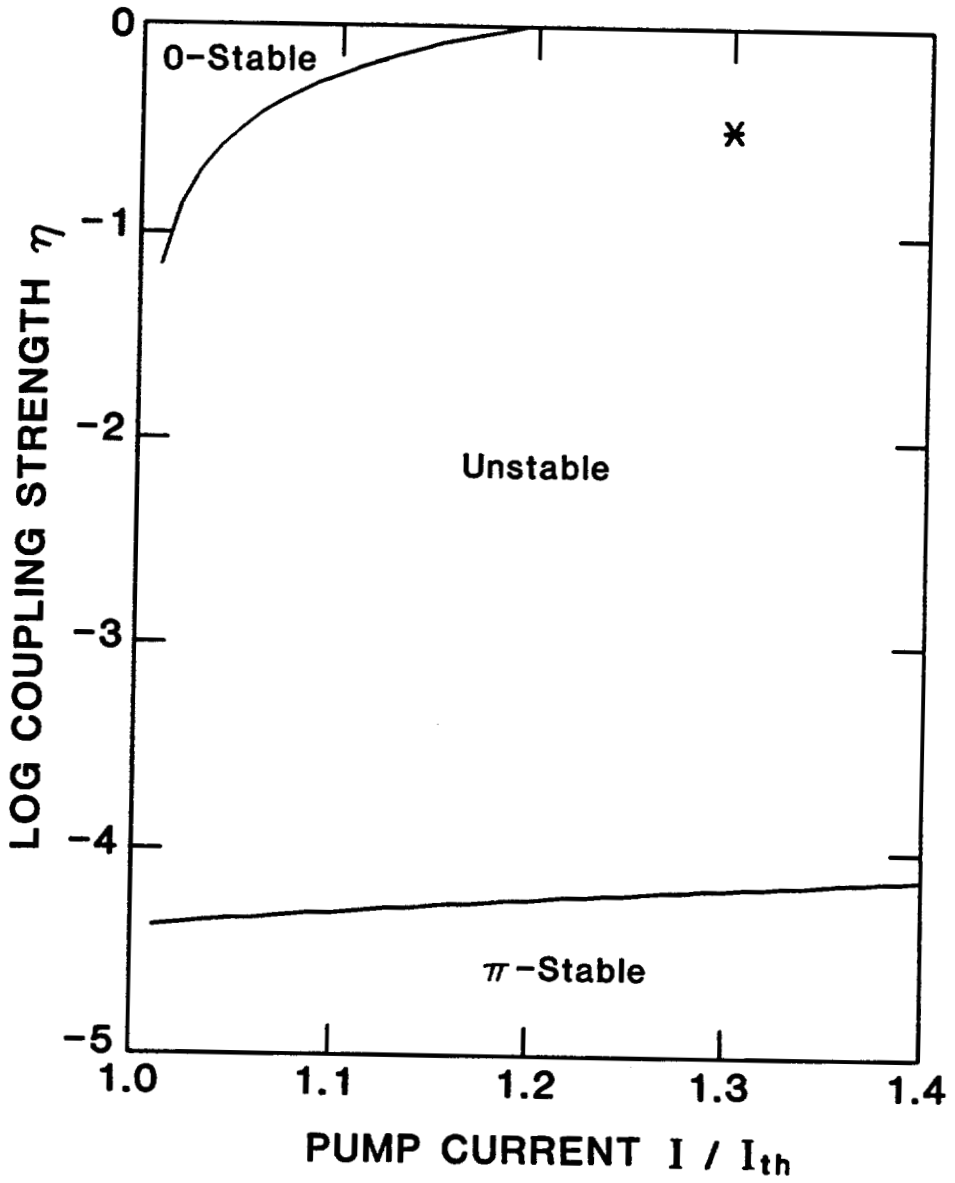

Figure 4.21 The stability diagram in the plane of the coupling strength and the normalized excess pump current.

Since the dominance of one mode in the emission spectrum is usually observed, it is necessary to allow complex coupling coefficient $\eta = \eta_R + i\eta_I$ for adequate modeling of real devices. A new model has extended the stability analysis into complex domain[148] as shown in Figure 4.22 for $I = 1.7I_{th}$. Since $\eta_R < 0$ has not been experimentally observed, the figure is a log-log plot of part of the $\eta_R > 0$ half of the complex η plane. The $\eta_I < 0$ and $\eta_I > 0$ quadrants have been joined at $|\eta_I| = 10^{-5}$, which for all practical purposes can be regarded as the real axis. The $\eta_R > 0$ half-plane is partitioned into three regions according to the linear asymptotic stability of the equilibrium points: in-phase stable, out-of-phase stable and neither stable. This is consistent with the results described in the previous paragraph when $\eta_I \to 0$. The star in this figure indicates the operation state of the array at $1.7\,I_{th}$ and it falls on the in-phase stability boundary.

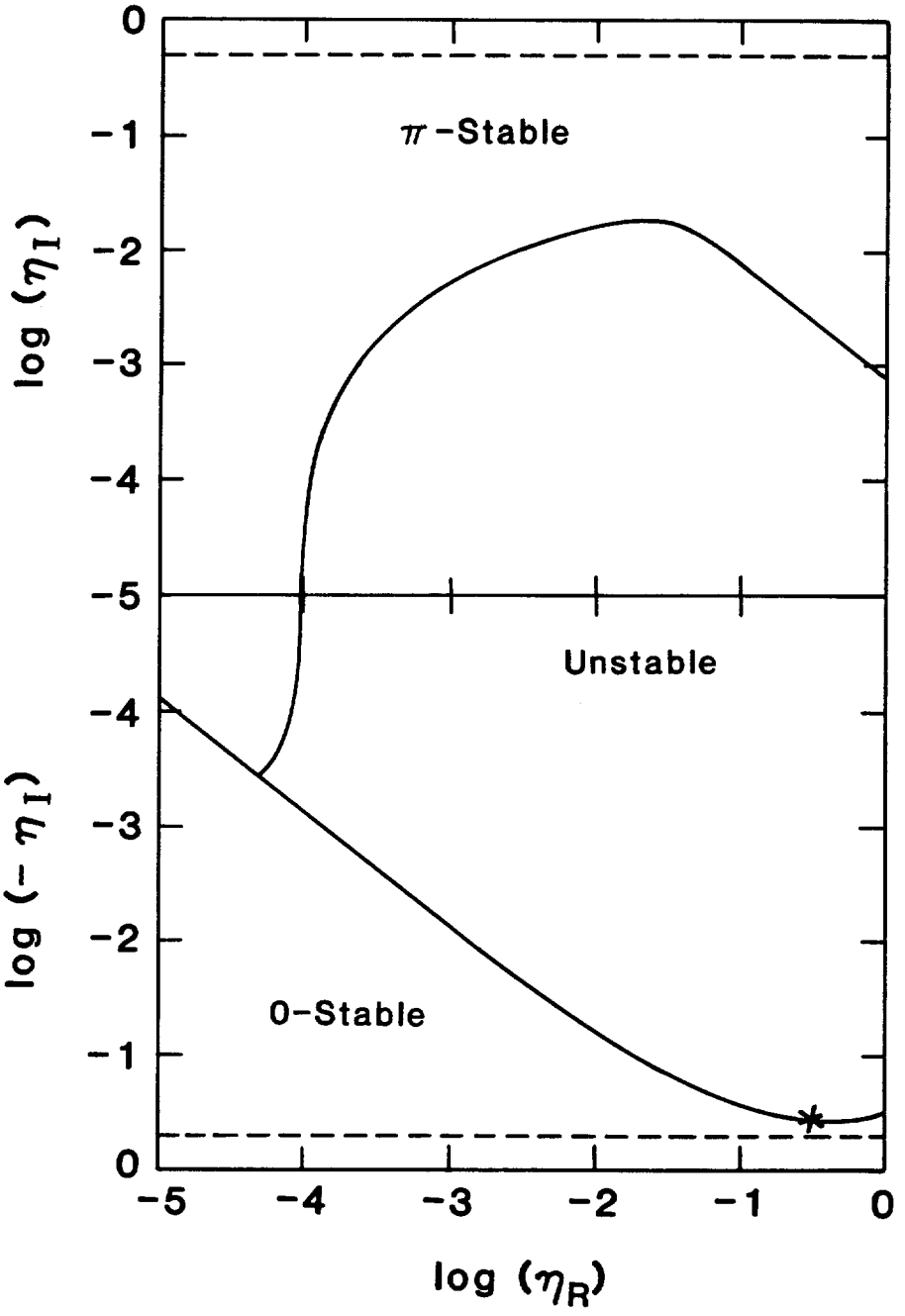

Figure 4.22 The stability diagram in the complex coupling strength plane.

Chapter 5
DYNAMIC CHARACTERISTICS OF INDEX-GUIDED ARRAYS

The lateral mode in gain-guided lasers is determined by the distribution of optical gain along the junction plane. The optical gain is determined by the carrier distribution that is influenced by both current spreading and carrier diffusion in the active region. As discussed in Chapter 4, gain-guided lasers have undesirable characteristics due to their poor beam quality. In index-guided laser structures, the laser structure is modified so as to introduce an effective index step large relative to the carrier-induced variation. Arrays of index-guided lasers have been fabricated, and are intrinsically more coherent and stigmatic than gain-guided devices. This chapter presents experimental characterization of two types of index-guided laser arrays. The devices studied here are a channeled-substrate-planar (CSP) laser array and a flared guide Y-coupled laser (FYCL) array.

5.1 Eight-Stripe Channeled-Substrate-Planar Arrays

The evanescently coupled channeled-substrate-planar array has achieved high-power CW and pulsed phase-locked operation[71]. The frequency response of five-stripe CSP arrays has been measured to be about 2.5 GHz at an output power of 50 mW indicating that they have a potential for high-speed direct

modulation[149,150]. Modeling analysis of widely spaced (7-10 μm center-to-center) CSP arrays by Evans and Butler pointed out that not only was the coupling weak, but that it took only negligible nonuniformity ($<<$ 1% in either gain or geometry) to decouple the array and produce a far-field characteristic of a number of superimposed single lasers rather than of a phase-locked array[151]. CSP arrays fabricated with large center-to-center spacings were experimentally found to exhibit exactly such behavior: i.e., the individual elements were uncoupled. The optical coupling between array elements is stronger in closely spaced CSP arrays resulting in near- and far-field distributions relatively insensitive to small nonuniformities in either gain or geometry. Eight-element CSP arrays fabricated with 4 μm center-to-center spacing have been experimentally demonstrated[151] to be capable of stable, coherent, single-spatial and single-longitudinal-mode phase-locked operation. However, the observation of regular self-sustained pulsations in the output of some such arrays operated under CW conditions has been recently reported[152].

In the following sections, a detailed experimental study[153] on the spatio-spectral and spatio-temporal properties of an eight-element CSP laser array is presented. The closely-spaced CSP array with strong optical coupling between array elements is characterized by a broad-area-laser-like operation in accordance with its spatial mode spectra. The spatio-temporal evolution of the near- and far-field exhibits complex dynamical behavior in the picosecond to nanosecond domain. Operating parameters for the laser device have been experimentally determined.

5.1.1 Device Structure and Performance

The CSP laser array structure used in this work is schematically drawn in Figure 5.1. The wafer was grown[151] by standard liquid-phase-epitaxy multibin techniques, zinc-diffused for current-confined injection through a photolithographically defined oxide stripe that covered the entire array area, contacted with Ti-Pt-Au and Au-Ge on the p- and n-sides, respectively, and facet-coated to produce a high reflectivity of 90% on the back facet and a low reflectivity of 10% on the front facet[154]. Incorporated into the growth was an MOCVD-deposited AlGaAs buffer layer to prevent meltback of the channels, and the use of mesas to ensure a planar growth profile of n-clad over the AlGaAs buffer layer.

The array consisted of eight V-shaped channels with a center-to-center channel separation of 4 μm and it was mounted p side down on a copper heat sink. Scanning electron micrograph (SEM) measurements[155] showed a laser cavity length of 200 μm, an active layer thickness of 0.12 μm and a stripe width of 3.5 μm which is defined by the base width of the V-shape of the channel[156]. Taking into account the 8 elements of the array, the total active volume is given by $V = 6.7\times10^{-10}$ cm^3.

The CW light-current characteristic of the CSP laser array is shown in Figure 5.2 to a power level beyond 100 mW. The threshold currents were 200 mA in the pulsed case and 215 mA in the CW case. Considering that the CSP laser array was facet-coated to produce reflectivities of $R_1 = 90\%$ on the back facet and $R_2 = 10\%$ on the front facet, we have from Equation (3.3.8) a facet loss $\alpha_m = 60$ cm^{-1}. The slope dP_{out}/dI of the L-I curve shown in Figure 5.2 is 0.6 mW/mA. At the lasing wavelength $\lambda = 8450$ Å, the internal loss α_i was

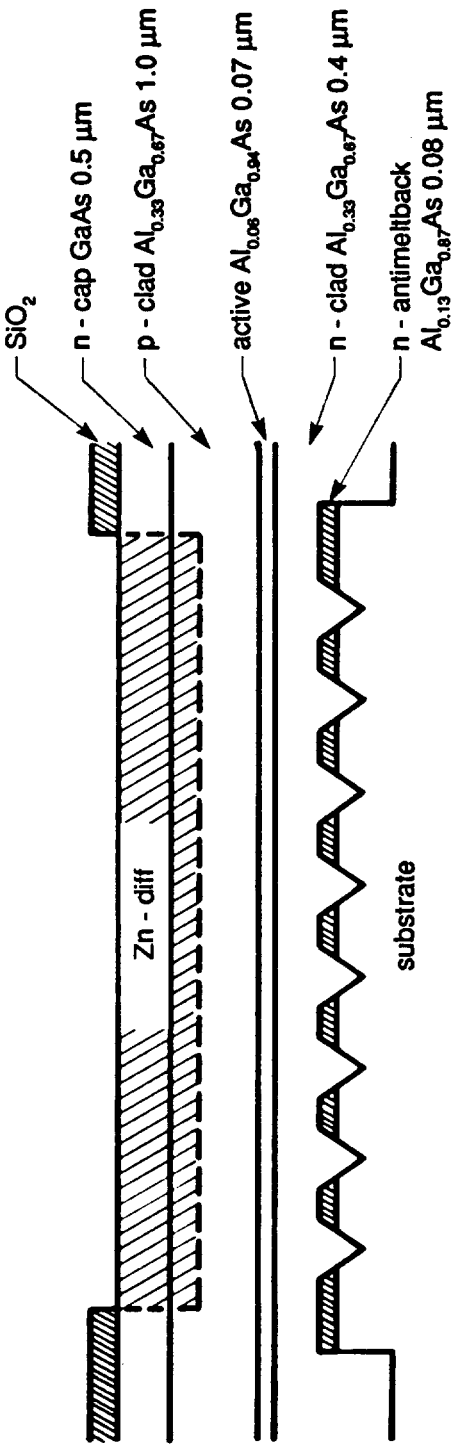

Figure 5.1 Schematic diagram of an eight-stripe CSP laser array.

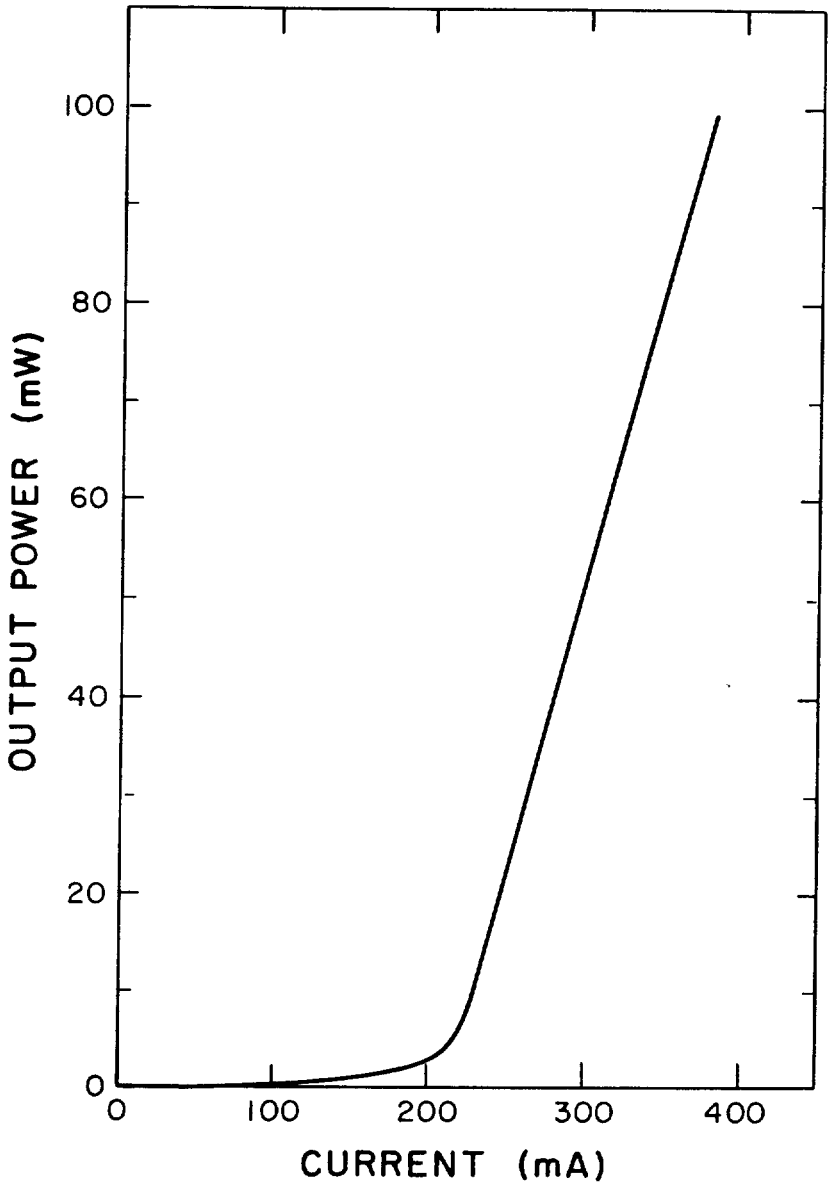

Figure 5.2 The L-I characteristic of the CSP laser array in CW operation.

calculated, using Equation (3.3.11), to be 82 cm^{-1}. Then the total loss $\alpha_t = \alpha_m + \alpha_i$ in the laser is 142 cm^{-1}. The beam divergence angle in the transverse direction was measured to be 35.1° with the technique described in Section 3.3.3. For the measured wavelength the spot size at the laser end facet was determined to be 0.44 μm. Using Equation (3.3.3), the confinement factor Γ was calculated to be 0.22. Therefore, Equation (3.3.12) gives the gain at threshold g_{th} = 645 cm^{-1}. The group index n_g = 4.5, calculated from the measured longitudinal mode spacing $\Delta\lambda$ = 4 Å and using Equation (3.3.6) yields a photon lifetime of τ_p = 1.1 ps when substituted into Equation (3.3.13). Figure 5.3 shows the measured delay time between the input pulse and output light pulse as a function of injection current level. From this graph, as described in Section 3.3, the carrier lifetime τ_s is found to be 2.1 ns. The CW threshold carrier density is 4.2×10^{18} cm^{-3} from Equation (3.3.2).

Fabry-Perot resonances were observable in the below threshold spectra of the CSP array down to 120 mA CW. Spectra were recorded at current intervals of 10 mA above this level to 230 mA. Figure 5.4(a) gives the measured wavelength shift for a longitudinal mode due to injected carrier density as a function of current. The shift has been corrected for the wavelength variation due to the increase in temperature with current using a linear heating correction factor of 2.7×10^{-2} Å/mA deduced from the measured wavelength shift above threshold[120,121]. From Equation (3.3.5), the slope -4.2×10^{-2} Å/mA of the line yields a value of -5.2×10^{-21} cm^3 for the carrier-induced index change dn/dN in terms of the carrier density N calculated as a function of current from the measurements of the carrier lifetime τ_s. Figure 5.4(b) shows the net gain dependence

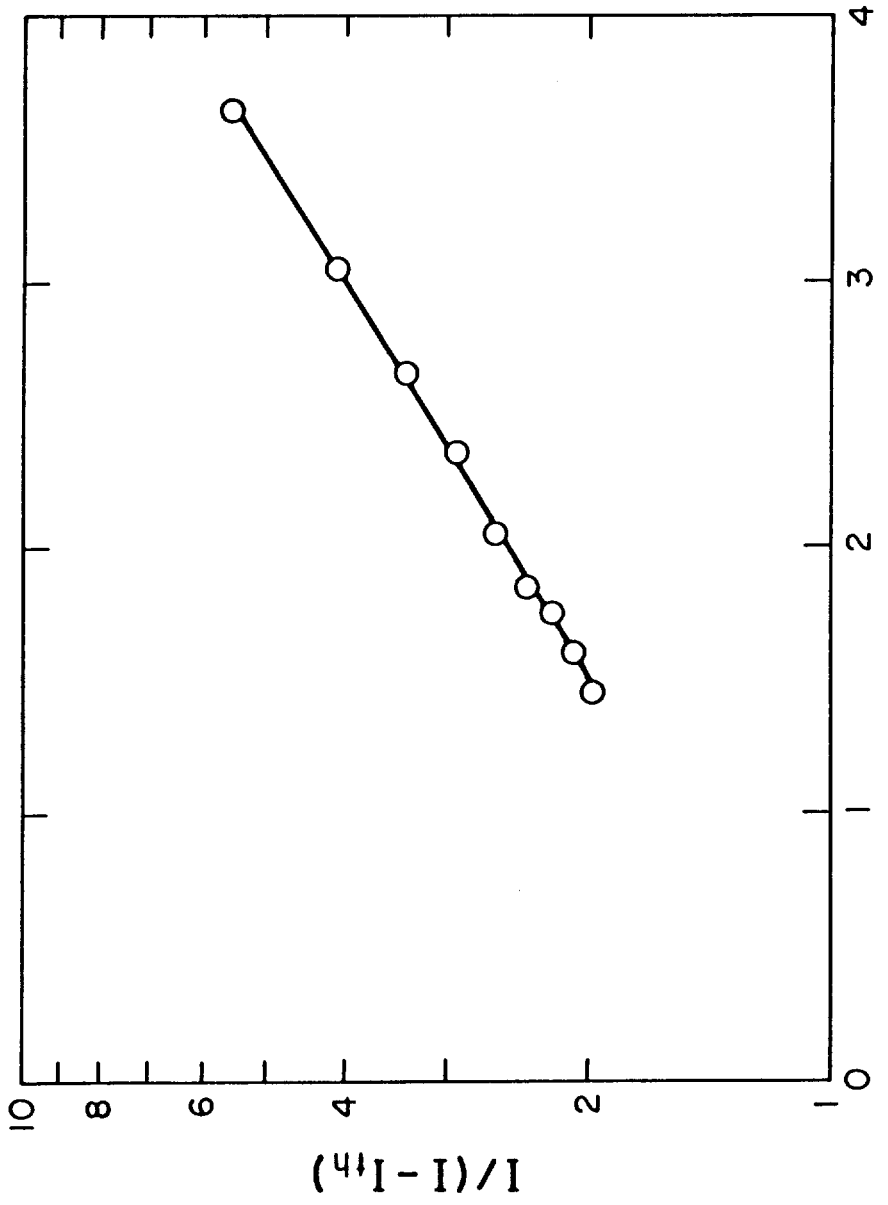

Figure 5.3 The drive current plotted vs laser light output delay for the CSP laser array.

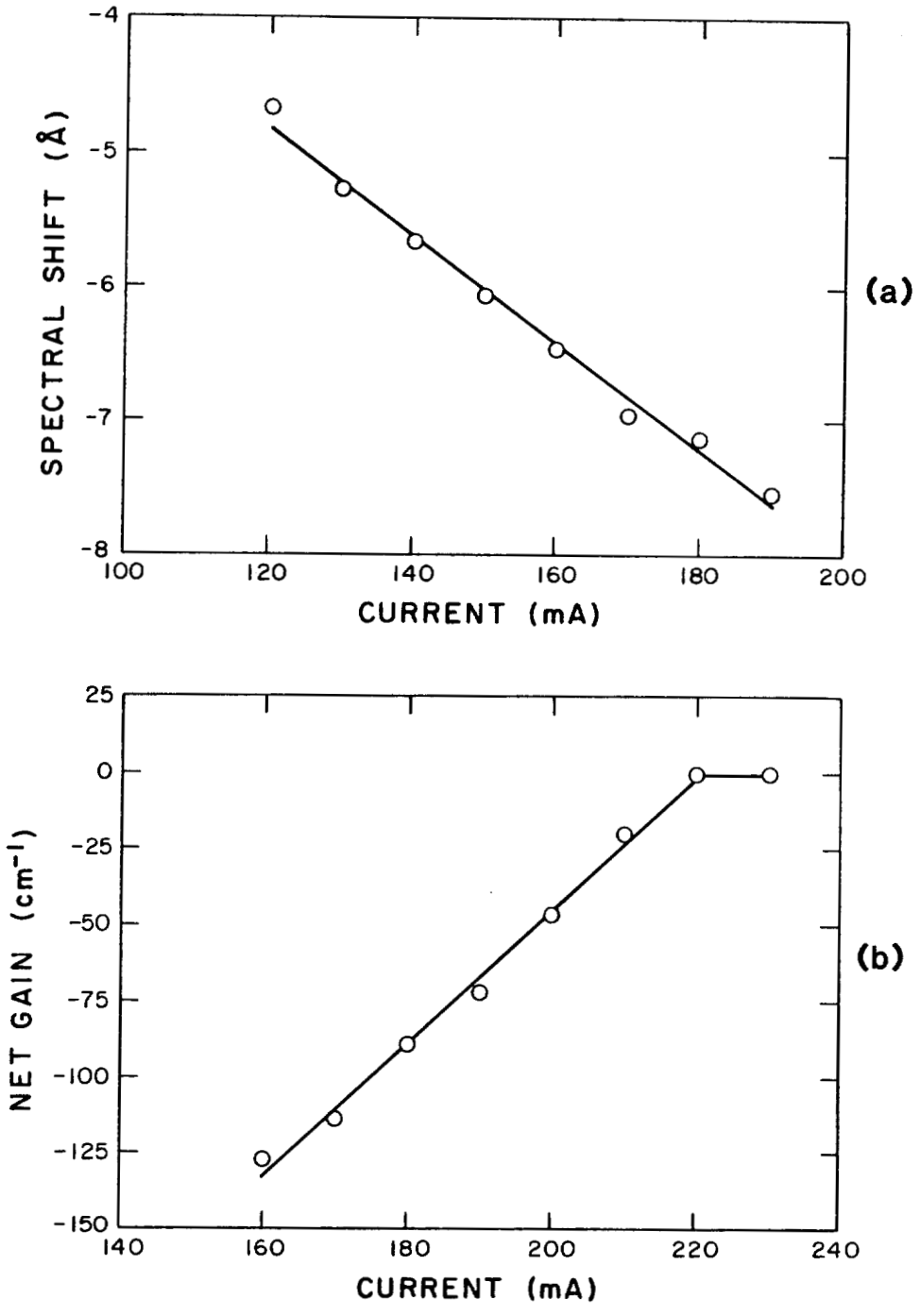

Figure 5.4 (a) Plot of measured wavelength shift as a function of drive current for the CSP laser array. (b) The net gain dependence on current for a wavelength of 8450Å.

on current at a wavelength of 8450 Å. The gain increases as a linear function of the current up to the lasing threshold. The slope dG/dI of the straight line fitted through the data points is 2.18 $cm^{-1}mA^{-1}$. Using the values α_t = 142 cm^{-1}, Γ = 0.22, and the carrier density N calculated as a function of current from the measurements of the carrier lifetime τ_s, we obtain the differential gain $dg/dN = 5.1\times10^{-16}$ cm^2 and the carrier density $N_0 = 2.9\times10^{18}$ cm^{-3}. Using the values of dn/dN and dg/dN at the lasing wavelength, the linewidth enhancement factor α was calculated to be 1.5. We notice that this value is lower than those of conventional CSP lasers. One possible reason for this discrepancy may be due to that this CSP array has a short cavity length (200 μm) which increases the carrier concentration and the lasing photon energy relative to that of the spontaneous emission peak[130]. The gain change and the refractive index change also increase with the increase of the lasing photon energy. However, since the gain change increases much faster than the refractive index change, the linewidth enhancement factor is greatly reduced.

All the parameter values measured for the CSP array are summarized in Table 5.1.

5.1.2 Spectral Properties

Since the CSP laser array under study contains a small emitter-to-emitter spacing (4 μm center-to-center) and small lateral index step[157], the coupling between the array elements may be strong. Strong coupling can blur the distinction between an array and a broad area laser, thus it would be interesting to know if the laser lateral modes are well described by coupled mode theory as

Table 5.1 Parameter Values of a CSP Laser Array

Parameter	Symbol	Value	Unit
Cavity length	L	200	μm
Stripe width	w	3.5	μm
Active layer thickness	d	0.12	μm
Active volume	V	6.7×10^{-10}	cm^3
Group index	n_g	4.5	
Group velocity	v_g	6.7×10^{9}	$cm\cdot s^{-1}$
Confinement factor	Γ	0.22	
Lasing wavelength	λ	8450	Å
Longitudinal mode spacing	$\Delta\lambda$	4	Å
Facet loss	α_m	60	cm^{-1}
Internal loss	α_i	82	cm^{-1}
Carrier lifetime	τ_s	2.1	ns
Photon lifetime	τ_p	1.1	ps
Threshold carrier density	N_{th}	4.2×10^{18}	cm^{-3}
Carrier density to reach zero gain	N_0	2.9×10^{18}	cm^{-3}
Gain at threshold	g_{th}	645	cm^{-1}
Gain derivative	dg/dN	5.1×10^{-16}	cm^2
Index derivative	dn/dN	-5.2×10^{-21}	cm^3
Line-width enhancement factor	α	1.5	

shown for the ten-stripe gain-guided array in Chapter 4 or resembles that of a broad area laser. To investigate this question, the spectral properties of the CSP laser array were examined by spectrally resolving its near-field patterns. The time averaged spectra of the CSP laser were measured during both CW and pulsed (50 ns wide square-wave, 20 kHz repetition frequency) operation for various drive current conditions with a 1.26 m spectrometer used in the first and second diffraction orders.

Spectrally resolved near-field patterns of the laser under pulsed conditions are shown in Figure 5.5. The laser exhibited multimode operation with three dominant longitudinal modes centered at 8450 Å. The longitudinal modes of the laser cavity are separated by 4 Å and each one has a family of lateral modes separated by approximately 0.5 Å. Figure 5.5(a) shows the spectrally resolved near-field at 1.1 times threshold current. Three lateral modes of the individual longitudinal modes can be seen in the figure. It should be noted that the fourth order mode has the lowest threshold. Here the order number of a lateral mode refers to the number of peaks in its near-field. By increasing the drive current, higher order lateral modes were observed successively at shorter wavelengths. Seven spectrally broadened lateral modes are displayed in Figure 5.5(b) for 1.4 times threshold current and up to eight modes were observed at higher drive currents. The spectral broadening of these lateral modes with an increase in the pulse current, as shown by comparison of Figures 5.5(a) and (b), is due to thermally induced frequency chirping. The intensity profiles of the lateral modes corresponding to one longitudinal mode in Figure 5.5(b) are shown in Figure 5.5(c). Note that the lobes of these array modes, except in the case of the mode

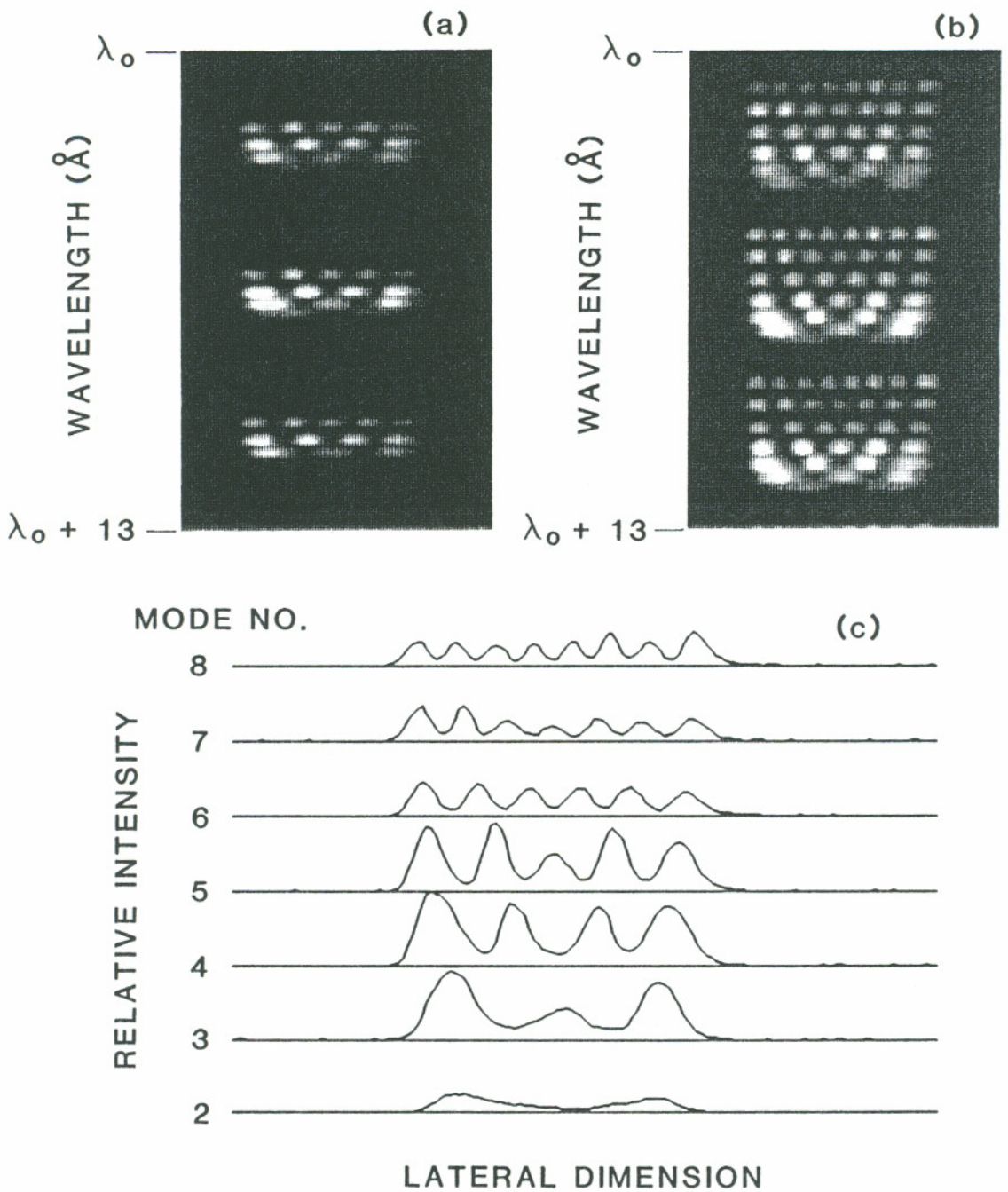

Figure 5.5 Spectrally resolved near-field patterns of the pulsed CSP laser array, (a) at 1.1 times threshold, (b) at 1.4 times threshold. λ_0 is approximately 8443Å. (c) The intensity distributions of the lateral modes for one longitudinal mode at 1.4 times threshold.

number eight, do not correspond to the location of the individual laser emitters, and the center lobes of the third-order and higher modes are less intense than the outer lobes, which is qualitatively similar to a Hermite-Gaussian mode structure. Further, these array modes can not be related to any of the conventional super-modes predicted by the coupled-mode theory[39,96]. This lateral-mode behavior may be explained in terms of a broad-area mode-coupling model[158] which considers the array as a broad-area laser perturbed by temperature effects and periodic index modulation. A temperature increase toward the center of the junction in a diode laser array[159,160] induces a refractive index change[161] with parabolic distribution across the array[160] which influences the lateral mode structure. Once the thermally induced index variation becomes dominant, the parabolic refractive-index profile gives rise to Hermite-Gaussian spatial modes[162]. Therefore, according to its spectral properties this CSP laser array operates as a broad area laser rather than a series of coupled waveguides.

Figure 5.6(a) and 5.6(b) show, respectively, the spectrally resolved near-field patterns and their intensity profiles at 1.4 times threshold current under CW operation. As shown in the figures, the laser operated in the first- through seventh-order lateral modes with the first- and fourth-order modes having weak intensity distributions. Note that the CW spectral data have a skew-symmetric structure. This is probably caused by an asymmetric thermal effect across the laser array. In the absence of chirping during CW operation, the observed lateral mode linewidth is narrower compared to the pulsed spectra.

The spectrally-integrated time-averaged far-field pattern of the laser are presented in Figure 5.7. In the figure, there are two major lobes separated by 7°

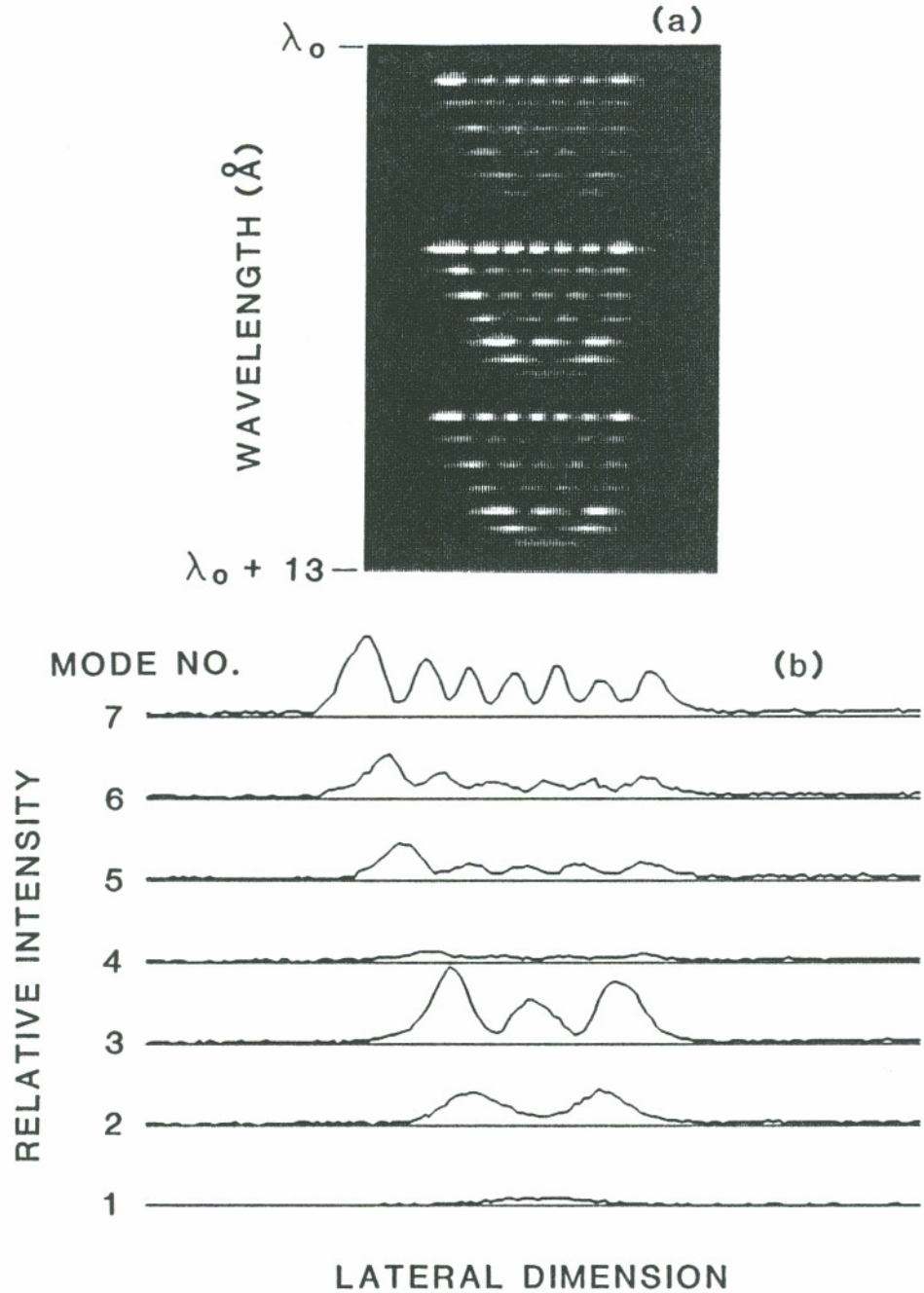

Figure 5.6 (a) The spectrally resolved near-field patterns, and (b) their intensity profiles at 1.4 times threshold CW.

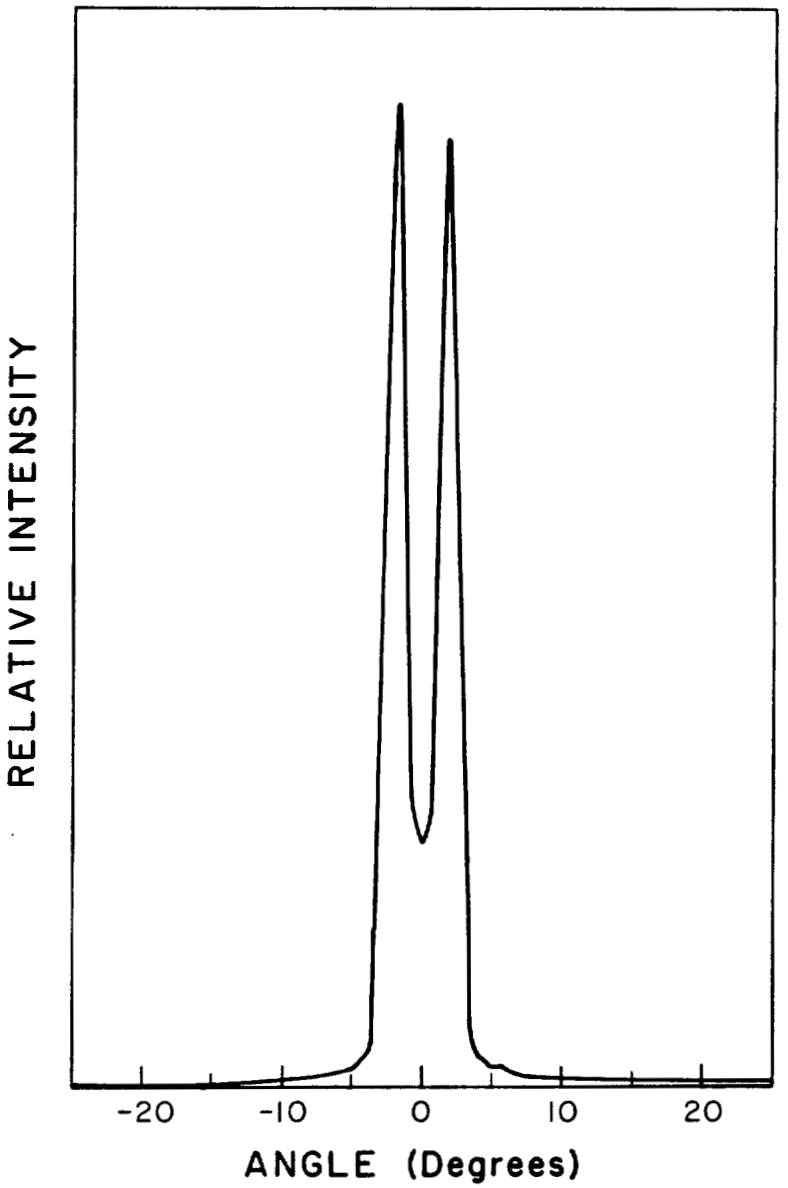

Figure 5.7 Lateral far-field pattern of the CSP laser array.

in the lateral direction, both with full-width-at-half-power (FWHP) of 2.7° which is 1.8 times the diffraction limit due in large part to the fact that the laser operated simultaneously in several lateral modes. This dual-lobed far-field clearly indicates the out-of-phase character of the lateral modes in the near-field which is consistent with Hermite-Gaussian spatial modes[162].

5.1.3 Picosecond Temporal Properties

Figure 5.8 is a halftone reproduction of the time evolution of the near field pattern for the CSP laser array under pulsed operation. The figure is made up of 230 vertical time pixels of 22 ps duration each. For the figure, the laser was pulsed from zero bias with a 280 mA current pulse ($\sim 1.4\ I_{th}$). Note nonuniformity of the lasing emission intensity across the array and the spatial variation in the traces of the inner emitters as they "walk-around" as time progresses. Referring to Figure 5.5, it is evident that these variations were caused by temporal fluctuations of the lateral mode superposition.

Figure 5.9(a) shows quantitatively the time evolution of the intensity of each of the emitters from the same device taken under the same operating conditions as Figure 5.8 and is typical of the CSP laser array at various drive currents. The well-known relaxation oscillations can be seen at the beginning of the pulse. These oscillations decay away after the first 1 ns and there are erratic fluctuations at a much reduced level which persist throughout the rest of the entire optical pulse duration. Figure 5.9(b) shows the intensity emitted from each stripe of the array averaged over 20 events such as that shown in Figure 5.9(a). This average is computed numerically by summation and normalization of the

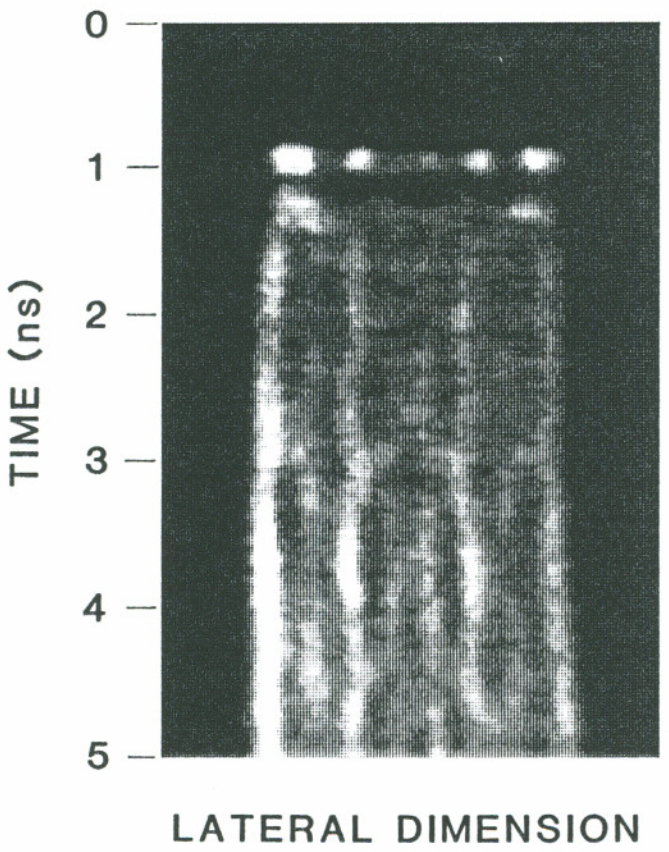

Figure 5.8 Halftone representation of the time evolution of the near-field intensity of the CSP laser array during pulsed operation at 1.4 times threshold at the beginning of the optical pulse.

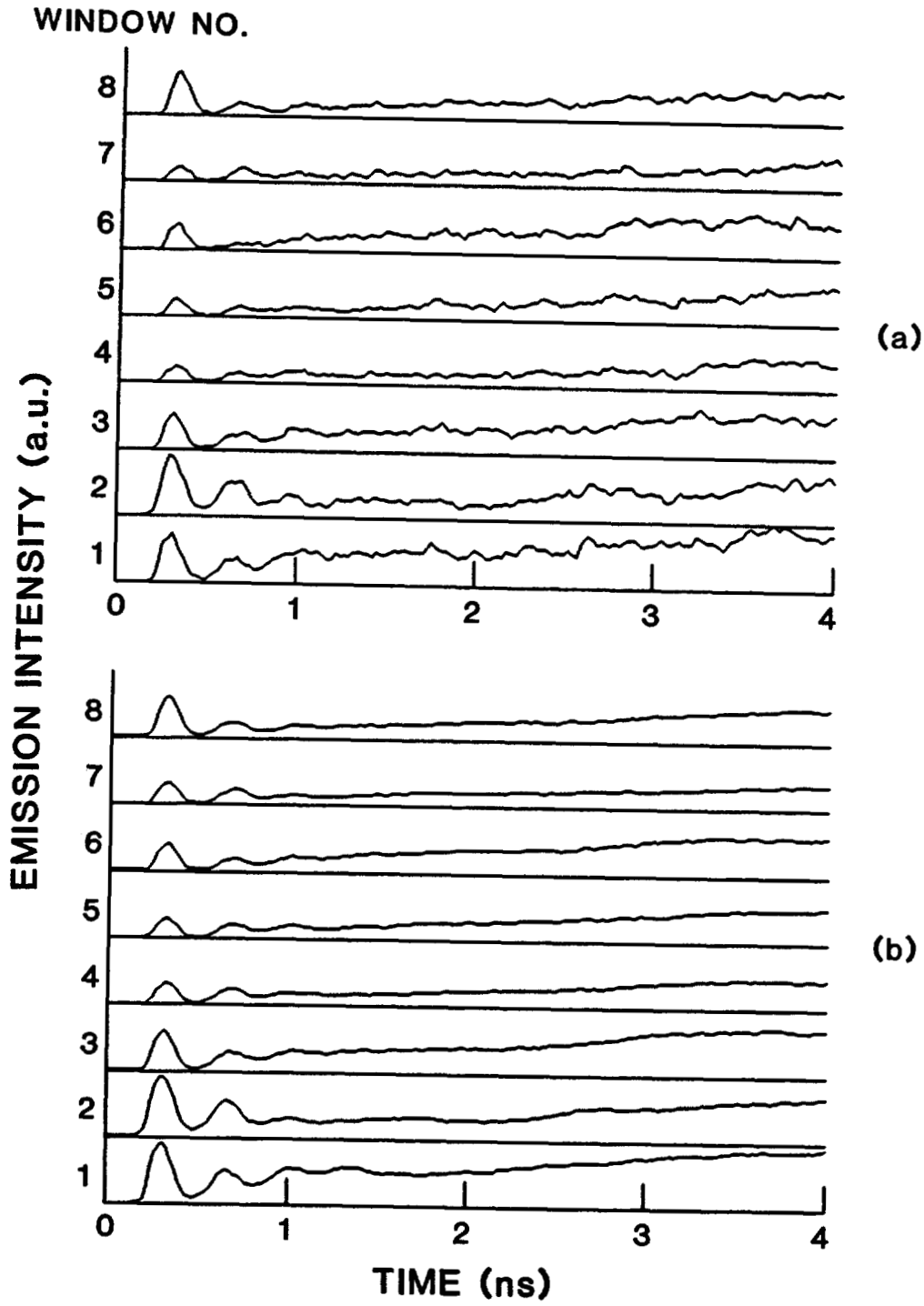

Figure 5.9 (a) Quantitative representation of time evolution of each of the emitters of the CSP laser array during pulsed operation at 1.4 times threshold. (b) Average temporal evolution of 20 such events.

intensity profiles comprising 20 events. It is clear from the figures that the erratic fluctuations are averaged out while the relaxation oscillations add constructively. Similar behavior was observed for gain-guided arrays[41]. Note the gradual increase of the light output at the transient seen in Figure 5.9. Since when the relaxation oscillation decay away after the first 1 ns the injected carrier concentration in the lasing region of individual stripes of the array is lower than that of the region between the stripes, considerable lateral carrier diffusion into the gain region results in additional carriers delivered for stimulated emission[163,164].

Using a discrete Fourier transform (DFT) algorithm, Fourier spectra calculated emitter-by-emitter within each of 20 frames and then averaged and normalized for graphical presentation are displayed in Figure 5.10. For each emitter, the first and second broad peaks represent the relaxation oscillation frequency and its first harmonic. The average relaxation oscillation frequency is approximately 1.6 GHz at a drive current of 220 mA. Figure 5.10 displays a relaxation oscillation frequency of approximately 2.7 GHz at 280 mA drive current.

Figure 5.11(a) shows the time evolution of each of the emitters during CW operation of the same device and is typical of the laser at various drive currents. The streak shown was initiated after the laser had been operating for several minutes at a CW drive current of 300 mA or approximately 1.4 times threshold. It is evident from the figure that the intensity has large erratic amplitude fluctuations. Figure 5.11(b) presents the Fourier spectra calculated in the same manner similar to that in Figure 5.10. The Fourier spectrum is broadband, indicative of optical chaos or noise.

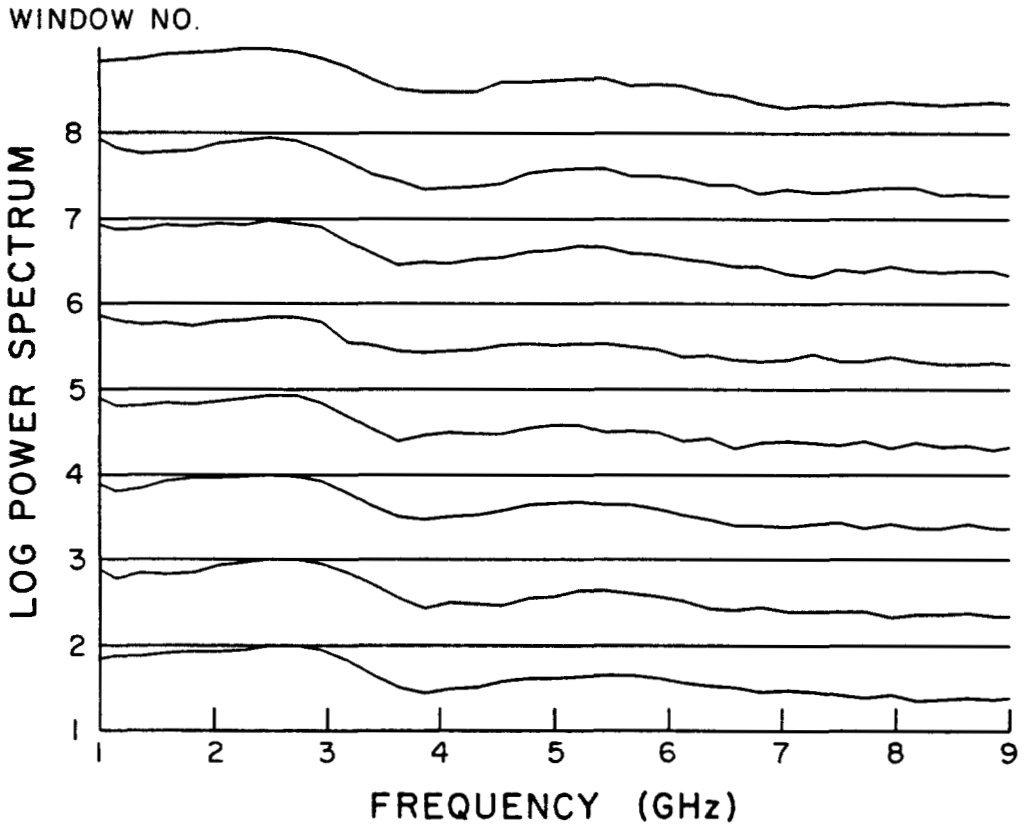

Figure 5.10 Average power spectra for a CSP laser operated with a 280 mA current pulse.

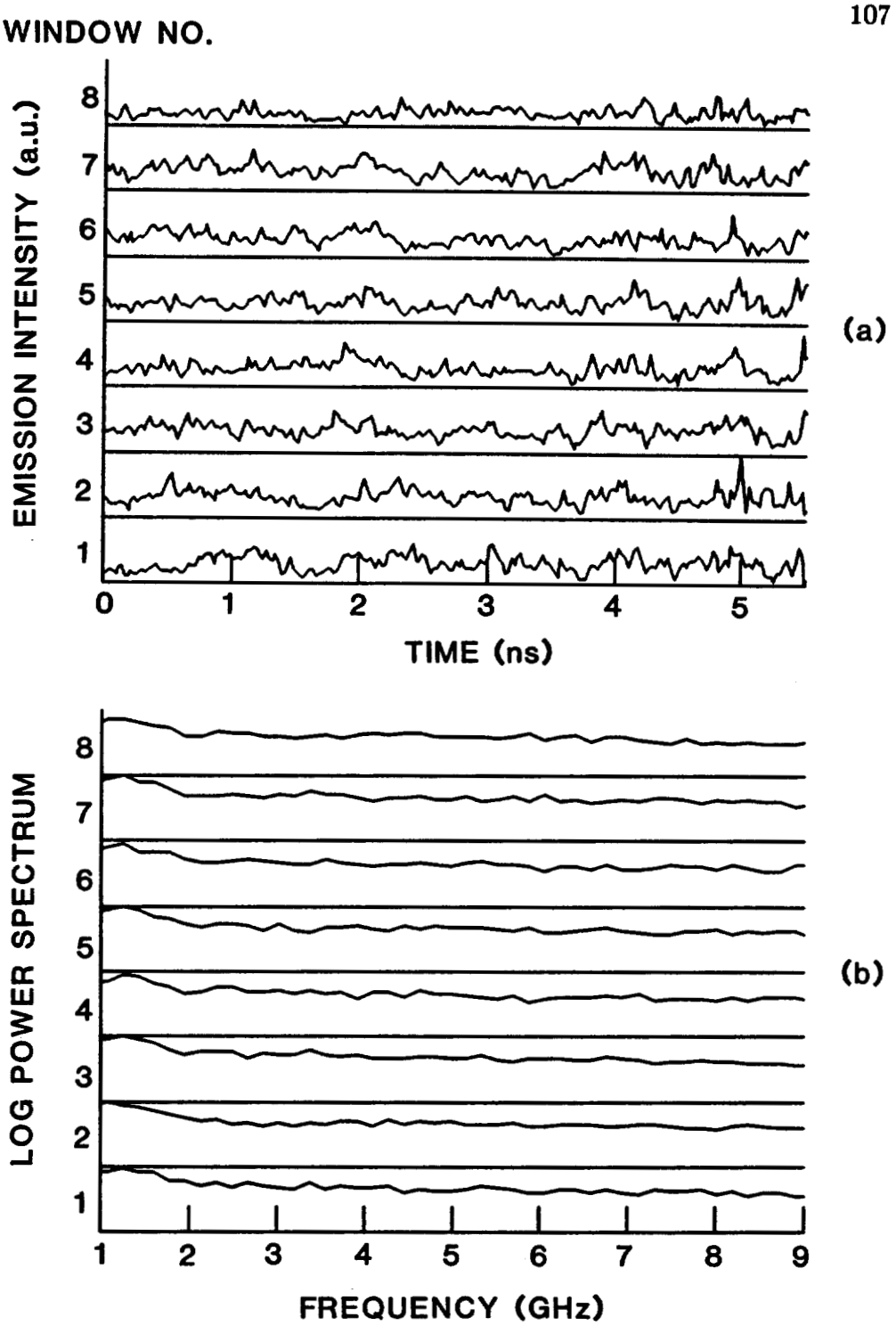

Figure 5.11 (a) Time evolution of each of the emitters during CW operation of the CSP laser array at 300 mA. (b) Average Fourier spectra for the CSP laser array operated at a 300 mA CW drive current.

The time evolution of the lateral far-field of the CSP array was also measured by placing a cylindrical lens with its axis of rotation perpendicular to the plane of the array behind a 20×, 0.4 NA microscope objective to image the array far-field pattern onto the input plane of the streak camera. Figures 5.12(a) through 5.12(d) are halftone reproductions of the time evolution of the far-field patterns for the same laser at pulsed current levels of 1.1×, 1.4×, 1.7×, and $2\times I_{th}$, respectively. These far-field patterns exhibit a variety of dynamic behaviors with regular spiking, beam steering and erratic fluctuation at different drive current levels. This appears to be a consequence of the variation of the lateral mode superposition with time (lateral mode instabilities). Figure 5.13 shows intensity traces of these two lobes for a 20 pulse average at 1.4 times threshold pulsed. The gradual increase of the light intensity at the transient can be seen in the figure. Figures 5.14(a) through 5.14(d) show the Fourier spectra of the measured time evolution of far-field patterns corresponding to those shown in Figure 5.12. The broadband power spectra are general for the CSP laser array and may serve as a indication for chaotic radiation of this device.

In conclusion, the spectral and temporal properties of a CSP laser array with 4 μm center-to-center spacing have been experimentally studied in detail under both pulsed and CW operating conditions. The intensity profiles of lateral modes show a Hermite-Gaussian mode structure which indicates this CSP array is operating as a broad area laser. The near- and far-field temporal evolution of the CSP array has been observed with streak cameras. Under pulsed operation, the optical output exhibited strong relaxation oscillations at the beginning of the pulse and erratic fluctuations throughout the entire pulse duration. The inten-

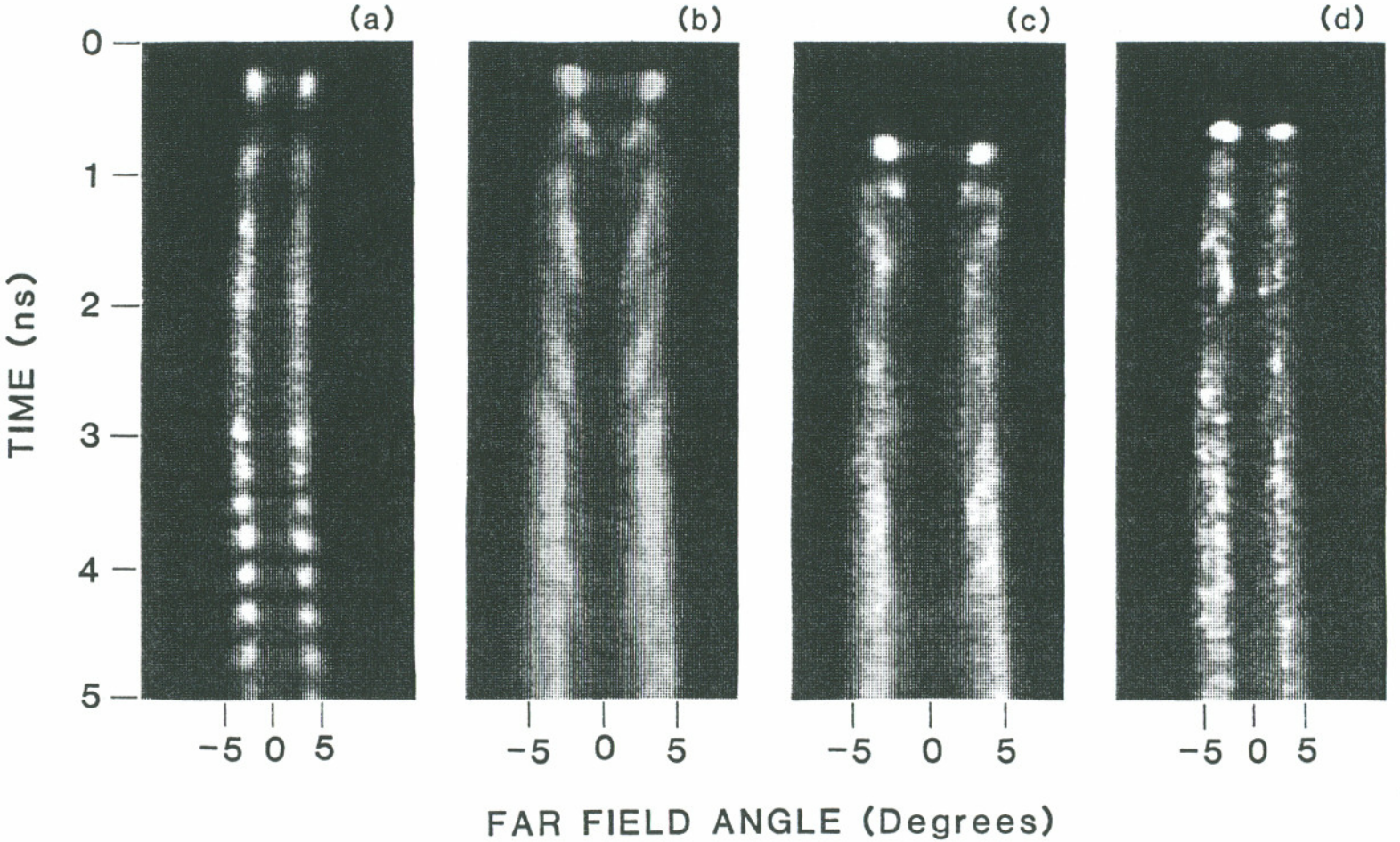

Figure 5.12 Halftone representations of the time evolution of far-field patterns for a pulsed CSP laser array (a) at 1.1×, (b) at 1.4×, (c) at 1.7×, and (d) at $2\times I_{th}$.

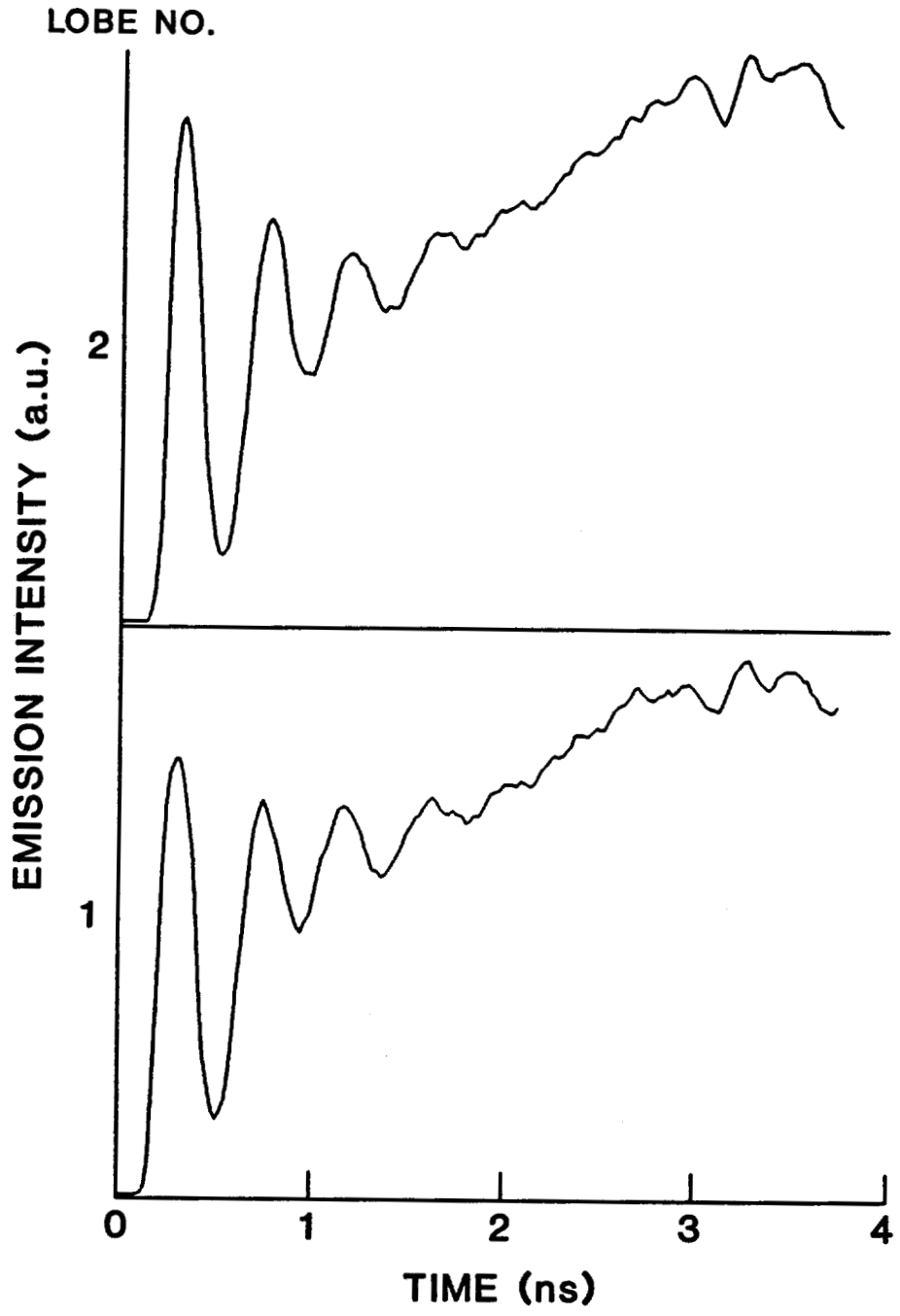

Figure 5.13 Streak traces of a far-field pattern for a 20 pulse average at 1.4 times threshold.

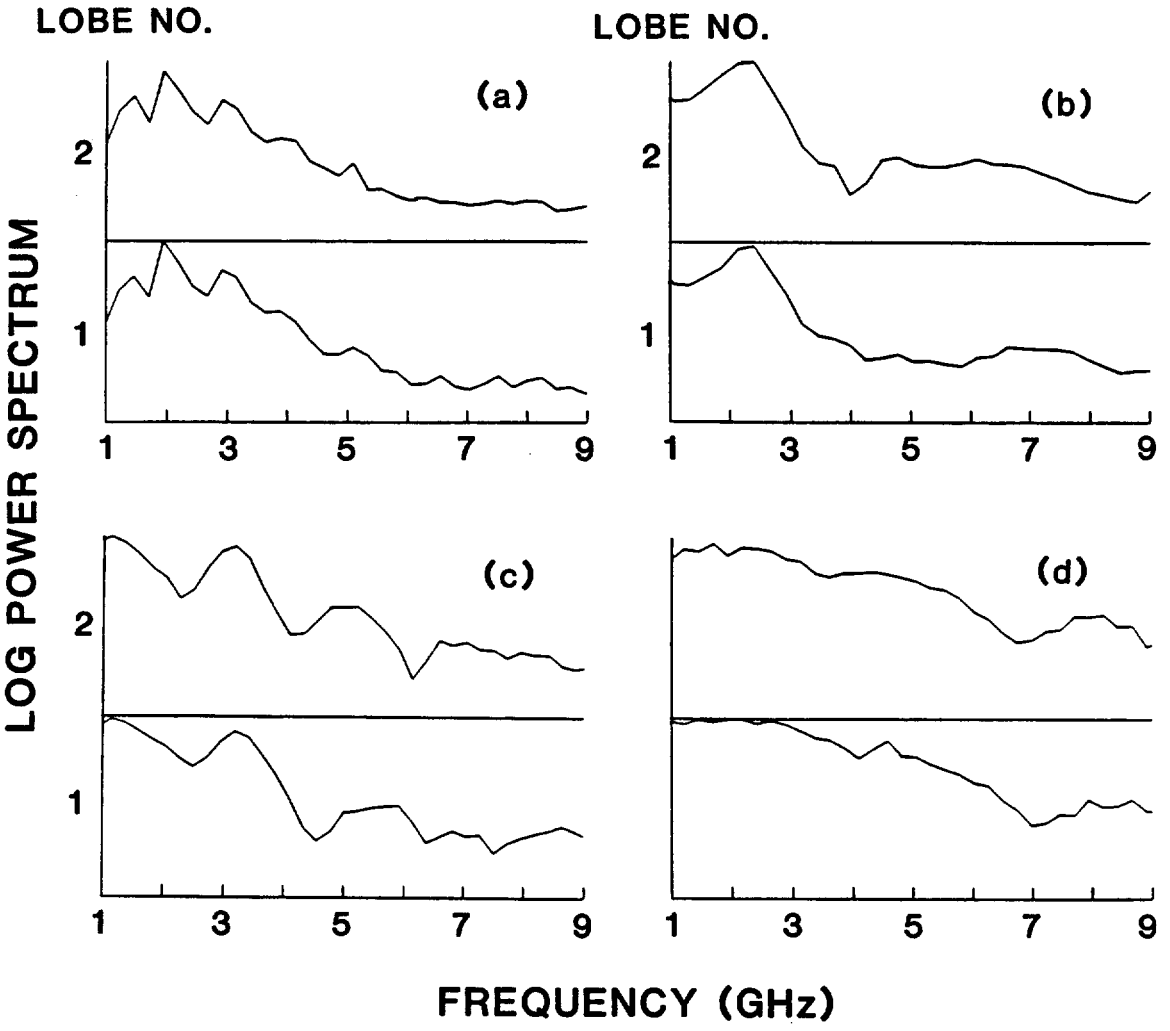

Figure 5.14 Average Fourier spectra of measured far-field time evolution for a pulsed CSP laser array (a) at 1.1×, (b) at 1.4×, (c) at 1.7×, and (d) at $2\times I_{th}$.

sity fluctuation behavior has also been observed during CW operation. Furthermore, device operating parameters have been determined experimentally. The values of these parameters are important for understanding the dynamical behavior of CSP laser arrays and designing devices with optimum characteristics for various applications.

5.2 Ten-Stripe Array with Y-Coupling

Evanescently coupled laser arrays typically select several higher-order array modes for which adjacent stripes are out-of-phase[63,71]. This limits spatial coherence of the output radiation, so that the lasers generally do not radiate in a single diffraction limited lobe. Even when in-phase operation has been achieved, other array modes emit simultaneously above threshold due to spatial hole burning as a result of the poor overlap of the optical wave with the lateral injected charge distribution[74,165]. *Y*-coupled laser arrays designs which were proposed by Scifres *et al*[84]. and more recently by Chen *et al*[166]. have recently been implemented with real refractive index guided lasers grown by both liquid phase epitaxy (LPE)[79,167] and metalorganic chemical vapor deposition (MOCVD)[86,87,168]. Such structures provide strong discrimination against out-of-phase field components, resulting in far-field patterns corresponding to in-phase near-field emission[169,170]. In the *Y*-junction arrays, the array mode exploits all the injected charges equally, except in the outermost guides. Thus no excess charge should remain to encourage other array modes to begin oscillating with increased pumping.

Interest in flared waveguide Y-coupled laser arrays has been spurred by the observation that they exhibit quasi-instantaneous (< 20 ps) phase-locking[42] upon the initiation of lasing action. Recent experiments have also shown that these devices exhibit far-field beam steering[42] during pulsed operation, regular sustained self-pulsations during both CW[43,171] and pulsed[44] operation and near diffraction limited output in an external cavity[94]. In this work, spatio-spectral and spatio-temporal properties of flared waveguide "Y" coupled laser arrays are investigated in both CW and pulsed operation. In each case, regular sustained self-pulsations at multigigahertz frequencies are exhibited. Destabilization of phase-locking, caused by amplitude-phase coupling, is thought to be the origin of the pulsations.

5.2.1 Flared Guide Y-Coupled Laser Arrays

Y-coupled arrays consist of parallel buried-heterostructure waveguide lasers interconnected in a particular fashion. Real-refractive-index differences are usually used to support only a single mode in the waveguides and they are not evanescently coupled along their lengths as in more conventional arrays but rather couple exclusively at Y-junctions. The waveguide and junction pattern is shown schematically in Figure 5.15. The light is coupled and then split between adjacent emitters resulting in a high degree of communication between the elements. The modal discrimination results from constructive and destructive interference in the Y-junction[172]. When the waves in the individual index guides are in phase, they combine constructively. However, if the waves are out of phase, they destructively interfere, and the light is radiated out of the waveguide.

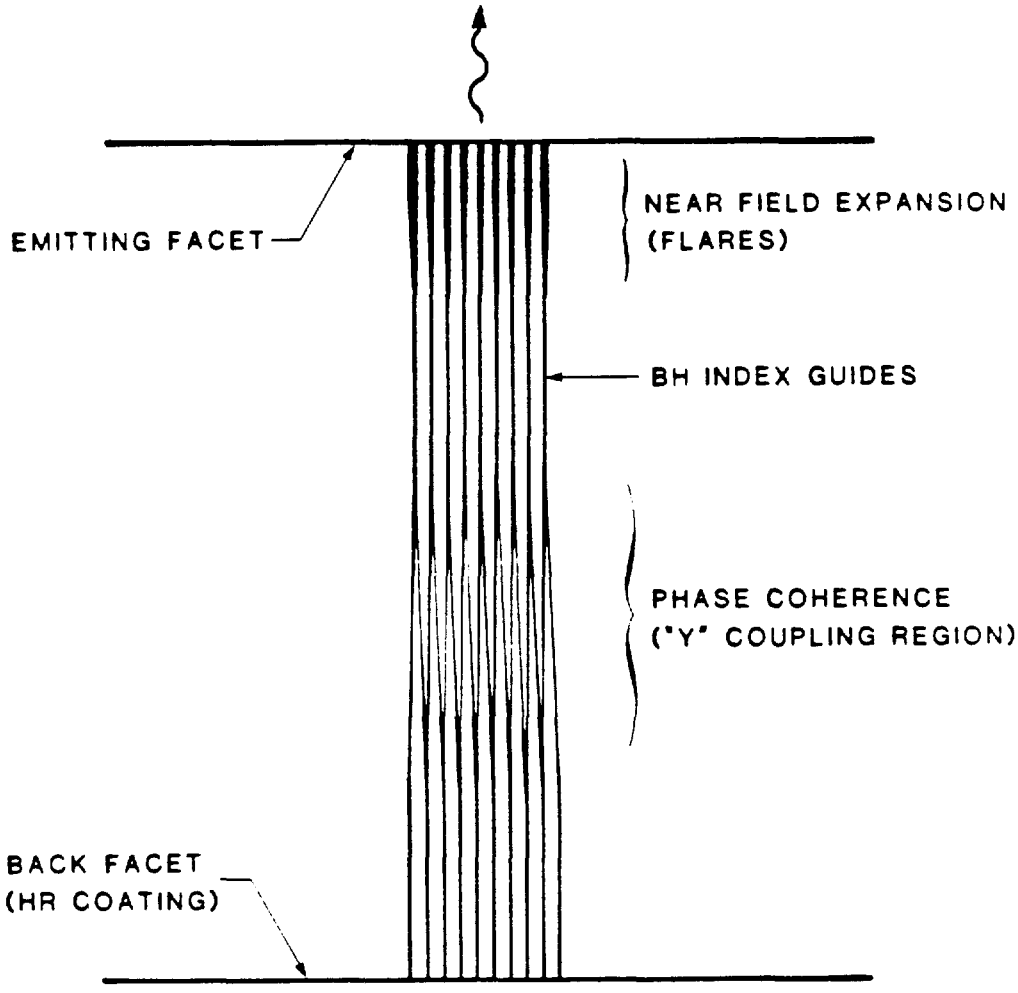

Figure 5.15 Schematic diagram of waveguide pattern of a flared *Y*-coupled laser array.

By virtue of the Y-junction, the mode that operates with all the emitters in-phase experiences the highest gain and will radiate at threshold, generating a predominantly single-lobe output beam up to substantial power levels[86]. The waveguides may be expanded or flared at the facet to enlarge the near-field spot size of individual emitters without supporting higher-order waveguide modes[173]. As a result of the flared waveguide, Y-couple arrays have achieved a near-field "fill factor" of greater than 80% with 70% of the optical power concentrated in a central far-field lobe.

The flared waveguide Y-coupled laser (FYCL) array used in this work was a ten-emitter buried heterostructure real refractive index Y-junction laser array grown by a two step MOCVD process[168]. The first series of layers, which includes the active layer and part of the p-cladding layer, were grown, and the wafer was removed from the reactor. After etching the Y-coupled lateral index guide structure in the wafer, additional cladding and contacting layers were then grown in a second MOCVD process. After n- and p-side metallization were deposited, the wafer was cleaved and the back facet coated for high reflectivity. The stripe period was 6 μm and the flare width was 4 μm, while the straight waveguides were 1.5 μm wide. The uniformity of the near-field intensity is excellent as shown in Figure 5.16. This indicates that there is a strong overlap of the in-phase array mode with the injected charge profile.

5.2.2 Spectral Properties

The average spectral properties[44] of the FYCL arrays were measured during CW operation with a SPEX 1269 spectrometer used in the first through third

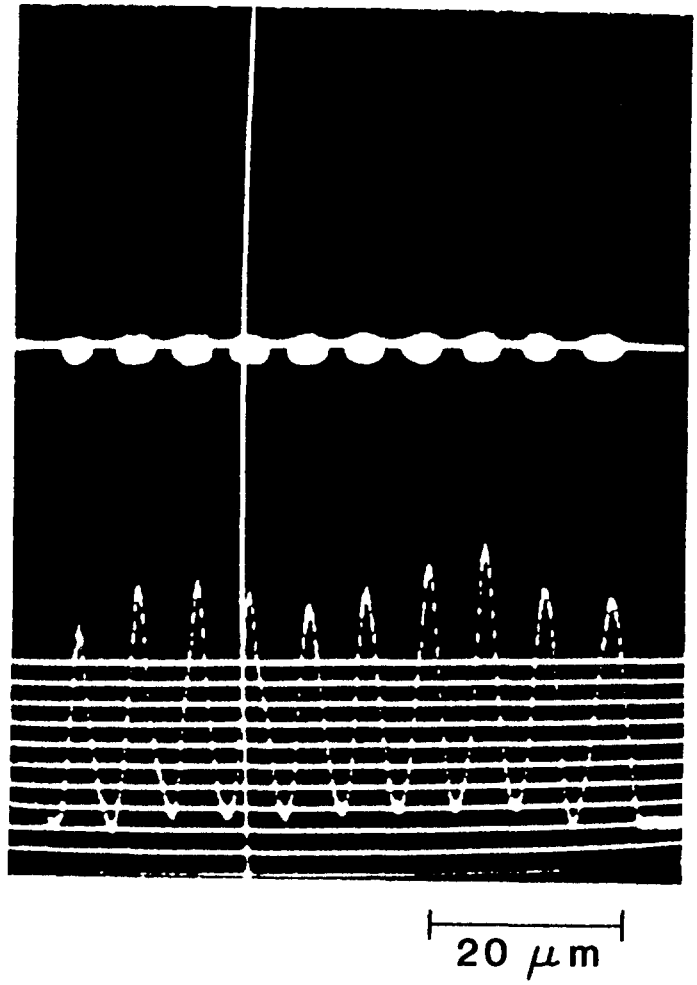

Figure 5.16 Near-field pattern of the Y-coupled laser array.

diffraction orders. Figure 5.17 shows the low resolution spatio-spectral properties of the device during CW operation at 1.6 times threshold. The spectral properties shown in the figure are qualitatively similar to those in reference (94). From the figure it may be seen that the FYCL array exhibits multiple longitudinal mode operation with an average mode separation of approximately 2.6 Å. While each of the emitters has approximately the same total optical output, emitters 1, 2 and 3 show nearly single longitudinal mode operation while 4 through 10 have decidedly multimode operation. Since coupling between widely separated segments decreases as the exponent of the number of intervening Y junctions[172], it becomes more difficult for a large number of segments to lock. The low resolution results depicted in Figure 5.17 do not show transverse mode splitting in the wavelength domain. This is to be expected for an ideal Y-guide array of identical emitters since transverse modes of such an array are known[172] to be energy degenerate. However, since actual Y-coupled laser array guides are only nearly identical, some broadening of the longitudinal mode is to be expected.

It is evident from Figure 5.18 that this is indeed the case. The Figure shows a high resolution spectral measurement of the dominant mode of emitter 1 at the same drive level above threshold as in Figure 5.17. The line has a width of about 0.6 Å and exhibits strong sidebands and a pronounced dip at the center. The substantial linewidth and the asymmetric sidebands are suggestive of the presence of considerable amplitude and phase modulation. To confirm the presence of amplitude modulation, direct measurements of the temporal evolution of the array output were undertaken under both pulsed and CW conditions.

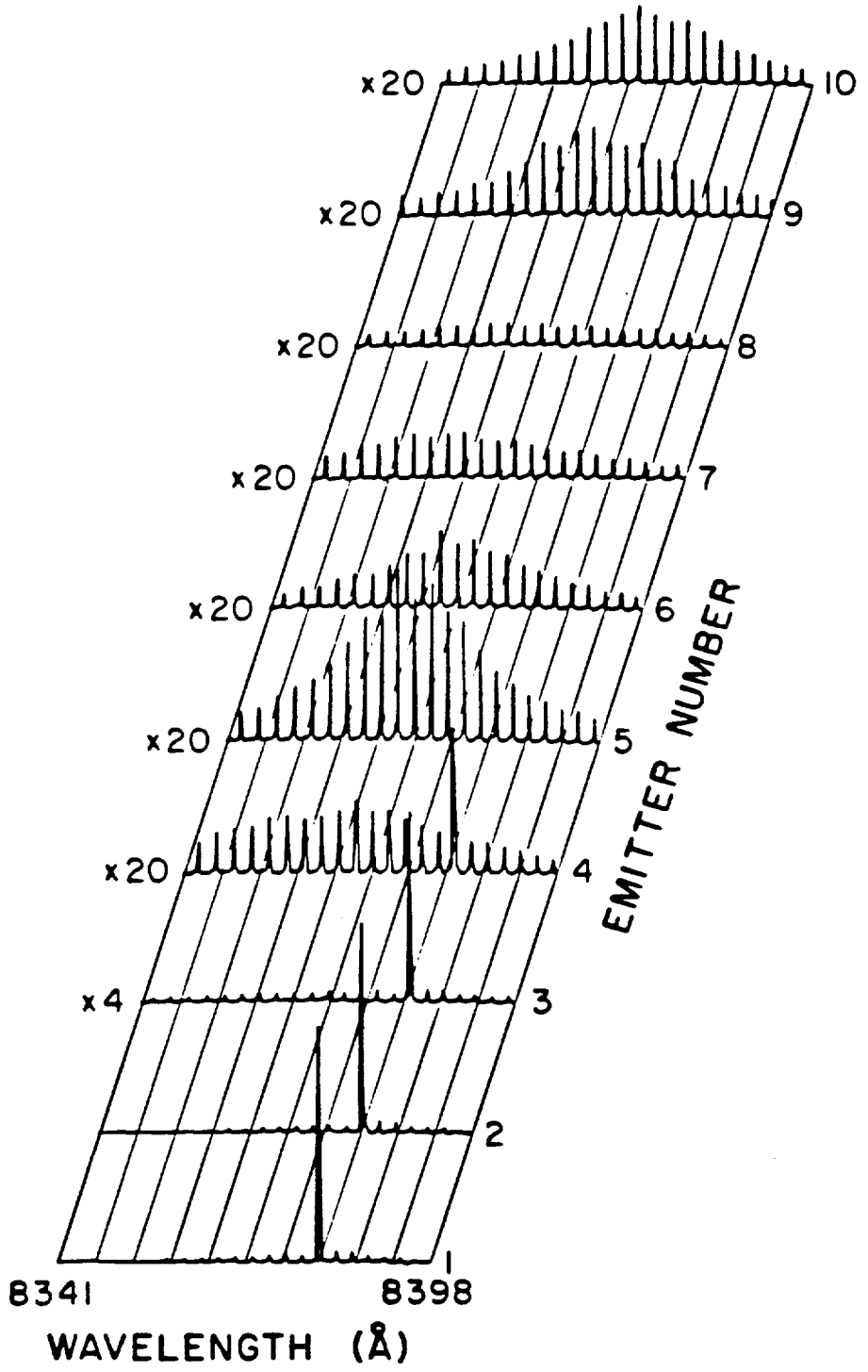

Figure 5.17 Low-resolution spatio-spectral properties of a Y-coupled laser array during CW operation at 1.6 times threshold.

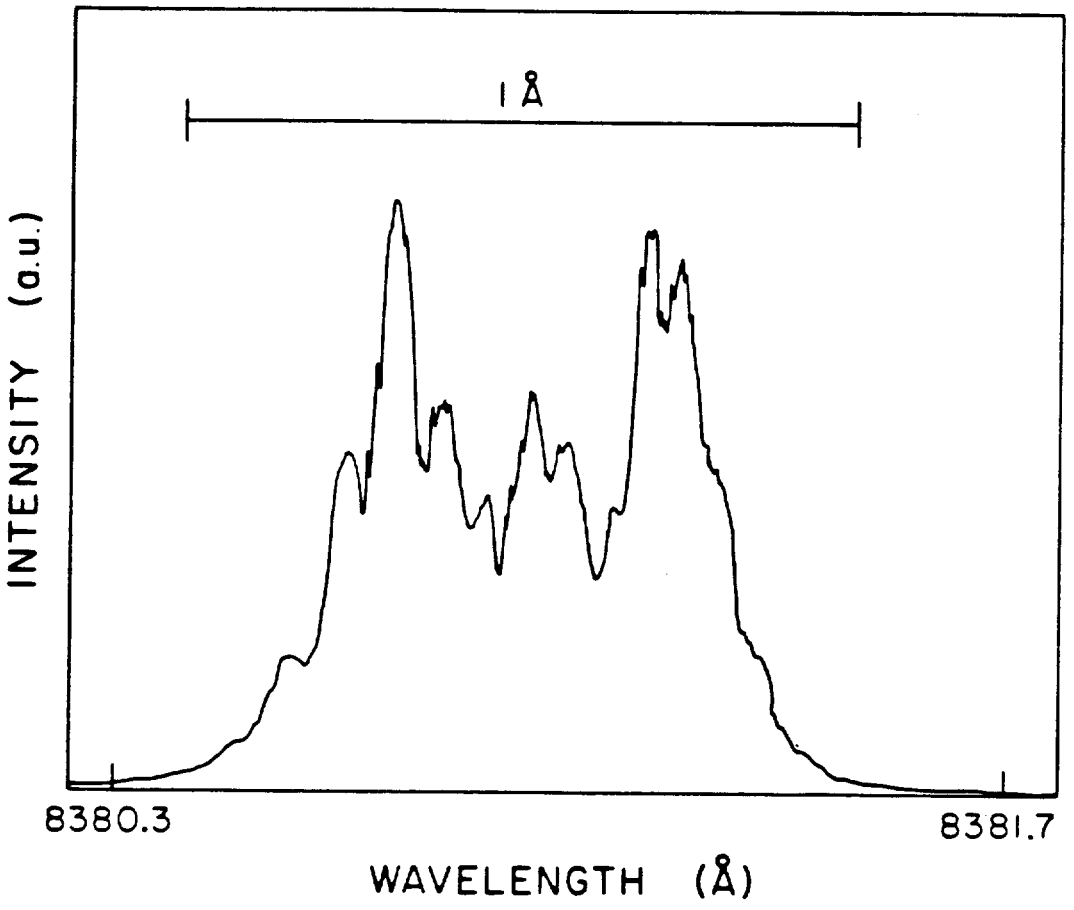

Figure 5.18 High-resolution spectral properties of the dominant mode of Emitter 1 shown in Figure 5.17.

5.2.3 Temporal Properties

Figure 5.19(a) is a halftone reproduction of the time evolution of the near-field pattern for a CW operating FYCL array. The figure shows the time evolution of the near field for each of the ten emitters in the array. The streak shown was initiated after the laser had been operating for several minutes at a CW drive current of 400 mA. The figure is made up of 192 vertical time pixels of 24 picoseconds duration each. The sustained self-pulsation of the array is clearly visible in the figure. A curious feature of the spatio-temporal self-organization of the array output under CW operation is the "temporal curvature" in which the inner emitters lag the outer ones in the phasing of the pulsations. It may be noted that during high resolution spectral studies of this array, we have observed an accompanying "spectral curvature" in which the inner emitters possess a longer wavelength than the outer emitters. We have observed similar spectral and temporal chirping in other YCL arrays we have studied. Figure 5.19(b) shows quantitatively the time evolution of emitter seven from Figure 5.19(a).

Sustained pulsing is also present during operation of the same device pulsed from zero bias. The lower picture in Figure 5.20 is an image of the time evolution of the near-field with a 500 mA current pulse. The horizontal dimension is the time with a 5 ns span. The temporal profiles are plotted in the upper part in Figure 5.20 for 10 emitters corresponding to the picture emitter by emitter. Figure 5.21 shows the time evolution of the near-field pattern during pulsed operation and averaged over 20 pulses at the same drive level as in Figure 5.20. It is interesting to note the spiking in emitters one through four has a fixed phase relationship from pulse to pulse relative to the initiation of lasing action as

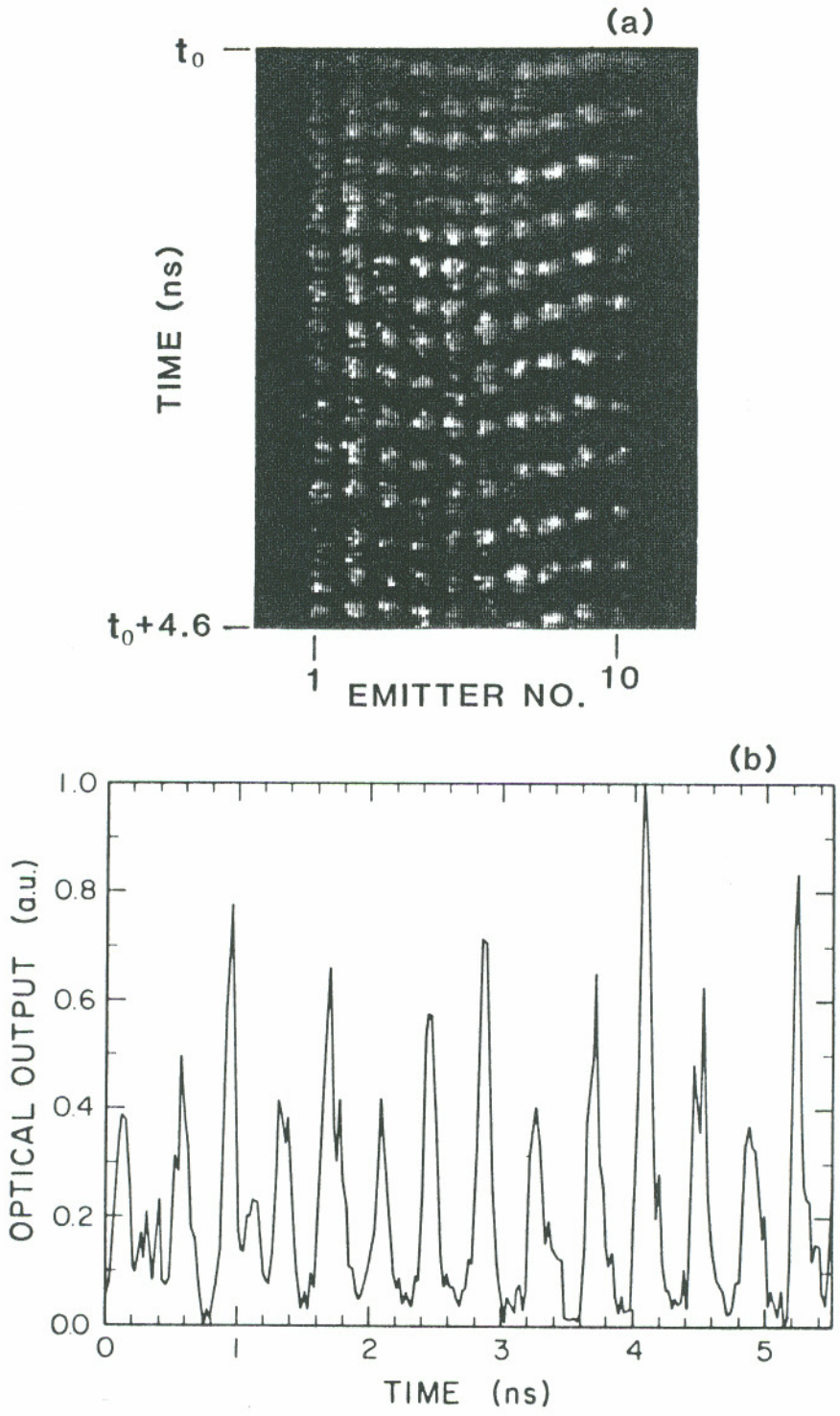

Figure 5.19 (a) Halftone representation of the time evolution of the Y-coupled laser array near field during CW operation at 400 mA. t_0 indicates several minutes after the initiation of lasing. (b) Time evolution of Emitter 7.

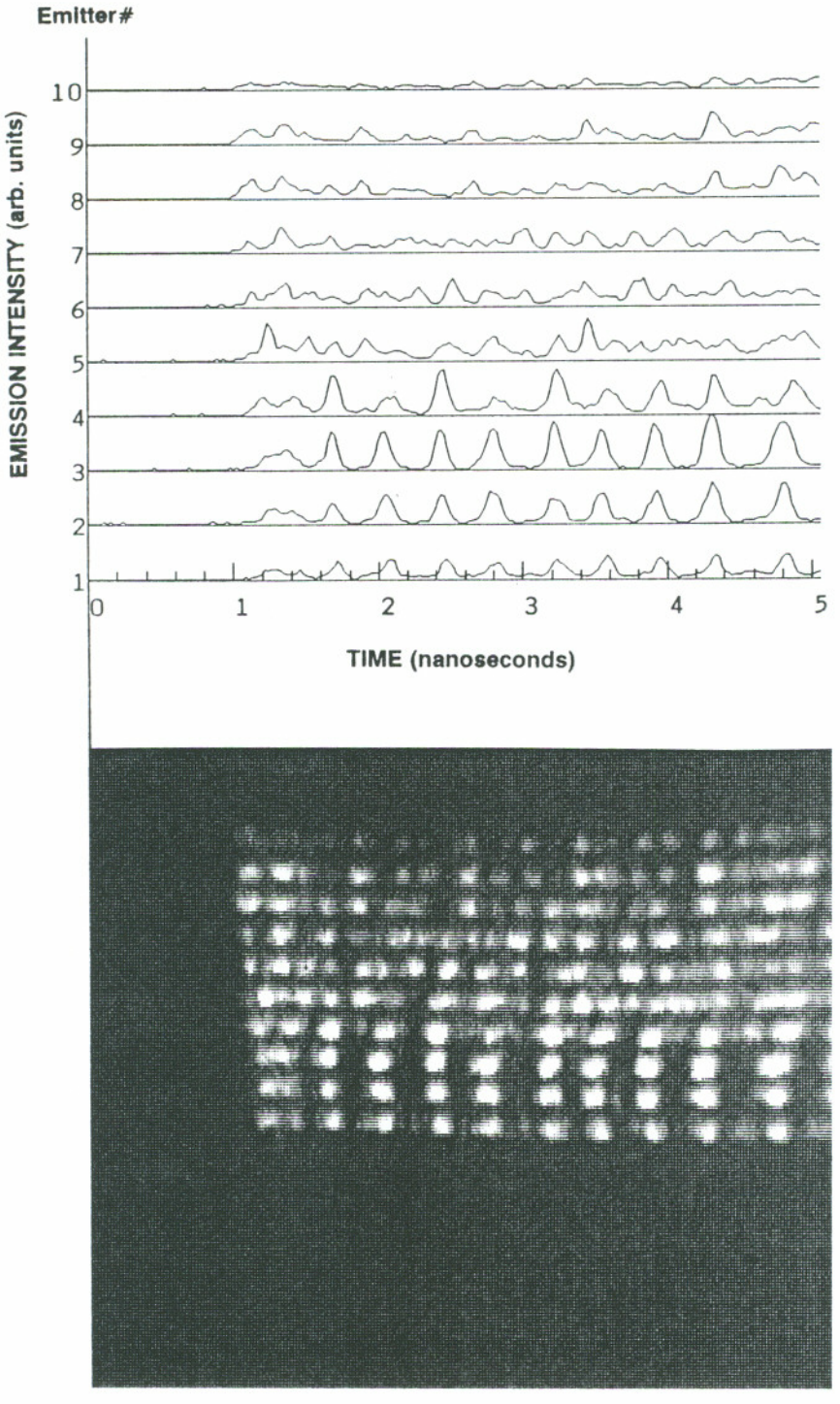

Figure 5.20 The time evolution of the near field of the Y-coupled laser array with a 500 mA current pulse.

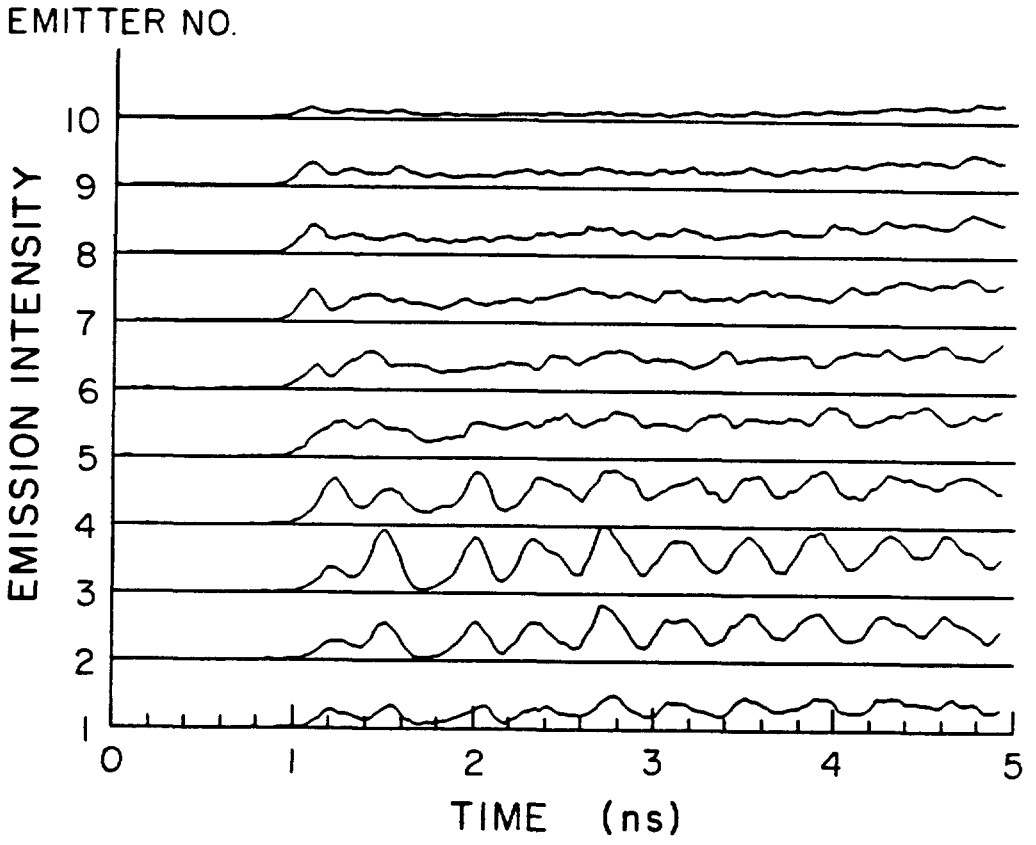

Figure 5.21 Average temporal evolution of the near field of the *Y*-coupled laser array averaged over 20 events with a 500 mA current pulse.

evidenced by the fact that it constructively adds over the 20 pulse averaging process while the spiking in emitters five through ten does not add constructively. This pulsed behavior may be compared to that of gain guided arrays where pulses with random phase relative to the initiation of lasing were observed[41].

Figure 5.22(a) shows the discrete Fourier transform modulus (DFTM) averaged over 20 video frames for the FYCL array operated at a CW drive current of 400 mA. Figure 5.22(b) shows similar data for the array operated at 500 mA CW. The DFTM was calculated emitter by emitter within each of 20 frames and then averaged and normalized for graphical presentation. At 400 mA drive current, the average DFTM peaks at 3.3 and 2.6 GHz for emitters 1 through 5 and 6 through 10, respectively. At 500 mA, it peaks at 3.99 and 3.07 GHz for the same stripes. These frequencies, when ratioed, fit the well known relationship[143] between the semiconductor relaxation oscillation frequency and the current overdrive,

$$f \propto \left(\frac{I}{I_{th}} - 1\right)^{\frac{1}{2}} .$$

Here, the CW I_{th} is approximately 260 mA. The temporal characteristics described here are typical in both the pulsed and CW drive cases of other YCL arrays we have observed. It was further observed that sustained self-pulsing occurs for all of the above-threshold drive currents used in the experiments described here.

In conclusion, Y-coupled index-guided laser arrays phase-lock in less than 20 ps and exhibit periodic sustained self-pulsations at multigigahertz frequencies in both pulsed and CW operation. These oscillations occur near the relaxation

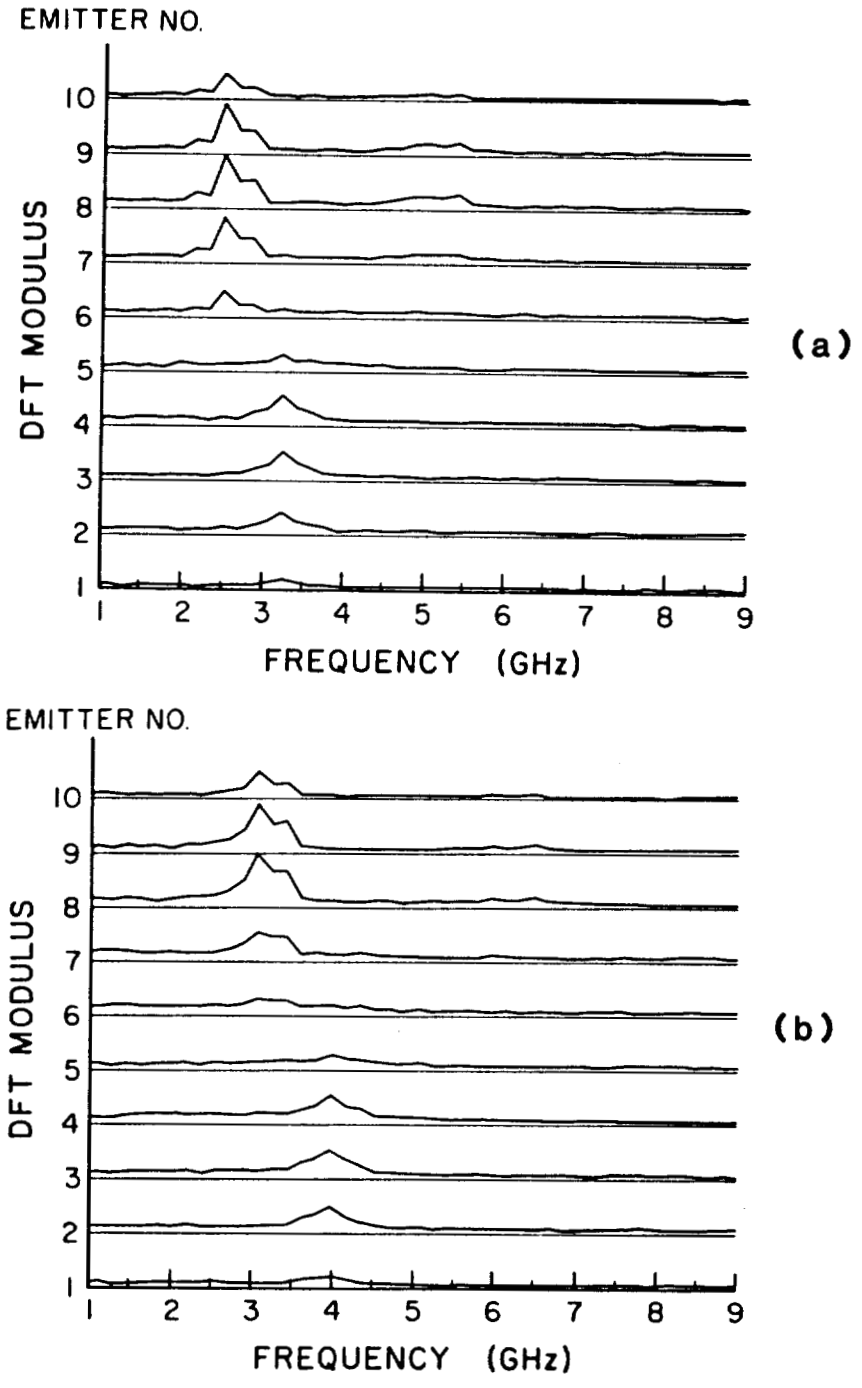

Figure 5.22 Average power spectra for the Y-coupled laser array operated, (a) at a 400 mA CW drive current, and (b) a 500 mA CW drive current.

resonance frequency of the laser and are likely driven by amplitude-phase coupling. Sustained self-pulsation is clearly evident, while a strong spatio-temporal organization, which is characteristic of Y-coupled arrays, is observed across the array.

Chapter 6

PHYSICAL MECHANISMS OF INSTABILITIES IN ARRAYS

All semiconductor laser arrays we have examed exhibit unstable behavior with intensity fluctuations. For optical communication applications, these are unwanted effects to be eliminated. On the other hand, self-pulsing can produce pulses shorter than 100 ps and thus could serve as a useful and simple source of short pulses. It is therefore important to understand the nature and mechanism of instabilities in these devices. There is only a limited theoretical and experimental studies on the dynamics of semiconductor laser arrays and little is known about the physical mechanisms which disturb the stability of the arrays. In this chapter, a brief discussion about some mechanisms that may cause or enhance the instability in diode laser arrays is given.

6.1 Amplitude-Phase Coupling

Using the nonlinear dynamic model described in Chapter 3, Winful and Wang performed a stability analysis of phase-locked semiconductor laser arrays[47]. Their results suggested that amplitude-phase coupling leads to instabilities in semiconductor laser arrays with evanescent coupling[48]. This is due to the fact that carrier induced amplitude-phase coupling intrinsic to semiconductor lasers destabilizes the coherent phase locking in diode laser arrays.

It is well known that any change in the imaginary part of the susceptibility (gain or loss) will be accompanied by a corresponding change in its real part (refractive index) via the Kramers-Kronig dispersion relations[174]. In semiconductor lasers, the lasing transition occurs between two energy bands, and this leads to asymmetry of the gain spectrum[126,175]. When Hilbert-transformed[176], this spectrum produces a dispersion curve of refractive index with its zero shifted from the gain-peak frequency[119,127,128,177]. Since the gain varies with the carrier density, the refractive index around the lasing frequency will also depend on the carrier density. The refractive index at the lasing wavelength decreases with increasing gain. Calculations of the refractive index dependence on the carrier concentration in GaAs[126-128], confirmed by numerous measurements of the carrier-induced wavelength shift in AlGaAs[118-120,128,178] and long-wavelength InGaAsP lasers[119,121,179-182], indicate that dn/dN, and hence α, is not zero in semiconductor lasers. The carrier induced changes in the refractive index play an important role in determining characteristics of semiconductor lasers.

The behavior of multistripe lasers will be strongly influenced by the waveguiding properties of the structure. The computed near- and far-field patterns of gain-guided laser arrays are sensitive to the values of α, with additional peaks in the near-field intensity profiles developing between the stripes and a three lobed far-field when $\alpha > 0$[95], in agreement with our experimental results presented in Chapter 4. The properties of twin-stripe lasers have been extensively studied by Shore *et al.* and their results indicated that an important factor in determining the stability of the optical field in two-stripe injection lasers was the relative strength of two mode-guiding mechanisms, namely, gain guiding

and refractive index anti-guiding[183]. They pointed out that the competition between the two guiding mechanisms is the cause of a near-field instability[184]. The couping coefficient between the array elements is proportional to the α factor[185]. In analysis of modal stabilities in uniform evanescently coupled diode laser arrays, Whiteaway *et al*[93,186]. suggested that the basic instability of the zero-order supermode could be at least partly explained by its tendency of self-focus due to the effect of the injected carries on refractive index.

A number of studies[101,125,187-190] have shown that the linewidth enhancement factor α that describes the coupling between carrier induced variations of real and imaginary parts of susceptibility is a key parameter in characterizing the linewidth broadening due to amplitude-phase coupling and the noise properties of semiconductor lasers. It has been shown by Henry[101,191], that the time variation of phase of the optical field is proportional to the α factor. Thus, α will appear in analysis of any phenomena where variations of phase are important. The coupling of phase and amplitude fluctuations leads to occurrence of α in a phase rate equation, and increases the laser linewidth[101] by $1 + \alpha^2$. For individual lasers, every elementary spontaneous emission event in the oscillating mode brings rise to two different contributions to the fluctuations of the phase of the laser field. The first one is due to the random phase of the spontaneous emitted photons, the second one is related to the consequent change of the field intensity. Besides the instantaneous phase change, there will be a delayed phase change in time resulting from the instantaneous change in intensity. The carrier density and hence gain will fluctuate to restore the laser field amplitude to the steady-state value, so that the laser will undergo relaxation oscillations. The time scale to restore

equilibrium is about 1 ns[101,192]. The change in the gain or imaginary part of the refractive index arising from this carrier density change is accompanied by a change in the real part of the refractive index. During relaxation oscillations index variations cause phase fluctuations in addition to those arising directly from the spontaneous emission events. In a laser array, an amplitude fluctuation in one laser leads to a carrier density fluctuation and a phase fluctuation in that same laser through α-factor. A change in relative phase leads to an amplitude change in a neighboring laser and accompanying change in its carrier density.

Also, the coupling strength between elements is the major parameter to determine the stability of the arrays because it is important to the time needed to send a signal from one element to its neighbors for controlling the type of oscillation of the outputs[50]. The analysis showed that instabilities occur for certain values of the coupling constant and the injection current when the α factor has nonzero values. In the simplest case of two-stripe arrays, the model provides stability diagrams and closed form expressions for the stability boundaries. Such boundaries are found to shift with the α value and the instability disappears as $\alpha \to 0$. When operated in the unstable regime, the light output of an array exhibits sustained periodic, quasi-periodic, or even chaotic pulsations.

6.2 Saturable Absorption

Presence of saturable absorption in the laser cavity is known to cause self-sustained pulsations in semiconductor lasers. It was first attempted by Basov[193] to relate the self-pulsation to saturable absorption effects in the active region of a diode laser. Since then, both experimental and theoretical studies have been

reported that show the presence of saturable absorber inside a semiconductor laser can yield unstable output. The saturable absorption mechanism can be understood as following.

Consider a semiconductor laser consisting of amplifying and absorbing regions. An increase of optical power within the laser cavity yields a decrease of carrier density and therefore also a decrease of gain in the amplifying region, but an increase of carrier number in the absorbing region. The increased carrier density in the absorbing region in turn yields a reduction of optical absorption, corresponding to a saturable absorber. If the decrease of absorption overcompensates the gain reduction, a net gain increase results which causes the stimulated emission to rise rapidly. The sudden increase of stimulated emission depletes the carrier density to a below-threshold level, and the stimulated emission stops. When the carrier density is built up again, the process repeats itself. Thus, the system is unstable and pulsation results due to such repetitive Q-switching process.

The exact nature of the absorption centers in semiconductor lasers is still not well known. There are suggestions that they may be deep-level traps[194,195], microdegradations distributed throughout the active region[196], mirror facet degradation[197], or proton-induced damage[198,199]. All of these mechanisms produce saturable absorption inside the laser cavity[200]. The exact cause of self-pulsation in any one particular laser is probably different from others, and there may even be more than one mechanism at work simultaneously. Self-pulsations are frequently observed in gain-guided lasers in which the laser stripe is defined by proton bombardment[198,201-203]. The properties of semiconductors after pro-

ton bombardment, and possible subsequent annealing, are not very well understood. But, it is believed that proton bombardment usually produces a high density of defects, which serve as centers of fast nonradiative recombination. These defects consequently increase the optical absorption and decrease the radiative efficiency and the equilibrium carrier concentration.

6.3 Feedback Effect

In the course of studying the dynamics of semiconductor laser arrays, it is important to eliminate unwanted sources that may unintentionally induce spectral and intensity instabilities. Particular attention has been paid to external optical feedback[204], that is, a portion of the laser output fed back into the laser waveguide cavity from an external reflecting surface, due to the fact that semiconductor laser behaviors can be significantly affected by external feedback. For certain amount of feedbacks, intabilities may occur[205-207]. Because of this concern optical feedback effects will be discussed in this section.

The characteristics of a semiconductor laser exposed to optical feedback from an external reflector have been studied both experimentally and theoretically[204,208-213], and five distinct regimes of feedback effects have been well characterized by the external feedback power ratio[211,214]. The first three regimes correspond to week optical feedback regimes with less than approximately -40 dB feedback power ratio. Such week feedback may yields linewidth broadening or narrowing, mode hoppings and related mode-hopping noise depending on the specific regime. A further increase of feedback beyond -40 dB causes the transition to the fourth regime of "coherence collapse". The operation

of a laser diode within the "coherence collapse" regime features strong instabilities, multiple external cavity modes, spectral linewidths of several 10 GHz, and large intensity noise. This regime has been termed "coherence collapse" because of the associated drastic reduction in the coherence length of the laser. The fifth regime occurs at the highest feedback levels, typically greater than -10 dB. The laser cavity is then formed essentially through an external cavity and the laser is relatively insensitive to additional external optical perturbations. The transition between regimes IV and V was observed for a laser diode with reduced facet reflectivities. Thus, the most detrimental operation for diode lasers occurs in the "coherence collapse" regime IV.

It is then necessary to quantify the amount of external optical feedback to the laser array from optical surfaces in our experimental setups. In the experimental arrangement, the light from the array was collected with a 20X microscope objective and focused onto a slit in the object plane of the streak camera's input optics. The microscope objective was located at about 5 mm from the array output facet. Assume that the light output from the array has an elliptical Gaussian wavefront with the beam waist located at the output facet of the array. The power feedback ratio is then calculated as

$$R_{ext} = \frac{w_{ox} w_{oy}}{w_x(l) w_y(l)} \tag{6.1}$$

where w_{ox}, w_{oy} are the output beam waists at the facet and $w_x(l)$, $w_y(l)$ are the beam radii of the light reflected back from a reflector located at distance $l/2$ from the laser output facet. Consider the reflectivity of the external reflector to be 0.04. For typical diode lasers, the calculated power feedback ratio with

$l = 1$cm is on the order of -80 dB. Therefore, the reflection from the microscope objective can be neglected. This estimation is in agreement with Tkach and Chraplyvy[211].

Another possible reflection may come from the input optics of the streak camera, which, if exists, is very difficult to estimate quantitatively. However, it is possible to analyze the pulsation frequency components to see if the observed pulsations are related to any external feedback in the experimental setup. It is well known that a variety of profound changes take place in the oscillation properties of a semiconductor laser when subjected to significant external feedback[204,208,215]. Among these changes is the increase in the output intensity fluctuations or pulsations. Experimental studies show that there are two kinds of components in the increased noise or pulsation frequency spectrum[205,215,216]. One is the high-frequency components, which are peaked at the frequency f_l and its integer multiples, where f_l corresponds to the reciprocal of the round-trip time for light to travel in the external cavity formed by the external reflector and the laser output facet. The other is the low-frequency components peaked at a frequency one or two orders of magnitude smaller than f_l. The high-frequency component can be understood as a result of resonance in the external cavity, while the physical nature of the low-frequency enhancement has not been clarified. Chinone *et al*[208]. have examined the external feedback effect for the case where the external mirror distance ranged between a few millimeters and several centimeters. It has been found that the oscillation period locked to the laser-to-mirror round-trip time was dominating. Temkin *et al*[217]. showed that under moderate feedback conditions (-35 to -15 dB power reflectivity), the pulsa-

tion period was determined by the external cavity length and takes a time of about ten round-trips in the external cavity. Cho and Umeda[218] reported experimental observations of chaotic output from semiconductor lasers with a feedback factor of about 30%. The fundamental frequency component coincided with the external cavity-mode separation, and chaos ceased at a feedback factor of 2%.

In our experiments, The pulsations observed in the output of the semiconductor laser arrays do not have either the low-frequency or the high-frequency features reported for feedback induced pulsations described above. For temporal property measurements, the distance between the output facet of the array and the input optics of the streak camera is typically between 30 to 45 cm. In particular case, such distance was measured to be 34 cm in the CW experiments with the gain-guided two-stripe laser. If there is significant feedback from the streak camera to induce pulsations, the fundamental frequency component f_l should be at about 440 MHz. The frequency spectrum of the pulsations for the two-stripe laser was calculated from the measured time evolution to be peaked at 1.5 GHz, as shown in Figure 4.15. This peak frequency is much higher than the corresponding feedback characteristic frequency f_l. It thus indicates that the observed self-pulsation in the output of the semiconductor arrays under our studies is not caused by external feedback effects.

Chapter 7
CONCLUSIONS

In the present dissertation the spatio-spectral and spatio-temporal properties have been experimentally characterized under both CW and pulsed operating conditions for AlGaAs monolithic 1-D coherent arrays of semiconductor diode lasers with the following structures: (1) ten-stripe gain-guided; (2) twin-stripe gain-guided; (3) eight-stripe channeled-substrate-planar; and (4) ten-stripe *Y*-coupled arrays. The experiments carried out to measure spatio-temporal and spatio-spectral properties as well as a variety of operating parameters demonstrate the capability for the study of the nonlinear dynamics in diode laser arrays. Streak camera observation of the time evolution of the near- and far-field radiation patterns reveals that these arrays are unstable in the picosecond to nanosecond domain with complex dynamic behavior such as periodicity, quasi-periodicity and chaos. Experimentally measured values for such array operating parameters as resonator dimensions, group refractive index, optical confinement factor, lasing wavelength, longitudinal mode spacing, mirror loss, internal loss, carrier lifetime, photon lifetime, threshold carrier density, transparency carrier density, threshold gain, differential gain, the linewidth enhancement factor, and the emitter-to-emitter complex coupling coefficient have also been reported for some of the arrays in an attempt to provide necessary experimental basis for

further theoretical research.

These experimental results also indicate an interesting and rich field of research on the nonlinear dynamics of semiconductor laser arrays exists. Studies in this area have just recently started. Though several important works have appeared in the last couple of years, there are may problems left to the future. In our experiments the time evolution of the array radiation patterns is recorded as a time series in a computer, and its power spectral density is calculated using the fast Fourier transform algorithm. Although power spectra make it possible to distinguish between periodic, quasiperiodic, and chaotic regimes. the broadband noise or broadband lines that suggest chaotic behavior could arise from stochastic as well as deterministic processes. A better method of analysis is needed to determine if erratic array radiation originates from random noise or characterizes a chaotic regime of an essentially deterministic system. On the other hand, observed intensity time series that display a variety of dynamic behaviors have not been adequately modeled. Further investigations of semiconductor laser array dynamics are likely to contribute to the development in the theoretical understanding of this phenomenon with the following more careful considerations:

(1) Coupled mode theory is an approximation and fails in strong coupling. A continuum model for laser array dynamics may be needed to treat the array as a single entity.

(2) Carrier diffusion has substantial effects on lateral mode instability in gain-guided and weakly index-guided arrays and should be taken into account.

(3) Spontaneous emission influences the array dynamic behavior and cannot be neglected.

For future experiments, stability of antiguide laser arrays remains to be examined since this kind of devices is the most promising approach to achieve stable, diffraction-limited beams to high power. Dynamic characterization could also extend to hybrid devices (e.g., longitudinally injection coupling or external cavity control) and 2-D grating-surface-emitting laser arrays.

References

1. J. Gowar, *Optical Communication Systems,* Prentice-Hall International, London, 1984.
2. M. J. Adams, A. G. Steventon, W. J. Devlin, and I. D. Henning, *Semiconductor Lasers for Lon-Wavelength Optical-Fiber Communications Systems,* Peter Peregrinus Ltd., London, 1987.
3. V. W. S. Chan, "Space coherent optical communication systems — An introduction," *IEEE J. Lightwave Technol.*, vol. LT-5, pp. 633-637, April 1987.
4. B. D. Seery and T. L. Holcomb, "High power laser diodes for the NASA direct detection laser transceiver experiment," *Proc. SPIE High Power Laser Diodes and Applications,* vol. 893, pp. 70-78, January 1988.
5. J. R. Lesh and M. D. Rayman, "Deep-space missions look to laser communications," *Laser Focus/Electro-Optics,* pp. 81-86, October 1988.
6. D. Botez, "High-power diode lasers for space communications: a review," *Opt. Eng.*, vol. 28, pp. 828-836, July 1989.
7. Y. A. Carts, "Tiny lasers promise high-speed communications," *Laser Focus World,* pp. 23-26, October 1989.
8. C. S. Wang, K. G. Lu, H. Firouzi, K. Ouyang, C. J. Hwang, J. L. Stevenson, S. Akiba, and R. A. Peters, "Reliability test of high power semiconductor laser for inter-satellite link," *Proc. SPIE Laser-Diode Technology and Applications II,* vol. 1219, pp. 138-149, January 1990.
9. E. S. Rothchild, "Rapid growth anticipated for optical disk systems and CD-ROM hardware," *Laser Focus/Electro-Optics,* pp. 118-123, February 1988.
10. L. E. Ravich, "Optical storage becomes multifaceted," *Laser Focus World,* pp. 115-122, March 1989.
11. D. Botez, "Laser diodes are power-packed," *IEEE Spectrum,* pp. 43-53, June 1985.
12. J. D. McClure, "Diode laser radar: applications and technology," *Proc. SPIE Laser-Diode Technology and Applications II,* vol. 1219, pp. 446-456, January 1990.
13. D. Welch, W. Streifer, and D. Scifres, "High power, coherent laser diodes," *Optics News,* pp. 7-10, March 1989.
14. W. Streifer, D. R. Scifres, G. L. Harnagel, D. F. Welch, J. Berger, and M. Sakamoto, "Advances in diode laser pumps," *IEEE J. Quantum Electron.*, vol. QE-24, pp. 883-894, June 1988.
15. H. Imai, M. Morimoto, K. Hori, M. Takusagawa, and H. Saito, "Long-lived high-power GaAlAs DH laser diodes," *J. Quantum Electron.*, vol. QE-16, pp. 248-250, March 1980.
16. C. S. Hong, J. J. Coleman, P. D. Dapkus, and Y. Z. Liu, "High-efficiency, low-threshold, Zn-diffused narrow stripe GaAs/GaAlAs double heterostructure lasers grown by metalorganic chemical vapor deposition," *Appl. Phys. Lett.*, vol. 40, pp. 208-210, 1 February 1982.

17. T. Hayakawa, N. Miyauchi, S. Yamamoto, H. Hayashi, S. Yano, and T. Hijikata, "Highly reliable and mode-stabilized operation in V-channeled substrate inner stripe lasers on p-GaAs substrate emitting in the visible wavelength region," *J. Appl. Phys.*, vol. 53, pp. 7224-7234, November 1982.

18. T. Hijikata, "Development and production of VSIS lasers," *Lasers & Applications*, pp. 57-60, February 1985.

19. T. Murakami, K. Ohtaki, H. Matsubara, T. Yamawaki, H. Saito, K. Isshiki, Y. Kokubo, A. Shima, H. Kumabe, and W. Susaki, "A very narrow-beam AlGaAs laser with a thin tapered-thickness active layer (T^3 laser)," *IEEE J. Quantum Electron.*, vol. QE-23, pp. 712-719, June 1987.

20. H. Jaeckel, H. P. Meier, G. L. Bona, W. Walter, D. J. Webb, and E. Van Gieson, "High-power fundamental mode AlGaAs quantum well channeled substrate laser grown by molecular beam epitaxy," *Appl. Phys. Lett.*, vol. 55, pp. 1059-1061, 11 September 1989.

21. K. Shinozaki, A. Watanabe, R. Furukawa, and N. Watanabe, "High-power operation of 830-nm AlGaAs laser diodes," *J. Appl. Phys.*, vol. 65, pp. 2907-2911, 15 April 1989.

22. D. F. Welch, H. Kung, M. Sakamoto, E. Zucker, W. Streifer, and D. Scifres, "Reliability characteristics of high power laser diodes," *Proc. SPIE Laser-Diode Technology and Applications II*, vol. 1219, pp. 113-116, 16-19 January 1990.

23. T. Yamaguchi, K. Yodoshi, K. Minakuchi, Y. Inoue, and K. Komeda, "A fundamental transverse mode 100 mW semiconductor laser with high reliability," *Proc. SPIE Laser-Diode Technology and Application II*, vol. 1219, pp. 126-133, 16-19 January 1990.

24. H. Naito, M. Kume, K. Hamada, H. Shimizu, and G. Kano, "Highly-reliable CW operation of 100 mW GaAlAs buried twin ridge substrate lasers with nonabsorbing mirrors," *IEEE J. Quantum Electron.*, vol. QE-25, pp. 1495-1499, June 1989.

25. K. Hamada, H. Naito, M. Kume, M. Yuri, and H. Shimizu, "High-power GaAlAs single-element lasers with nonabsorbing mirrors," *Proc. SPIE Laser-Diode Technology and Applications II*, vol. 1219, pp. 117-125, 16-19 January 1990.

26. K. Honda, T. Mamine, and M. Ayabe, "Single stripe high power laser diodes made by metal-organic chemical vapor deposition," *Proc. SPIE High Power Laser Diodes and Applications*, vol. 893, pp. 16-20, 14-15 January 1988.

27. R. G. Waters, P. L. Tihanyi, D. S. Hill, and B. A. Soltz, "Progress in single quantum well structures for high power laser device applications," *Proc. SPIE High Power Laser Diodes and Applications*, vol. 893, pp. 203-209, 14-15 January 1988.

28. H. Yamanaka, K. Iwamoto, N. Yamaguchi, K. Honda, T. Mamine, and C. Kojima, "Progress in super high power laser diodes with a broad area structure," *Technical Digest of Conference on Lasers and Electro-Optics*, vol. 7, pp. 468-469, Anaheim, CA, 21-25 May 1990.

29. D. F. Welch, B. Chan, W. Streifer, and D. R. Scifres, "High-power, 8 W CW single-quantum-well laser diode array," *Electron. Lett.*, vol. 24, pp. 113-115, 21 January 1988.

30. M. Sakamoto, D. F. Welch, J. G. Endriz, D. R. Scifres, and W. Streifer, "76 watt continuous-wave monolithic laser diode arrays," *Appl. Phys. Lett.*, vol. 54, pp. 2299-2300, 5 June 1989.

31. K. Iga, F. Koyama, and S. Kinoshita, "Surface emitting semiconductor lasers," *IEEE J. Quantum Electron.*, vol. QE-24, pp. 1845-1855, September 1988.

32. M. Y. A. Raja, S. R. J. Brueck, M. Osinski, C. F. Schaus, J. G. McInerney, T. M. Brennan, and B. E. Hammons, "Resonant periodic gain surface-emitting semiconductor lasers," *IEEE J. Quantum Electron.*, vol. QE-25, pp. 1500-1512, June 1989.

33. T. H. Windhorn and W. D. Goodhue, "Monolithic GaAs/AlGaAs diode laser/deflector devices for light emission normal to the surface," *Appl. Phys. Lett.*, vol. 48, pp. 1675-1677, 16 June 1986.

34. J. N. Walpole and Z. L. Liau, "Monolithic two-dimensional arrays of high-power GaInAsP/InP surface-emitting diode lasers," *Appl. Phys. Lett.*, vol. 48, pp. 1636-1638, 16 June 1986.

35. J. Puretz, R. K. DeFreez, R. A. Elliott, J. Orloff, and T. L. Paoli, "300 mW operation of a surface-emitting phase-locked array of diode lasers," *Electron. Lett.*, vol. 23, pp. 130-131, January 1987.

36. G. A. Evans, N. W. Carlson, J. M. Hammer, M. Lurie, J. K. Butler, S. L. Palfrey, R. Amantea, L. A. Carr, F. Z. Hawrylo, E. A. James, C. J. Kaiser, J. B. Kirk, and W. F. Reichert, "Two-dimensional coherent laser arrays using grating surface emission," *IEEE J. Quantum Electron.*, vol. QE-25, pp. 1525-1538, June 1989.

37. D. F. Welch, R. Parke, A. Hardy, W. Streifer, and D. R. Scifres, "Low-threshold grating-coupled surface-emitting lasers," *Appl. Phys. Lett.*, vol. 55, pp. 813-815, 28 August 1989.

38. G. A. Evans, N. W. Carlson, J. M. Hammer, and R. A. Bartolini, "Surface emitters support 2-D diode-laser technology," *Laser Focus World*, pp. 97-106, November 1989.

39. E. Kapon, J. Katz, and A. Yariv, "Supermode analysis of phase-locked arrays of semiconductor lasers," *Opt. Lett.*, vol. 10, pp. 125-127, April 1984.

40. J. K. Butler, D. E. Ackley, and D. Botez, "Coupled-mode analysis of phase-locked injection laser arrays," *Appl. Phys. Lett.*, vol. 44, pp. 293-295, 1 February 1984.

41. R. A. Elliott, R. K. DeFreez, T. L. Paoli, R. D. Burnham, and W. Streifer, "Dynamic characteristics of phase-locked multiple quantum well injection lasers," *IEEE J. Quantum Electron.*, vol. QE-21, pp. 598-602, June 1985.

42. R. K. DeFreez, R. A. Elliott, K. Hartnett, and D. F. Welch, "Quasi-instantaneous ($<$ 20 ps) phase locking in single-lobe Y-coupled laser diode arrays," *Electron. Lett.*, vol. 23, pp. 589-590, 21 May 1987.

43. N. Yu, R. K. DeFreez, D. J. Bossert, R. A. Elliott, H. G. Winful, and D. F. Welch, "Observation of sustained self-pulsation in CW operated flared *Y*-coupled laser arrays," *Electron. Lett.*, vol. 24, pp. 1203-1204, 15 September 1988.

44. R. K. DeFreez, D. J. Bossert, N. Yu, K. Hartnett, R. A. Elliott, and H. G. Winful, "Spectral and picosecond temporal properties of flared guide *Y*-coupled phase-locked laser arrays," *Appl. Phys. Lett.*, vol. 53, pp. 2380-2382, 12 December 1988.

45. R. K. DeFreez, D. J. Bossert, N. Yu, J. M. Hunt, H. Ximen, R. A. Elliott, G. A. Evans, M. Lurie, N. W. Carlson, J. M. Hammer, S. L. Palfrey, R. Amantea, H. G. Winful, and S. S. Wang, "Picosecond optical properties of a grating surface emitting two-dimensional coherent laser array," *Photon. Tech. Lett.*, vol. 1, pp. 209-211, August 1989.

46. R. K. DeFreez, N. Yu, D. J. Bossert, M. Felisky, G. A. Wilson, R. A. Elliott, H. G. Winful, G. A. Evans, N. W. Carlson, and R. Amantea, "Experimental characterization of the picosecond spatio-temporal properties of coherent semiconductor laser arrays," *Proceedings of OSA Topical Meeting on Nonlinear Dynamics in Optical Systems*, Afton, Oklahoma, 4-8 June 1990.

47. S. S. Wang and H. G. Winful, "Dynamics of phase-locked semiconductor laser arrays," *Appl. Phys. Lett.*, vol. 52, pp. 1774-1776, 23 May 1988.

48. H. G. Winful and S. S. Wang, "Stability of phase locking in coupled semiconductor laser arrays," *Appl. Phys. Lett.*, vol. 53, pp. 1894-1896, 14 November 1988.

49. H. G. Winful and L. Rahman, "Synchronized chaos in arrays of coupled lasers," *Proceedings of OSA Topical Meeting on Nonlinear Dynamics in Optical Systems*, Afton, Oklahoma, 4-8 June 1990.

50. S. S. Wang and H. G. Winful, "Dynamics of lateral modes in semiconductor laser arrays," *Proceedings of OSA Topical Meeting on Nonlinear Dynamics in Optical Systems*, Afton, Oklahoma, 4-8 June 1990.

51. H. G. Winful, S. S. Wang, and R. K. DeFreez, "Periodic and chaotic beam scanning in semiconductor laser arrays," *Proceedings of OSA Topical Meeting on Nonlinear Dynamics in Optical Systems*, Afton, Oklahoma, 4-8 June 1990.

52. E. Garmire, P. Menendez-Caldes, M. Ohtaka, and M. Ramadas, "Transverse-mode competition in gain-guided semiconductor laser arrays modelled as a single strongly-coupled multimode laser," *Proceedings of OSA Topical Meeting on Nonlinear Dynamics in Optical Systems*, Afton, Oklahoma, 4-8 June 1990.

53. P. K. Jakobsen, R. A. Indik, A. C. Newell, and J. V. Moloney, "Transverse instabilities in laser diode arrays under free-running and injection-locking conditions," *Proceedings of OSA Topical Meeting on Nonlinear Dynamics in Optical Systems*, Afton, Oklahoma, 4-8 June 1990.

54. K. Otsuka and K. Ikeda, "Self-induced phase turbulence and chaotic itinerancy in coupled-waveguide lasers," *Proceedings of OSA Topical Meeting on Nonlinear Dynamics in Optical Systems*, Afton, Oklahoma, 4-8 June

1990.

55. K. Otsuka, "Chaotic far-field interference and spot dancing with coupled-waveguide lasers," *Proceedings of OSA Topical Meeting on Nonlinear Dynamics in Optical Systems*, Afton, Oklahoma, 4-8 June 1990.
56. D. Botez and D. E. Ackley, "Phase-locked arrays of semiconductor diode lasers," *IEEE Circuits and Devices*, vol. 2, pp. 8-17, January 1986.
57. G. T. Forrest, "Diode-laser arrays achieve increased power and brightness," *Laser Focus/Electro-Optics*, pp. 59-66, August 1988.
58. G. T. Forrest, "CW diode lasers supply powerful photon fluxes," *Laser Focus World*, pp. 113-119, January 1990.
59. J. E. Ripper and T. L. Paoli, "Optical coupling of adjacent stripe-geometry junction lasers," *Appl. Phys. Lett.*, vol. 17, pp. 371-373, 1 November 1970.
60. D. R. Scifres, R. D. Burnham, and W. Streifer, "Phase-locked semiconductor laser array," *Appl. Phys. Lett.*, vol. 33, pp. 1015-1017, 15 December 1978.
61. D. E. Ackley and W. H. Engelmann, "High-power leaky-mode multiple-stripe laser," *Appl. Phys. Lett.*, vol. 39, pp. 27-29, 1 July 1981.
62. V. I. Malakhova, Y. A. Tambiev, and S. D. Yakubovich, "Regular integrated arrays of stripe injection lasers," *Sov. J. Quantum Electron.*, vol. 11, pp. 1351-1352, October 1981.
63. D. R. Scifres, R. D. Burnham, and W. Streifer, "Continuous wave high-power, high-temperature semiconductor laser phase-locked arrays," *Appl. Phys. Lett.*, vol. 41, pp. 1030-1032, 1 December 1982.
64. D. R. Scifres, C. Lindstrom, R. D. Burnham, W. Streifer, and T. L. Paoli, "Phase-locked (GaAl)As laser diode emitting 2.6 W CW from a single mirror," *Electron Lett.*, vol. 19, pp. 169-171, 3 March 1983.
65. D. F. Welch, M. Devito, M. Cardinal, M. Abraham, H. Kung, G. Harnagel, P. Cross, D. Scifres, and W. Streifr, "Performance characteristics of high-brightness, cw, diode laser arrays," *Electron. Lett.*, vol. 23, pp. 892-894, 13 August 1987.
66. D. R. Scifres, D. F. Welch, G. Harnagel, M. Sakamoto, H. Kung, W. Streifer, and J. Berger, "Power limits, efficiency, and reliability of 1-D and 2-D laser diodes and diode arrays," *Proc. SPIE High Power Laser Diodes and Applications*, vol. 893, pp. 2-6, 1988.
67. G. L. Harnagel, J. M. Haden, G. S. Browder, Jr., M. Cardinal, J. G. Endriz, and D. R. Scifres, "High power quasi-cw linear laser diode arrays emitting in excess of 200 watts of optical power," *Proc. SPIE Laser-Diode Technology and Applications II*, vol. 1219, pp. 186-192, January 1990.
68. D. R. Scifres, R. D. Burnham, and W. Streifer, "High power coupled multiple stripe quantum well injection lasers," *Appl. Phys. Lett.*, vol. 41, pp. 118-120, 15 July 1982.
69. J. P. Van Der Ziel, R. M. Mikulyak, H. Temkin, R. A. Logan, and R. D. Dupuis, "Optical beam characteristics of Schottky barrier confined arrays of phase-coupled multiquantum well GaAs lasers," *IEEE J Quantum Electron.*, vol. QE-20, pp. 1259-1266, November 1984.

70. D. E. Ackley, "Single longitudinal mode operation of high power multiple-stripe injection lasers," *Appl. Phys. Lett.*, vol. 42, pp. 152-154, 15 January 1983.

71. D. Botez and J. C. Connolly, "High-power phase-locked arrays of index-guided diode lasers," *Appl. Phys. Lett.*, vol. 43, pp. 1096-1098, 15 December 1983.

72. D. E. Ackley, "Phase-locked injection laser arrays with nonuniform stripe spacing," *Electron. Lett.*, vol. 20, pp. 695-696, 16 August 1984.

73. Y. Twu, A. Dienes, S. Wang, and J. R. Whinnery, "High power coupled ridge waveguide semiconductor laser arrays," *Appl. Phys. Lett.*, vol. 45, pp. 709-711, 1 October 1984.

74. S. Mukai, C. Lindsey, J. Katz, E. Kapon, Z. Rav-Noy, S. Marglit, and A. Yariv, "Fundamental mode oscillation of a buried ridge waveguide laser array," *Appl. Phys. Lett.*, vol. 45, pp. 834-835, 15 October 1984.

75. I. Suemune, T. Terashige, and M. Yamanishi, "Phase-locked, index-guided multiple-stripe lasers with large refractive index differences," *Appl. Phys. Lett.*, vol. 45, pp. 1011-1013, 15 November 1984.

76. E. Kapon, L. T. Lu, Z. Rav-Noy, M. Yi, S. Margalit, and A. Yariv, "Phased arrays of buried-ridge InP/InGaAsP diode lasers," *Appl. Phys. Lett.*, vol. 46, pp. 136-138, 15 January 1985.

77. H. Temkin, R. A. Logan, J. P. van der Ziel, C. L. Reynolds,Jr., and S. M. Tharaldsen, "Index-guided arrays of schottky barrier confined lasers," *Appl. Phys. Lett.*, vol. 46, pp. 465-467, 1 March 1985.

78. C. B. Morrison, L. M. Zinkiewicz, A. Burghard, and L. Figueroa, "Improved high-power twin-channel laser with blocking layer," *Electron. Lett.*, vol. 21, pp. 337-338, 11 April 1985.

79. M. Taneya, M. Matsumoto, S. Matsui, S. Yano, and T. Hijikata, "0° phase mode operation in phased-array laser diode with symmetrically branching waveguide," *Appl. Phys. Lett.*, vol. 47, pp. 341-343, 15 August 1985.

80. R. D. Dupuis and P. D. Dapkus, "Preparation and properties of $Ga_{1-x}Al_xAs-GaAs$ heterostructure lasers grown by metalorganic chemical vapor deposition," *IEEE J. Quantum Electron.*, vol. QE-15, pp. 128-135, March 1979.

81. H. C. Casey and M. B. Panish, *Heterostructure Lasers: Part B: Materials and Operating Characteristics*, Academic Press, New York, 1978. Chapter 6

82. D. R. Scifres, R. D. Burnham, and W. Streifer, "Lateral grating array high power cw visible semiconductor laser," *Electron. Lett.*, vol. 18, pp. 549-550, 24 June 1982.

83. J. J. J. Yang, R. D. Dupuis, and P. D. Dapkus, "Theoretical analysis of single-mode AlGaAs-GaAs double heterostructure lasers with channel-guide structure," *J. Appl. Phys.*, vol. 53, pp. 7218-7223, November 1982.

84. D. R. Scifres, W. Streifer, and R. D. Burnham, "High-power coupled-multiple-stripe phase-locked injection laser," *Appl. Phys. Lett.*, vol. 34, pp. 259-261, 15 February 1979.

85. D. R. Scifres, W. Streifer, and R. D. Burnham, "Experimental and analytic studies of coupled multiple stripe diode lasers," *IEEE J. Quantum Electron.*, vol. QE-15, pp. 917-922, September 1979.

86. D. F. Welch, P. Cross, D. Scifres, W. Streifer, and R. D. Burnham, "In-phase emission from index-guided laser array up to 400mW," *Electron. Lett.*, vol. 22, pp. 293-294, 12 March 1986.

87. D. F. Welch, P. S. Cross, D. R. Scifres, and W. Streifer, "Single-lobe 'Y' coupled laser diode arrays," *Electron. Lett.*, vol. 23, pp. 270-272, 12 March 1987.

88. L. Mawst, D. Botez, T. J. Roth, P. Hayashida, and E. Anderson, "Stable, single-array-mode operation from phase-locked interferometric arrays of index-guided AlGaAs/GaAs diode lasers," *Proc. SPIE High Power Laser Diodes and Applications*, vol. 893, pp. 10-15, 1988.

89. D. Botez, L. Mawst, P. Hayashida, G. Peterson, and T. J. Roth, "High-power, diffraction-limited-beam operation from phase-lock diode-laser of closely spaced 'leaky' waveguides (antiguides)," *Appl. Phys. Lett.*, vol. 53, pp. 464-466, 8 August 1988.

90. L. J. Mawst, D. Botez, T. J. Roth, G. Peterson, and J. J. Yang, "Diffraction-coupled, phase-locked arrays of antiguide, quantum-well lasers grown by metalorganic chemical vapour deposition," *Electron. Lett.*, vol. 24, pp. 958-959, 21 July 1988.

91. E. Kapon, C. P. Lindsey, J. S. Smith, S. Margalit, and A. Yariv, "Inverted-V chirped phased arrays of gain-guided GaAs/GaAlAs diode lasers," *Appl. Phys. Lett.*, vol. 45, pp. 1257-1259, 15 December 1984.

92. T. R. Chen, K. L. Yu, B. Chang, A. Hasson, S. Margalit, and A. Yariv, "Phase-locked InGaAsP laser array with diffraction coupling," *Appl. Phys. Lett.*, vol. 43, pp. 136-137, 15 July 1983.

93. J. E. A. Whiteaway, G. H. B. Thompson, and A. R. Goodwin, "Mode stability in real index-guide semiconductor laser arrays," *Electron. Lett.*, vol. 21, pp. 1194-1195, 5 December 1985.

94. J. Berger, D. F. Welch, W. Steifer, and D. R. Scifres, "Narrowing the far-field of a *Y*-junction laser array using a customized spatial filter in an external cavity," *Appl. Phys. Lett.*, vol. 52, pp. 1560-1562, 9 May 1988.

95. G. P. Agrawal, "Lateral-mode analysis of gain-guided and index-guided semiconductor-laser arrays," *J. Appl. Phys.*, vol. 58, pp. 2922-2931, 15 October 1985.

96. J. K. Butler, D. E. Ackley, and M. Ettenberg, "Coupled-mode analysis of gain and wavelength oscillation characteristics of diode phased arrays," *IEEE J. Quantum Electron.*, vol. QE-21, pp. 458-464, May 1985.

97. G. P. Agrawal and N. K. Dutta, *Long-Wavelength Semiconductor Lasers*, Van Nostrand Reinhold, New York, 1986. Chapter 6

98. N. Minorsky, *Nonlinear Oscillations*, Van Nostrand, Princeton, 1962.

99. J. -P. Eckmann, "Roads to turbulence in dissipative dynamical systems," *Rev. Mod. Phys.*, vol. 53, pp. 643-654, October 1981.

100. E. Ott, "Strange attractors and chaotic motions of dynamical systems," *Rev. Mod. Phys.*, vol. 53, pp. 655-671, October 1981.

101. C. H. Henry, "Theory of the linewidth of semiconductor lasers," *IEEE J. Quantum Electron.*, vol. QE-18, pp. 259-264, February 1982.

102. T. Hertsens, "Measuring diode laser characteristics," *Laser & Optronics*, pp. 37-42, February 1989.

103. J. G. Fujimoto and M. M. Salour, "Ultrafast picosecond chronography," *Proc. SPIE Picosecond Laser and Applications*, vol. 322, pp. 137-165, 1982.

104. Y. Tsuchiya, A. Takeshima, E. Inuzuka, K. Suzuki, M. Koishi, and K. Kinoshita, "Universal streak camera," *Proceedings of 16th International Congress on Speed Photography and Photonics*, pp. 86-94, Strasbourg, France, 27-31 August 1984.

105. A. J. Campillo and S. L. Shapiro, "Picosecond streak camera fluorometry — a review," *IEEE J. Quantum Electron.*, vol. QE-19, pp. 585-603, April 1983.

106. N. H. Schiller, "Picosecond streak camera photonics," *Semiconductor Probed by Ultrafast Spectroscopy*, vol. II, pp. 441-458, Academic Press, Orlando, 1984.

107. A. M. Prokhorov and M. Ya. Schelev, "Streak-camera technology makes rapid strides," *Laser Focus World*, pp. 85-92, February 1989.

108. R. K. DeFreez, R. A. Elliott, T. L. Paoli, R. D. Burnham, and W. Streifer, "Dynamic properties of phased-array multiple quantum well injection lasers," *Thirteenth International Quantum Electronics Conference*, Anaheim, CA, 18-21 June 1984. Paper PD-B3

109. K. A. Hartnett, *Streak Camera Analysis of Dynamic Characteristics of Current Modulated Diode Laser Arrays*, March 1988. M. S. Thesis, Oregon Graduate Center

110. A. J. Lee and D. P. Casasent, "Computer generated hologram recording using a laser printer," *Appl. Opt.*, vol. 26, pp. 136-138, 1 January 1987.

111. J. E. Ripper, "Measurement of spontaneous carrier lifetime from stimulated emission delays in semiconductor lasers," *J. Appl. Phys.*, vol. 43, pp. 1762-1763, April 1972.

112. R. W. Dixon and W. B. Joyce, "Generalized expressions for the turn-on delay in semiconductor lasers," *J. Appl. Phys.*, vol. 50, pp. 4591-4595, July 1979.

113. K. Konnerth and C. Lanza, "Delay between current pulse and light emission of a gallium arsenide injection laser," *Appl. Phys. Lett.*, vol. 4, pp. 120-121, 1 April 1964.

114. N. K. Dutta, R. L. Hartman, and W. T. Tsang, "Gain and carrier lifetime measurements in AlGaAs multiquantum well lasers," *IEEE J. Quantum Electron.*, vol. QE-19, pp. 1613-1616, November 1983.

115. G. P. Agrawal and N. K. Dutta, *Long-Wavelength Semiconductor Lasers*, Van Nostrand Reinhold, New York, 1986. Chapter 2

116. A. E. Siegman, *Lasers*, University Science Books, Mill Vally, California, 1986. Chapter 17

132. T. L. Paoli, W. Streifer, and R. D. Burnham, "Observation of supermodes in a phase-locked diode laser array," *Appl. Phys. Lett.*, vol. 45, pp. 217-219, 1 August 1984.

133. W. T. Tsang, "Extremely low threshold (AlGa)As modified multiquantum well heterostructure lasers grown by molecular-beam epitaxy," *Appl. Phys. Lett.*, vol. 39, pp. 786-788, 15 November 1981.

134. C. Lindstrom, R. D. Burnham, T. L. Paoli, W. Streifer, and D. R. Scifres, "CW high-power single-mode operation of gain-guided stripe-geometry multiple-quantum-well lasers," *Electron. Lett.*, vol. 19, pp. 104-105, 3 February 1983.

135. G. L. Harnagel, T. L. Paoli, R. L. Thornton, R. D. Burnham, and D. L. Smith, "Accelerated aging of 100-mW cw multiple-stripe GaAlAs lasers grown by metalorganic chemical vapor deposition," *Appl. Phys. Lett.*, vol. 46, pp. 118-120, 15 January 1985.

136. G. P. Agrawal and N. K. Dutta, *Long-Wavelength Semiconductor Lasers*, Van Nostrand Reinhold, New York, 1986. Chapter 9

137. Y. Arakawa and A. Yariv, "Theory of gain, modulation response, and spectral linewidth in AlGaAs quantum well lasers," *IEEE J. Quantum Electron.*, vol. QE-21, pp. 1666-1674, October 1985.

138. Y. Arakawa and A. Yariv, "Quantum well lasers — gain, spectra, dynamics," *IEEE J. Quantum Electron.*, vol. QE-22, pp. 1887-1899, September 1986.

139. Y. Arakawa, K. Vahala, and A. Yariv, "Quantum noise and dynamics in quantum well and quantum wire lasers," *Appl. Phys. Lett.*, vol. 45, pp. 950-952, 1 November 1984.

140. M. Born and E. Wolf, *Principles of Optics*, Pergamon Press, New York, 1975. Chapter 15

141. J. M. T. Thompson and H. B. Stewart, *Nonlinear Dynamics and Chaos*, John Wiley & Sons Ltd., Chichester, 1986. Chapter 6

142. H. Kressel and J. K. Butler, *Semiconductor Lasers and Heterojunction LEDs*, Academic Press, New York, 1977. Chapter 17

143. G. H. B. Thompson, *Physics of Semiconductor Laser Devices*, John Wiley & Sons, New York, 1980. Chapter 7

144. D. D. Cook and F. R. Nash, "Gain-induced guiding and astigmatic output beam of GaAs lasers," *J. Appl. Phys.*, vol. 46, pp. 1660-1672, April 1975.

145. P. A. Kirkby, A. R. Goodwin, G. H. B. Thompson, and P. R. Selway, "Observations of self-focusing in stripe geometry semiconductor lasers and the development of a comprehensive model of their operation," *IEEE J. Quantum Electron.*, vol. QE-13, pp. 705-719, August 1977.

146. T. L. Paoli, "Magnitude of the intrinsic resonant frequency in a semiconductor laser," *Appl. Phys. Lett.*, vol. 39, pp. 522-524, 1 October 1981.

147. H. Leipholz, *Stability Theory*, Academic Press, New York, 1970.

148. G. A. Wilson, R. K. DeFreez, and H. G. Winful, "Modulation of phased-array semiconductor lasers at k-band frequencies," *submitted to IEEE J.*

Quantum Electron., 1990.

149. T. Kadowaki, T. Aoyagi, S. Hinata, N. Kaneno, Y. Seiwa, K. Ikeda, and W. Susaki, "Long-lived phase-locked laser arrays mounted on a Si-submount with Au-Si solder with a junction-down configuration," *10th IEEE International Semiconductor Laser Conference*, pp. 84-85, Kanazawa, Japan, October 1986.

150. Y. Seiwa, T. Aoyagi, S. Hinata, T. Kadowaki, N. Kaneno, K. Ikeda, and W. Susaki, "High power cw operation over 400 mW on five-stripe phase-locked laser arrays assembled by new junction down mounting," *J. Appl. Phys.*, vol. 61, pp. 440-442, 1 January 1987.

151. B. Goldstein, N. W. Carlson, G. A. Evans, N. A. Dinkel, and V. J. Masin, "Performance of a channelled-substrate-planar high-power phase-locked array operating in the diffraction limit," *Electron. Lett.*, vol. 23, pp. 1136-1138, 8 October 1987.

152. N. W. Carlson, S. K. Liew, G. A. Evans, and J. K. Butler, "Observation of self-sustained pulsations from a highly coherent channeled-substrate-planar diode laser array," *Technical Digest of Conference on Lasers and Electro-Optics, Baltimore, MD*, p. 302, 24-28 April, 1989.

153. N. Yu, R. K. DeFreez, D. J. Bossert, G. A. Wilson, R. A. Elliott, S. S. Wang, and H. G. Winful, "Spatio-spectral and picosecond spatio-temporal properties of a broad-area-operating channeled-substrate-planar laser array," *submitted to Appl. Opt.*, 1990.

154. G. A. Evans, *Private Communication.*

155. N. W. Carlson, *Private Communication.*

156. J. K. Butler, G. A. Evans, and B. Goldstein, "Analysis and performance of channeled-substrate-planar double-heterojunction lasers with geometrical asymmetries," *IEEE J. Quantum Electron.*, vol. QE-23, pp. 1890-1899, November 1987.

157. G. A. Evans, J. K. Butler, and V. J. Masin, "Lateral optical confinement of channeled-substrate-planar lasers with GaAs/AlGaAs substrates," *IEEE J. Quantum Electron.*, vol. QE-24, pp. 737-749, May 1988.

158. J. M. Verdiell and R. Frey, "A broad-area mode-coupling model for multiple-stripe semiconductor lasers," *IEEE J. Quantum Electron.*, vol. 26, pp. 270-279, February 1990.

159. E. M. Garmire and M. T. Tavis, "Heatsink requirements for coherent operation of high-power semiconductor laser arrays," *IEEE J. Quantum Electron.*, vol. QE-20, pp. 1277-1283, November 1984.

160. J. R. Andrews, "Variable focusing due to refractive-index gradients in a diode-array traveling-wave amplifier," *J. Appl. Phys.*, vol. 64, pp. 2134-2137, 15 August 1988.

161. F. R. Nash, "Mode guidance parallel to the junction plane of double-heterostructure GaAs lasers," *J. Appl. Phys.*, vol. 44, pp. 4696-4707, October 1973.

162. G. H. B. Thompson, *Physics of Semiconductor Laser Devices*, John Wiley & Sons, New York, 1980. Chapter 4

163. N. Chinone, K. Aiki, M. Nakamura, and R. Ito, "Effects of lateral mode and carrier density profile on dynamic behaviors of semiconductor lasers," *IEEE J. Quantum Electron.*, vol. QE-14, pp. 625-631, August 1978.

164. K. Petermann, *Laser Diode Modulation and Noise*, Kluwer Academic Publishers, Dordrecht, 1988. Chapter 4

165. D. F. Welch, D. Scifres, P. Cross, H. Kung, W. Streifer, R. D. Burnham, J. Yaeli, and T. L. Paoli, "High power cw operation of phased array diode lasers with diffraction limited output beam," *Appl. Phys. Lett.*, vol. 47, pp. 1134-1136, 1 December 1985.

166. K.-L. Chen and S. Wang, "Single-lobe symmetric coupled laser arrays," *Electron. Lett.*, vol. 21, pp. 347-349, 11 April 1985.

167. M. Taneya, M. Matsumoto, H. Kawanishi, S. Matsui, S. Yano, and T. Hijikata, "Phased-array with the 'YY' shaped symmetrically branching waveguide (SBW)," *Jpn. J. Appl. Phys.*, vol. 25, pp. L432-L434, June 1986.

168. D. F. Welch, P. S. Cross, D. R. Scifres, W. Streifer, and R. D. Burnham, "High-power (CW) in-phase locked 'Y' coupled Laser Arrays," *Appl. Phys. Lett.*, vol. 49, pp. 1632-1634, 15 December 1986.

169. W. Streifer, P. S. Cross, D. F. Welch, and D. R. Scifres, "Analysis of a *Y*-junction semiconductor laser array," *Appl. Phys. Lett.*, vol. 49, pp. 58-60, 14 July 1986.

170. K.-L. Chen and S. Wang, "Analysis of symmetric *Y*-junction laser arrays with uniform near-field distribution," *Electron. Lett.*, vol. 22, pp. 644-645, 5 June 1986.

171. R. K. DeFreez, N. Yu, D. J. Bossert, R. A. Elliott, H. G. Winful, and D. F. Welch, "Sustained self-pulsation of CW operated *Y*-coupled diode laser arrays," *Proceedings of IEEE Lasers and Electro-Optics Society 1988 Annual Meeting*, pp. 459-460, Santa Clara, California, 2-4 November 1988.

172. W. Streifer, D. F. Welch, P. S. Cross, and D. R. Scifres, "*Y*-junction semiconductor laser arrays: Part I - Theory," *IEEE J. Quantum Electron.*, vol. QE-23, pp. 744-751, June 1987.

173. D. F. Welch, W. Streifer, P. S. Cross, and D. R. Scifres, "*Y*-Junction semiconductor laser arrays: Part II - experiments," *IEEE J. Quantum Electron.*, vol. QE-23, pp. 752-756, June 1987.

174. A. Yariv, *Quantum Electronics*, John Wiley & Sons, New York, 1989. Third Edition

175. G. Lasher and F. Stern, "Spontaneous and stimulated recombination radiation in semiconductors," *Phys. Rev.*, vol. A133, pp. A553-A563, 20 January 1964.

176. G. B. Arfken, *Mathematical Methods for Physicists, Third Edition*, p. 85, Academic Press, Orlando, 1985. Chapter 7

177. R. Lang, "Injection locking properties of a semiconductor laser," *IEEE J. Quantum Electron.*, vol. QE-18, pp. 976-983, June 1982.

178. M. Ito and T. Kimura, "Carrier density dependence of refractive index in AlGaAs semiconductor lasers," *IEEE J. Quantum Electron.*, vol. QE-16, pp. 910-911, September 1980.

179. K. Kishino, S. Aoki, and Y. Suematsu, "Wavelength variation of 1.6 μm wavelength buried heterostructure GaInAsP/InP lasers due to direct modulation," *IEEE J. Quantum Electron.*, vol. QE-18, pp. 343-351, March 1982.

180. S. E. H. Turley, "Anomalous effect of carriers on dielectric constant of (In, Ga)(As, P) lasers operating at 1.3μm wavelength," *Electron Lett.*, vol. 18, pp. 590-592, 8 July 1982.

181. J.-C. Bouley, J. Charil, Y. Sorel, and G. Chaminant, "Injected carrier effects on modal properties of 1.55 μm GaInAsP lasers," *IEEE J. Quantum Electron.*, vol. QE-19, pp. 969-974, June 1983.

182. C. H. Henry, L. F. Johnson, R. A. Logan, and D. P. Clarke, "Determination of the refractive index of InGaAsP epitaxial layers by mode line luminescence spectroscopy," *IEEE J. Quantum Electron.*, vol. QE-21, pp. 1887-1892, December 1985.

183. K. A. Shore and P. J. Hartnett, "Diffusion and waveguiding effects in twin-stripe injection lasers," *Opt. Quantum Electron.*, vol. 14, pp. 169-176, 1982.

184. T. E. Rozzi and K. A. Shore, "Spatial and temporal instabilities in multistripe semiconductor lasers," *J. Opt. Soc. Am. B*, vol. 2, pp. 237-249, January 1985.

185. J. Katz, E. Kapon, C. Lindsey, S. Margalit, and A. Yariv, "Coupling coefficient of gain-guided lasers," *Appl. Opt.*, vol. 23, pp. 2231-2233, 15 July 1984.

186. G. H. B. Thompson and J. E. A. Whiteaway, "Analysis of the stability of the highest-order supermode in semiconductor laser arrays," *Electron. Lett.*, vol. 23, pp. 444-446, 23 April 1987.

187. J. P. van der Ziel, "Spectral broadening of pulsating $Al_xGa_{1-x}As$ double heterostructure lasers," *IEEE J. Quantum Electron.*, vol. QE-15, pp. 1277-1281, November 1979.

188. W. Elsasser and E. O. Gobel, "Spectral linewidth of gain- and index-guided InGaAsP semiconductor lasers," *Appl. Phys. Lett.*, vol. 45, pp. 353-355, 15 August 1984.

189. J. Harrison and A. Mooradian, "Spectral characteristics of (GaAl)As diode lasers at 1.7 K," *Appl. Phys. Lett.*, vol. 45, pp. 318-320, 15 August 1984.

190. N. Ogasawara, R. Ito, and R. Morita, "Linewidth enhancement factor in GaAs/AlGa/As multi-quantum-well lasers," *Jpn. J. Appl. Phys.*, vol. 24, pp. L519-L521, July 1985.

191. C. H. Henry, "Theory of the phase noise and power spectrum of a single mode injection laser," *IEEE J. Quantum Electron.*, vol. QE-19, pp. 1391-1397, September 1983.

192. D. Welford and A. Mooradian, "Output power and temperature dependence of the linewidth of single-frequency cw (GaAl)As diode lasers," *Appl. Phys. Lett.*, vol. 40, pp. 865-867, 15 May 1982.

193. N. G. Basov, "Dynamics of injection lasers," *IEEE J. Quantum Electron.*, vol. QE-4, pp. 855-864, November 1968.

194. H. Imai, K. Isozumi, and M. Takusagawa, "Deep level associated with the slow degradation of GaAlAs DH laser diodes," *Appl. Phys. Lett.*, vol. 33, pp. 330-332, 15 August 1978.

195. J. A. Copeland, "Semiconductor-laser self pulsing due to deep level traps," *Electron. Lett.*, vol. 14, pp. 809-810, 7 December 1978.

196. D. Kato, "Microscale degradation in (GaAl)As double-heterostructure diode lasers," *Appl. Phys. Lett.*, vol. 31, pp. 588-590, 1 November 1977.

197. R. W. Dixon and W. B. Joyce, "A possible model for sustained oscillations (pulsations) in (Al,Ga)As double-heterostructure lasers," *IEEE J. Quantum Electron.*, vol. QE-15, pp. 470-474, June 1979.

198. J. P. van der Ziel, J. L. Merz, and T. L. Paoli, "Study of intensity pulsations in proton-bombarded stripe-geometry double-heterostructure $Al_xGa_{1-x}As$ lasers," *J. Appl. Phys.*, vol. 50, pp. 4620-4637, July 1979.

199. J. C. Campbell, S. M. Abbott, and A. G. Dentai, "A comparison of "normal" lasers and lasers exhibiting light jumps," *J. Appl. Phys.*, vol. 51, pp. 4010-4013, August 1980.

200. C. H. Henry, "Theory of defect-induced pulsations in semiconductor injection lasers," *J. Appl. Phys.*, vol. 51, pp. 3051-3061, June 1980.

201. A. J. Schorr and W. T. Tsang, "Development of self-pulsations due to self-annealing of proton bombarded regions during aging in proton bombarded stripe-geometry AlGaAs DH lasers grown by molecular beam epitaxy," *IEEE J. Quantum electron.*, vol. QE-16, pp. 898-901, August 1980.

202. R. P. Brouwer, C. H. F. Velzel, and B. Yeh, "Lateral modes and self-oscillations in narrow-stripe double-heterostructure GaAl-As injection lasers," *IEEE J. Quantum Electron.*, vol. QE-17, pp. 694-701, May 1981.

203. M. Kuznetsov, "Pulsations of semiconductor lasers with a proton bombarded segment: well-developed pulsations," *IEEE J. Quantum Electron.*, vol. QE-21, pp. 587-592, June 1985.

204. R. Lang and K. Kobayashi, "External optical feedback effects on semiconductor injection laser properties," *IEEE J. Quantum Electron.*, vol. QE-16, pp. 347-349, March 1980.

205. M. Fujiwara, K. Kubota, and R. Lang, "Low-frequency intensity fluctuation in laser diodes with external optical feedback," *Appl. Phys. Lett.*, vol. 38, pp. 217-220, 15 February 1981.

206. C. H. Henry and R. F. Kazarinov, "Instability of semiconductor lasers due to optical feedback from distant reflectors," *IEEE J. Quantum Electron.*, vol. QE-22, pp. 294-301, February 1986.

207. G. C. Dente, P. S. Durkin, K. A. Wilson, and C. E. Moeller, "Chaos in the coherence collapse of semiconductor lasers," *IEEE J. Quantum Electron.*, vol. QE-24, pp. 2441-2447, December 1988.

208. N. Chinone, K. Aiki, and R. Ito, "Stabilization of semiconductor laser outputs by a mirror close to a laser facet," *Appl. Phys. Lett.*, vol. 33, pp. 990-

991, 15 December 1978.

209. L. Goldberg, H. F. Taylor, A. Dandridge, J. F. Weller, and R. O. Miles, "Spectral characteristics of semiconductor lasers with optical feedback," *IEEE J. Quantum Electron.*, vol. QE-18, pp. 555-564, April 1982.

210. P. Spano, S. Piazzolla, and M. Tamburrini, "Theory of noise in semiconductor lasers in the presence of optical feedback," *IEEE J. Quantum Electron.*, vol. QE-20, pp. 350-357, April 1984.

211. R. W. Tkach and A. R. Chraplyvy, "Regimes of feedback effects in 1.5-μm distributed feedback lasers," *J. Lightw. Tech.*, vol. LT-4, pp. 1655-1661, November 1986.

212. E. G. Vicente De Vera and E. Bernabeu, "External feedback effects on I/L characteristics of laser diode," *Electron. Lett.*, vol. 25, pp. 976-978, 20 July 1989.

213. J. O. Binder and G. D. Cormack, "Mode selection and stability of a semiconductor laser with weak optical feedback," *IEEE J. Quantum Electron.*, vol. QE-25, pp. 2255-2259, November 1989.

214. K. Petermann, *Laser Diode Modulation and Noise*, Kluwer Academic Publishers, Dordrecht, 1988. Chapter 9

215. Ch. Risch and C. Voumard, "Self-pulsation in the output intensity and spectrum of GaAs-AlGaAs cw diode lasers coupled to a frequency-selective external optical cavity," *J. Appl. Phys.*, vol. 48, pp. 2083-2085, May 1977.

216. I. Ikushima and M. Maeda, "Self-coupled phenomena of semiconductor lasers caused by an optical fiber," *IEEE J. Quantum Electron.*, vol. QE-14, pp. 331-332, May 1978.

217. H. Temkin, N. A. Olsson, J. H. Abeles, R. A. Logan, and M. B. Panish, "Reflection noise in index-guided InGaAsP lasers," *IEEE J. Quantum Electron.*, vol. QE-22, pp. 286-293, February 1986.

218. Y. Cho and T. Umeda, "Chaos in laser oscillations with delayed feedback: numerical analysis and observation using semiconductor lasers," *J. Opt. Soc. Am. B*, vol. 1, pp. 497-498, June 1984.

APPENDIX A

This appendix is a source listing of the FORTRAN programs f.norm.jitter.f and cw.norm.f for pulsed and CW time-intensity data pre-processing respectively.

```
C*********************************************************************
C Program f.norm.jitter.f

      real wl,wr,zero(5)
      double precision ar(20,10,235),arr(235,20)
      double precision maxi,mini
      double precision b,s,s1,s2,s3
      double precision signalm,hsignalm
      double precision sum(235)
      integer n,m,i,ii,j,jj,ll,nfile,ldigit,rdigit,ta
      integer pldigit,prdigit
      integer signal(20),on(20)
      integer maxj
      character prefix*1,oprefix*1,suffixl*1,suffixr*1,name*6,dot*1
      character psuffixl*1,psuffixr*1
      character prefixo*3,suffixo*4,suffixout*4,nameout*11

      logical debug
      debug = .false.

C define the dimensions of the array--m denotes the number of emitters
      print *, 'input number of emitters/windows...'
      read *, m
C read the number of frames in the data set
      print *, 'input number of frames in the data set...'
      read *, nfile
      print *, 'input initial character of file prefix...'
      read *, prefix
      print *, 'input initial character of output file prefix...'
      read *, oprefix
C read the output triggering data file prefix
      print *, 'input prefix of triggering data file (3 char.)...'
      read *,prefixo
C set the length of the file
      n=235
C calculate the filenames of each of the array files

      dot = '.'
      mini=100.0
      maxi=0.0
      do 200 ii=1,nfile
           pldigit = ii/10
           prdigit = ii-10*pldigit
           psuffixl= char(pldigit + 48)
           psuffixr= char(prdigit + 48)
           do 100 jj=1,m
                ldigit = jj/10
                rdigit = jj-10*ldigit
                suffixl= char(ldigit + 48)
```

```
                suffixr= char(rdigit + 48)
                name = prefix//psuffixl//psuffixr//dot//suffixl//suffixr
C open each of these array files and read the data into ar(ii,jj,kk)
                open(4,file= name)
                read(4,45) wl
                read(4,45) wr
45              format (i3)
                do 50 ll=1,5
                   read(4,45) zero(ll)
50              continue
                do 80 kk=1,n
                   read(4,85) ta
85                 format(i3)
                   ar(ii,jj,kk)=ta
                   if (mini.gt.ar(ii,jj,kk)) then
                         mini=ar(ii,jj,kk)
                   end if
                   if (maxi.lt.ar(ii,jj,kk)) then
                         maxi=ar(ii,jj,kk)
                   end if
80              continue
                close(4)
100         continue
200   continue
      print *,mini
      print *,maxi
     nn=10
     do 1000 ii=1,nfile
          pldigit = ii/10
          prdigit = ii-10*pldigit
          psuffixl= char(pldigit + 48)
          psuffixr= char(prdigit + 48)
          maxijk=0
          do 400 jj=1,m
                ldigit = jj/10
                rdigit = jj-10*ldigit
                suffixl= char(ldigit + 48)
                suffixr= char(rdigit + 48)
                name = oprefix//psuffixl//psuffixr//dot//suffixl//suffixr
C open each of these array files and write the data into the files
                open(4,file= name)
                b=0.0
                s=0.0
                do 300 kk=1,n
                   arr(kk,jj)=(ar(ii,jj,kk)-mini)*63.0/(maxi-mini)
                   if (kk.le.15) then
                         b=b+arr(kk,jj)
                         s=s+arr(kk,jj)*arr(kk,jj)
                   end if
```

```
300             continue
                b=b/15.0
                s=dsqrt(s/15.0-b*b)
                do 350 j=1,n
                   arr(j,jj)=arr(j,jj)-(b-1.0*s)
                   if (arr(j,jj).lt.0) then
                         arr(j,jj)=0.0
                   end if
                   write(4,330) arr(j,jj)
330                format(f6.3)
350             continue
                close(4)
400          continue
             nn=nn+1
             do 500 i=1,n
                   sum(i)=0.0
                   do 450 j=1,m
                      sum(i)=sum(i)+arr(i,j)
450                continue
                   write (nn,465) i, sum(i)
465                format (i4,2x,f7.2)
500          continue
             s1=0.0
             s2=0.0
             do 600 i=1,15
                   s1=s1+sum(i)
                   s2=s2+sum(i)*sum(i)
600          continue
             b=s1/15.0
             s=dsqrt(s2/15.0-b*b)
             b=b+3.0*s
             do 700 i=21,n
                   if (b.lt.sum(i)) then
                         signal(ii)=i
                         goto 710
                   end if
700          continue
710          s3=0.0
             do 800 i=signal(ii),n
                   s3=s3+sum(i)
800          continue
             signalm=s3/dfloat(n-signal(ii)+1)
             hsignalm=signalm/2.0
             do 900 i=1,n
                   if (hsignalm.lt.sum(i)) then
                         on(ii)=i
                         print *,on(ii)
                         goto 1000
                   end if
```

```
900         continue
1000  continue
C determine the largest delay element, maxj
C set maxj to be the first element
      maxj=on(1)
      do 2500 j=1,nfile
            if (on(j).gt.maxj) then
                  maxj=on(j)
            end if
2500  continue
C calculate the output file name
      suffixo='.trg'
      suffixout='.max'
      nameout=prefixo//suffixo//suffixout
C write the data to this file, adding the maximum delay value
C at the beginning of the file
      open (1, file=nameout)
      write (1,2850) maxj
      write (1,2850) (on(j), j=1,nfile)
2850  format (i3)
      close (1)
      stop
      end
```

```
C*********************************************************************
C Program cw.norm.f

      real wl,wr,zero(5)
      double precision ar(20,10,235),arr(235,20)
      double precision maxi,mini
      double precision sum(235)
      integer n,m,i,ii,j,jj,ll,nfile,ldigit,rdigit,ta
      integer pldigit,prdigit
      character prefix*1,oprefix*1,suffixl*1,suffixr*1,name*6,dot*1
      character psuffixl*1,psuffixr*1
      logical debug
      debug = .false.
C define the dimensions of the array--m denotes the number of emitters
      print *, 'input number of emitters/windows...'
      read *, m
C read the number of frames in the data set
      print *, 'input number of frames in the data set...'
      read *, nfile
      print *, 'input initial character of file prefix...'
      read *, prefix
      print *, 'input initial character of output file prefix...'
      read *, oprefix
C set the length of the file
      n=235
C calculate the filenames of each of the array files
      dot = '.'
      mini=100.0
      maxi=0.0
      do 200 ii=1,nfile
            pldigit = ii/10
            prdigit = ii-10*pldigit
            psuffixl= char(pldigit + 48)
            psuffixr= char(prdigit + 48)
            do 100 jj=1,m
                  ldigit = jj/10
                  rdigit = jj-10*ldigit
                  suffixl= char(ldigit + 48)
                  suffixr= char(rdigit + 48)
                  name = prefix//psuffixl//psuffixr//dot//suffixl//suffixr
C open each of these array files and read the data into ar(ii,jj,kk)
                  open(4,file= name)
                  read(4,45) wl
                  read(4,45) wr
45                format (i3)
                  do 50 ll=1,5
                     read(4,45) zero(ll)
50                continue
                  do 80 kk=1,n
```

```
                read(4,85) ta
85              format(i5)
                ar(ii,jj,kk)=ta
                if (mini.gt.ar(ii,jj,kk)) then
                    mini=ar(ii,jj,kk)
                end if
                if (maxi.lt.ar(ii,jj,kk)) then
                    maxi=ar(ii,jj,kk)
                end if
80             continue
               close(4)
100         continue
200   continue
      print *,mini
      print *,maxi
     nn=10
     do 1000 ii=1,nfile
          pldigit = ii/10
          prdigit = ii-10*pldigit
          psuffixl= char(pldigit + 48)
          psuffixr= char(prdigit + 48)
          do 400 jj=1,m
               ldigit = jj/10
               rdigit = jj-10*ldigit
               suffixl= char(ldigit + 48)
               suffixr= char(rdigit + 48)
               name = oprefix//psuffixl//psuffixr//dot//suffixl//suffixr
C open each of these array files and write the data into the files
               open(4,file= name)
               do 300 kk=1,n
C                  arr(kk,jj)=(ar(ii,jj,kk)-mini)*63.0d0/(maxi-mini)
                   arr(kk,jj)=ar(ii,jj,kk)*64.0d0/maxi
                   write(4,330) arr(kk,jj)
330                format(f12.9)
300             continue
               close(4)
400         continue
          nn=nn+1
          do 500 i=1,n
               sum(i)=0.0
               do 450 j=1,m
                  sum(i)=sum(i)+arr(i,j)
450             continue
C              write (nn,465) i, sum(i)
465            format (i4,2x,f7.2)
500         continue
1000  continue
      stop
      end
```

APPENDIX B

This appendix is a source listing of the FORTRAN program mkarray.b.f. This program forms the array files from the time-intensity data files of the individual emitters.

```
C**********************************************************************
C program mkarray.b.f...this program opens and reads the trigger-
C                ing data file 'xxx.trg.max'; extracts delay
C                information for each frame and the total length
C                allowed by the maximum delay for the data set.
C                This provides the compensation necessary for the
C                observed triggering instability . The program then
C                opens and reads the individual emitter data files
C                which comprise one frame grabbed image. These
C                files are read into an array, a(j,i) where i ranges
C                from 1-m --the nth column in the array corresponds
C                to the data file for the nth emitter.  The array is
C                normalized to 1 and is then written to a file of the
C                form 'xxx.ar.nn' where nn is the frame number and
C                xxx is the output file prefix given as input to this
C                program (note:this prefix xxx is the same as that for
C                the triggering data files xxx.trg and xxx.trg.max).
C
      double precision a(234,10), anorm(234,10), junk(100,10)
      double precision ia(234,10)
      integer m,i,ii,id,j,jj,top,length
      integer ldigit,rdigit,pldigit,prdigit
      character prefix*1,suffixl*1,suffixr*1,suffix*4,name*6,dot*1
      character psuffixl*1,psuffixr*1
      character frame*2,outprefix*3, nameout*9
      print *, 'input delay factor...'
      read *, id
C read the number of emitters
      print *, 'input number of emitters/windows...'
      read *, m
C read the number of frames in the data set
      print *, 'input number of frames in the data set...'
      read *, nfile
C read the data file prefix
      print *, 'input initial character of file prefix...'
      read *, prefix
C read the data file prefix, output array file prefix and frame number
      print *, 'input output array file prefix...'
      read *, outprefix
      do 1000 jj=1,nfile
         pldigit = jj/10
         prdigit = jj -10*pldigit
         psuffixl = char(pldigit +48)
         psuffixr = char(prdigit +48)
         frame=psuffixl//psuffixr
C call the triggering data subroutine to handle the compensation for
C triggering instability
         call trigger(frame,outprefix,length,top)
C for each of the m data files calculate the filename,
```

```
C open the file and read the data into array a(j,ii),
        length=length+id
        dot = '.'
        do 10 ii=1,m
            ldigit = ii/10
            rdigit = ii -10*ldigit
            suffixl = char(ldigit +48)
            suffixr = char(rdigit +48)
            name= prefix//frame//dot//suffixl//suffixr
            open(1,file=name)
            do 20 j=1,top-id
                  read(1,18) junk(j,ii)
20           continue
            do 30 j=1,length
                  read(1,18) ia(j,ii)
                  a(j,ii)=ia(j,ii)
18                format (f7.3)
30           continue
            close(1)
10       continue
C normalize the array
        call norm(a,length,m,anorm)
C calculate the filename for the array file
        suffix = '.ar.'
        nameout = outprefix//suffix//frame
C open the array file and write the normalized
C array to it
        open(1,file=nameout)
        do 40 i=1,m
            do 50 j=1,length
                  write(1,800) anorm(j,i)
50           continue
40       continue
        close(1)
800      format(f8.4)
1000  continue
     print *,length
     stop
     end
C*********************************************************************
C Subroutine normalize...this subroutine normalizes an array of
C                  dimension up to (234,234).  A search through
C                  the array determines the largest element,rmax,
C                  and then each element of the array is divided
C                  by this value, rmax.  If rmax is 0 no division
C                  is performed and a warning is written to the
C                  screen that the array to be normalized is a
C                  zero array.
```

```
      subroutine norm(rarray,n,m,rnorm)
      double precision rarray(234,234), rmax, rnorm(234,234)
      integer i,j
C set rmax to be the first element
      rmax = rarray(1,1)
C search through the array comparing rmax to rarray(j,i)
C if rarray is bigger then it becomes rmax...
      do 100 i=1,m
           do 200 j=1,n
                if(rarray(j,i) .gt. rmax) then
                  rmax = rarray(j,i)
                end if
200        continue
100   continue
C if the array is a zero array then bypass the normalization and
C return
      if(rmax .eq. 0) then
        print *, 'rmax is 0'
        return
      end if
C now divide rarray(j,i) by rmax to normalize
      do 300 i=1,m
           do 400 j=1,n
                rnorm(j,i) = rarray(j,i)/rmax
400        continue
300   continue
      return
      end
C*********************************************************************
C Subroutine trigger...this subroutine opens the triggering data file
C                      and reads the first line which contains the maximum
C                      value and then the line corresponding to the current
C                      frame being analyzed. This information is sent back
C                      to the main program so that an array can be formed
C                      which compensates for the triggering instability.
      subroutine trigger(frame,outprefix,length,top)
      integer i,itop,itopp1,itopt,itopo,t(50),top,tmax,length
      character frame*2,outprefix*3,suffixt*8,namet*11

C calculate the index 'itop' in 2 parts--the 10's digit 'itopt' and then
C the 1's digit 'itopo'
C the value of 'itop' corresponds to the number of the frame in the set
C knowing this, the triggering information for this frame can then be
C read from the appropriate row in the triggering data file
      itopt = ichar(frame(1:1))-(48-(ichar(frame(1:1))-48)*9)
      itopo = ichar(frame(2:2))-48
      itop = itopt + itopo
C calculate the triggering data filename--the one that has the maximum
C value of the triggering delay written as the first line in the file
```

```
      suffixt = '.trg.max'
      namet = outprefix//suffixt
C open the file and read all of the data up to 'itop'+1 --this includes
C the max value and the delay value for this frame
      open(1,file=namet)
      itopp1 = itop + 1
      do 10 i=1,itopp1
          read(1,900) t(i)
10    continue
      close(1)
C 'top' contains the delay information for this frame
C 'tmax' contains the maximum delay for the data set--all frames
      top = t(itopp1)
      tmax = t(1)
C calculate the maximum length of the arrays for this data set
C note: in all frame-grabbed data files,there are 2 window numbers
C and 5 zeros written to the beginning and 14 zeros written to
C the end...these are of no value and will be removed
      length = 235-tmax
900   format(i3)
      return
      end
```

APPENDIX C

This appendix is a source listing of the FORTRAN 77 program analyser.F used to do the statistical analysis on the time-intensity profiles for each emitter of the laser array.

```
C*********************************************************************
C
C Program analyser.F
C
C     This program opens and reads the 'nfile' array files of a
C given run (specified by the common 3 character file prefix).
C The array files are of the form: ixx.ar.##  --where xx is the
C drive current without the decimal point and ## is the frame # of
C the array file.  For each of the 'nfile' intensity data files
C DFTs and correlations are calculated.  These results are then
C averaged, as is the intensity data.  The result files are of the
C form: ixx.ar.00.aft, ixx.ar.00.acr, and ixx.ar.00 respectively.
C The DFT and correlation of the average intensity data are
C calculated and written to files of the form: ixx.ar.00.dft and
C ixx.ar.00.crl.  The DFT and correlation results are written to
C files for only the four array file frame numbers: 05,10,15,20.
C These files are of the form: ixx.ar.05.dft;ixx.ar.05.crl for
C example. These files are all compatible with the graphics routine
C 'gr'.  This program is an extension of Program statc.crl.trg.F
C ( by K. A. Hartnett ).
C
C Nu Yu, Department of Applied Physics & Electrical Engineering,
C Oregon Graduate Center, 19600 NW Von Nuemann Dr., Beaverton,
C OR 97006
C
C Date begun: 9/26/87; Last update 11/27/88
C
C*********************************************************************
C
#define MAXROWS 256       /* max nr. of pixels per emitter */
#define MAXROWS_2 128     /* MAXROWS/2 (for dft routine) */
#define MAXCOLS 10  /* max nr. of emitters */

      double precision a(MAXROWS,MAXCOLS),aa(MAXROWS,MAXCOLS)
      double precision ar(MAXROWS,MAXCOLS),sumar(MAXROWS,MAXCOLS)
      double precision sumft(MAXROWS,MAXCOLS),sumcrl(MAXROWS,MAXCOLS)
      double precision aravg(MAXROWS,MAXCOLS),aaravg(MAXROWS,MAXCOLS)
      double precision ftavg(MAXROWS,MAXCOLS),crlavg(MAXROWS,MAXCOLS)
      double precision ftres(MAXROWS,MAXCOLS),ftavout(MAXROWS,MAXCOLS)
      double precision crlres(MAXROWS,MAXCOLS),crlavout(MAXROWS,MAXCOLS)
      double precision sumone(MAXCOLS),oneavg(MAXCOLS)
      double precision sumfr(MAXROWS),avgfr(MAXROWS),avgtot(MAXROWS)
      double precision apl(MAXROWS,MAXCOLS)
      double precision cjm1,avgfrmax,avgtotmax,rmax,unitl
      integer n,n2,m,i,ii,iii,index,j,jj,jjj,jm1,nfile,ldigit,rdigit
      character prefix*3,suffixl*1,suffixr*1,suffix*2,name*9,dot*4
      character suffixft*4,suffixcr*4,nameaft*13,nameacr*13,prefixft*7
      character dotav*4,nameav*9,dotfr*4,namefr*9
      character suffixplt*4,nameplt*13
```

```
      logical debug
      common unitl
      debug = .false.
C define the dimensions of the array--m denotes the number of emitters
      print *, 'input number of emitters/windows...'
      read *, m
C read the length of the file--of an individual emitter
      print *, 'input length of a column in array data file...'
      read *, n
      n2=(n+1)/2
C read the unit length of the file--of an individual emitter
      print *, 'input unit (ps/channel) of a column...'
      read *, unitl
      unitl=unitl*1.0d-03
C read the number of frames in the data set
      print *, 'input number of frames in the data set...'
      read *, nfile
C initially set the sum arrays to 0
      do 10 i=1,m
           do 20 j=1,n
              sumar(j,i)=0.0d0
20         continue
           do 30 jj=1,n2
              sumft(jj,i)=0.0d0
30         continue
           do 40 jjj=1,n
              sumcrl(jjj,i)=0.0d0
40         continue
10    continue
      do 50 j=1,n
           avgtot(j)=0.0d0
50    continue
      avgtotmax=0.0d0
C the number of files to be averaged is nfile
C read the filename prefix of the array files to be averaged
      print *, 'input file prefix--first 3 characters of filename...'
      read *, prefix
C calculate the filenames of each of the array files
      do 100 ii=1,nfile
           ldigit = ii/10
           rdigit = ii-10*ldigit
           suffixl= char(ldigit + 48)
           suffixr= char(rdigit + 48)
           dot = '.ar.'
           name = prefix//dot//suffixl//suffixr
C open each of these array files and read the data into ar(j,i)
C make two copies of ar(j,i) to be used for DFT and correlation analysis
           open(4,file= name)
           do 110 i=1,m
```

```
                do 120 j=1,n
                    read(4,850) ar(j,i)
                    a(j,i) = ar(j,i)
                    aa(j,i) = ar(j,i)
120              continue
110          continue
             close(4)
      if ((ii .eq. 5) .or.
     +    (ii .eq. 10) .or.
     +    (ii .eq. 15) .or.
     +    (ii .eq. 20) .or.
     +    (ii .eq. 0)) then
C calculate the new filename
             suffixplt = '.plt'
             nameplt = name//suffixplt
             open(1,file=nameplt)
C write the data to the file incrementing
C each 'column' by 1
             do 130 i=1,m
                   do 125 j=1,n
                        jm1=j-1
                        cjm1=jm1*unitl
                        im1=i
                        apl(j,i) = ar(j,i) +im1
                        write(1,122) cjm1, apl(j,i)
122                     format(f7.4,f8.4)
                        if (i.eq.m) go to 125
                        if (j.eq.n) write(1,123)
123                      format(" ")
125                 continue
130          continue
             close(1)
      end if
C calculate the average intensity for a frame
C first zero the sum array 'sumfr'
             do 145 j=1,n
                  sumfr(j) = 0.0d0
145          continue
C form the sum
             avgfrmax=0.0d0
             do 150 j=1,n
                  do 175 i=1,m
                       sumfr(j) = sumfr(j) + ar(j,i)
175                continue
                  avgfr(j) = sumfr(j)/dfloat(m)
                  if (avgfrmax.lt.avgfr(j)) then
                       avgfrmax=avgfr(j)
                  end if
                  avgtot(j)=avgtot(j)+avgfr(j)
```

```
                if (avgtotmax.lt.avgtot(j)) then
                    avgtotmax=avgtot(j)
                end if
150          continue
            if ((ii .eq. 5) .or.
     +      (ii .eq. 10) .or.
     +      (ii .eq. 15) .or.
     +      (ii .eq. 20) .or.
     +      (ii .eq. 0)) then
C calculate the filename for the average intensity for a frame
                dotfr = '.fr.'
                namefr = prefix//dotfr//suffixl//suffixr
                open(1,file=namefr)
                do 200 j=1,n
                    jm1 = j-1
                    cjm1=jm1*unitl
                    avgfr(j)=avgfr(j)/avgfrmax
                    write(1,905) cjm1, avgfr(j)
200              continue
                close(1)
            endif
C calculate the average intensity for each emitter
            do 325 i=1,m
                sumone(i) = 0.0d0
325          continue
            do 350 i=1,m
                do 375 j=1,n
                    sumone(i) = sumone(i) + ar(j,i)
375              continue
                oneavg(i) = sumone(i)/dfloat(n)
350          continue
            if ((ii .eq. 5) .or.
     +      (ii .eq. 10) .or.
     +      (ii .eq. 15) .or.
     +      (ii .eq. 20) .or.
     +      (ii .eq. 0)) then
C calculate the filename for the average intensity of each emitter
                dotav = '.av.'
                nameav = prefix//dotav//suffixl//suffixr
                open(1,file=nameav)
                do 385 i=1,m
                    write(1,910) i, oneavg(i)
385              continue
                close(1)
            endif
C calculate the DFT and correlation of each array file
            call dft(a,n,m,name,ii,ftres)
            call corrltn(aa,n,m,name,ii,crlres)
C determine the sum arrays of the intensity,DFT and correlation
```

```
C results of the nfile array files
          do 400 i=1,m
               do 500 j=1,n
                    sumar(j,i)=sumar(j,i) + ar(j,i)
500             continue
               do 525 jj=1,n2
                    sumft(jj,i)=sumft(jj,i) + ftres(jj,i)
525             continue
               do 550 jjj=1,n
                    sumcrl(jjj,i)=sumcrl(jjj,i) + crlres(jjj,i)
550             continue
400        continue
C next file...
100   continue
C normalize the sum arrays
     call norm(sumar,n,m,aravg)
     call norm(sumft,n2,m,ftavg)
C     call normcrl(sumcrl,n,m,crlavg)
C duplicate aravg(j,i) to be userd in determining the correlation
C of the average array file
C note: the DFT routine(NAG/c06eaf) returns the results in aravg(j,i)
C making it necessary to use another copy of aravg(j,i) for the
C correlation analysis
     do 575 i=1,m
          do 600 j=1,n
               aaravg(j,i) = aravg(j,i)
600        continue
575   continue
C define the value of ii and the average array filename
     ii=0
     suffix= '00'
     prefixft=name(1:7)
     name=prefixft//suffix
C calculate the name of the average array file
     nameplt= prefix//dot//suffix//suffixplt
C open this file and write the normalized array to it
     open(4, file=nameplt)
     do 650 i=1,m
          do 700 j=1,n
               jm1=j-1
               cjm1=jm1*unitl
               im1=i
               apl(j,i) = aravg(j,i) +im1
               write(4,122) cjm1, apl(j,i)
               if (i.eq.m) go to 700
               if (j.eq.n) write(4,123)
700        continue
650   continue
     close(4)
```

```
      namefr = prefix//dotfr//suffix
      open(1,file=namefr)
      do 655 j=1,n
           jm1 = j-1
           cjm1=jm1*unitl
           avgtot(j)=avgtot(j)/avgtotmax
           write(1,905) cjm1, avgtot(j)
655   continue
      close(1)
      do 660 i=1,m
           sumone(i) = 0.0d0
660   continue
      do 670 i=1,m
           do 665 j=1,n
              sumone(i) = sumone(i) + aravg(j,i)
665        continue
           oneavg(i) = sumone(i)/dfloat(n)
670   continue
      nameav = prefix//dotav//suffix
      open(1,file=nameav)
      do 680 i=1,m
           write(1,910) i, oneavg(i)
680   continue
      close(1)
C determine the DFT and correlation of the average array file
      call dft(aravg,n,m,name,ii,ftavout)
      call corrltn(aaravg,n,m,name,ii,crlavout)
C  calculate the name of the average correlation file
      suffixcr = '.acr'
      nameacr = name//suffixcr
C  open this file and write the results to it, incrementing
C  the values in the nth column by (n-1)
      open (3, file = nameacr)
      rmax=sumcrl(1,1)
      do 1620 i=1,m
             do 1610 j=1,n
               if (sumcrl(j,i).gt.rmax) then
                   rmax=sumcrl(j,i)
               end if
1610           continue
1620  continue
      do 710 i=1,m
        do 720 j=1,n
               im1 = i
               crlavg(j,i) = sumcrl(j,i)/rmax + im1 - 0.5
720           continue
710   continue
      do 730 i=1,m
           do 740 j=1,(n/2 + 1)
```

```
                jm1 = j-1
                iii = (n/2 + jm1)
                index = (-n/2 + jm1)-1
                cjm1=index*unitl
                write(3,905) cjm1, crlavg(iii,i)
740         continue
            do 750 j=(n/2 + 2),n
                jm1 = j-1
                jj =(jm1 - n/2)
                index = jj - 1
                cjm1=index*unitl
                write(3,905) cjm1, crlavg(jj,i)
                if (i.eq.m) go to 750
                if (j.eq.n) write (3,915)
750         continue
730   continue
      close (3)
C calculate the name of the average DFT file
      suffixft = '.aft'
      nameaft = name//suffixft
C open this file and write the average DFT array to it
      open(4, file=nameaft)
      do 800 i=1,m
C           do 815 j=1,2
C               jm1 = j-1
C               cjm1=jm1/(dfloat(n)*unitl)
C               im1 = i
C               write(4,905) cjm1, 0.0+im1
C815          continue
            do 825 j=4,n2
                jm1 = j-1
                cjm1=jm1/(dfloat(n)*unitl)
                im1 = i
                ftavg(j,i) = ftavg(j,i) + im1
                write(4,905) cjm1, ftavg(j,i)
                if (i.eq.m) go to 825
                if (j.eq.n2) write(4,915)
825         continue
800   continue
      close(4)
      write (*,899) 7
899   format (a1)
850   format(f8.4)
900   format(i4,f8.4)
905   format(f8.3,f8.4)
910   format(i2,f8.4)
915   format(" ")
      stop
      end
```

```
C*********************************************************************
C Subroutine dft...this subroutine calculates the discrete fourier
C             transform of each column in the array. This corresponds
C             to a DFT in the time domain since the columns contain
C             intensity information as a function of time for a single
C             emitter.  The data in the 2D array is read a column at
C             a time into a real 1D array required by the NAG routine
C             c06eaf. The original sequence is a real sequence and
C             consequently the DFT is a particular type of complex
C             sequence, a Hermitian sequence with the following
C             properties:  a(N-k)=a(k)
C                          b(N-k)=-b(k) , b(0)=0 , b(N/2)=0 for N even
C             where DFT{z(k)} = a(k) + ib(k)  when z(k)=x(k) (z real).
C             A Hermitian sequence of N complex values can then be
C             uniquely specified by N independent real values. The NAG
C             routine c06eaf writes the real parts a(k) for 0<k<N/2 in
C             the first (N/2 + 1) components of array x. The non-zero
C             imaginary components b(k) are written in reverse order
C             to the remaining (N/2 - 1) components of array x.
C             The results are normalized to one and read back
C             into an array file.
C
      subroutine dft(f,n,m,name,ii,ftout)
      integer i,im1, ifail, j, jm1, n2, nj ,kk, n,m
      logical debug
      double precision cjm1,unitl,pi
      double precision f(MAXROWS,MAXCOLS), rnorm(MAXROWS,MAXCOLS)
      double precision x(MAXROWS)
      double precision r(MAXROWS_2), im(MAXROWS_2),c(MAXROWS_2)
      double precision arft(MAXROWS,MAXCOLS),ftout(MAXROWS,MAXCOLS)
      character name*9,suffix*4,namedft*13
      common unitl
      data pi/3.14159265358979324d0/
C  read the elements of each column of the array
C  into x, one at a time
      do 500 kk = 1, m
           do 40 j = 1, n
         x(j)=f(j,kk)*0.5d0*(1.0d0-dcos(2.0d0*pi*j/dfloat(n)))
40          continue
            ifail = 0
C  call the NAG routine that calculates the DFT
C  of a real array x of length n
            call c06eaf(x,n,ifail)
C  real and imaginary components are returned to
C  x(j) see the above program description for the
C  specific locations of the components r(j), im(j)
C  the first components are given by
            r(1) = x(1)
            im(1) = 0.0d0
```

```
        c(1)=r(1)*r(1)
C  now determine the remaining DFT components
        n2 = (n+1)/2
        do 60 j=2,n2
            nj = n -j + 2
            r(j) = x(j)
            im(j) = x(nj)
C  find the modulus of the complex value of the DFT
            c(j) = r(j)*r(j) + im(j)*im(j)
60        continue
C  determine the last value if n is even
        if (mod(n,2) .ne. 0) go to 80
        r(n2 + 1) = x(n2 + 1)
        im(n2 + 1) = 0.0d0
        c(n2 + 1) = r(n2 + 1)*r(n2 + 1) +im(n2 + 1)*im(n2 + 1)
C  write the square of the DFT results to array, arft(j,kk)
C  as each column is operated on
        if (debug) print *, 'arft'
80        do 100 j=4,n2
            arft(j,kk) = c(j)
C             arft(j,kk) = dsqrt(c(j))
            if (debug) print *, kk, j, arft(j,kk)
100       continue
C  now repeat the process for the next column
500   continue
C  normalize the DFT results stored in arft to one
C  and return the normalized results in rnorm
     call norm(arft,n2,m,ftout)
     if ((ii .eq. 5) .or.
    +    (ii .eq. 10) .or.
    +    (ii .eq. 15) .or.
    +    (ii .eq. 20) .or.
    +    (ii .eq. 0)) then
        go to 550
     end if
     return
550   continue
C  compute the filename for the results file
     suffix = '.dft'
     namedft = name//suffix
C  open this file and write the normalized result array to it,
C  incrementing the values of the mth column by (m-1)
     open (2, file = namedft)
     do 600 i = 1, m
C         do 650 j=1,2
C             jm1 = j-1
C             cjm1=jm1/(dfloat(n)*unitl)
C             im1 = i
C             write(2,900) cjm1, 0.0+im1
```

```
C650        continue
          do 700 j=4,n2
              jm1 = j - 1
              cjm1=jm1/(dfloat(n)*unitl)
              im1 = i
              rnorm(j,i) = ftout(j,i) + im1
              write(2,900) cjm1, rnorm(j,i)
              if (i.eq.m) go to 700
              if (j.eq.n2) write(2,910)
700         continue
600   continue
      close (2)
900   format (f7.4,f8.4)
910   format (" ")
      return
      end


C*********************************************************************
C Subroutine corrltn...this subroutine determines the correlation of
C                      the first column of the array with each of the
C                      columns.  Before this is calculated, the mean of
C                      each of the columns is determined and is sub-
C                      tracted off from the values.  A copy of the first
C                      column vector is needed since the NAG routine
C                      c06ekf writes the result array back into the
C                      first column vector and the correlation of this
C                      column with all other columns is still to be
C                      determined.
C
      subroutine corrltn(cr,n,m,name,ii,crlout)
      integer i,ii,ifail,j,jj,jm1,n,kk,index
      double precision cr(MAXROWS,MAXCOLS), mean(MAXCOLS), sum(MAXCOLS)
      double precision cjm1,unitl
      double precision xa(MAXROWS),xxa(MAXROWS)
      double precision ya(MAXROWS),yya(MAXROWS)
      double precision crl(MAXROWS,MAXCOLS),crlout(MAXROWS,MAXCOLS)
      double precision crloutt(MAXROWS,MAXCOLS)
      double precision denoml,denomr
      character name*9,suffix*4,namecrl*13
      common unitl

C  initialize the sum array to zero
C  and then sum the column of the array
      do 100 kk=1,m
           sum(kk) = 0
           do 150 j=1,n
                sum(kk) = sum(kk) + cr(j,kk)
150         continue
```

```
C  determine the mean
           mean(kk) = sum(kk)/MAXROWS
100   continue
C  subtract off the mean from the values of the array
C  copy this array, xa, into xxa since c06ekf writes
C  the correlation results back into xa
      if (m.eq.1) then
           mc=m
      else
           mc=m/2.0
      endif
      do 200 j=1,n
           xa(j) = cr(j,mc) - mean(mc)
           xxa(j) = xa(j)
200   continue
      do 250 kk=1,m
           do 300 j=1,n
                xa(j) = xxa(j)
                ya(j) = cr(j,kk) - mean(kk)
C               xa(j) = ya(j)
C               xxa(j) = xa(j)
                yya(j) = ya(j)
300        continue
      ifail = 0
C  call the NAG program that does correlations by
C  giving the first argument of the call as 2 and
C  then giving the two vectors to be compared and their length
C  (the argument '2' directs the NAG routine c06ekf to do a
C   correlation of the two vectors--a first argument of '1'
C   would result in a fourier transform of the correlation)
      call c06ekf(2,xa,ya,n,ifail)
C  normalize this by dividing by the product of the sum of the squared
C  intensities of each of the two emitters to the 1/2 power.
      do 350 j=1,n
           denoml = xxa(j)*xxa(j) + denoml
           denomr = yya(j)*yya(j) + denomr
350   continue
      do 375 j=1,n
           crl(j,kk) = xa(j)/dsqrt((denoml*denomr))
375   continue
      denoml = 0
      denomr = 0
250   continue

C  normalize the results to one
      call normcrl(crl,n,m,crlout)
      if ((ii .eq. 5) .or.
     +    (ii .eq. 10) .or.
     +    (ii .eq. 15) .or.
```

```
     +    (ii .eq. 20) .or.
     +    (ii .eq. 0)) then
            go to 275
          end if
          return
275       continue
C  compute the new filename for the result file
          suffix = '.crl'
          namecrl = name//suffix
C  open this file and write the results to it, incrementing
C  the values in the nth column by (n-1)
          open (unit =3, file = namecrl, status ='new')
          do 400 i=1,m
            do 450 j=1,n
                    im1 = i
                    crloutt(j,i) = crlout(j,i) + im1 - 0.5
450               continue
400       continue
          do 500 i=1,m
              do 600 j=1,(n/2 +1)
                    jm1 = j-1
                    ii = (n/2 + jm1)
                    index = (-n/2 + jm1) - 1
                    cjm1=index*unitl
                    write(3,900) cjm1, crloutt(ii,i)
600           continue
              do 700 j=(n/2 + 2),n
                    jm1 = j-1
                    jj =(jm1 - n/2)
                    index = jj - 1
                    cjm1=index*unitl
                    write(3,900) cjm1, crloutt(jj,i)
                    if (i.eq.m) go to 700
                    if (j.eq.n) write (3,915)
700           continue
500       continue
          close (3)
C increase to f8.4 since the correlation is often 1 and for
C the 10th column this means that jm1 and crlout(j,i) run together
C ploot interprets this as a huge number...
900       format (f8.4,f8.4)
915       format ('' '')
          return
          end

C*********************************************************************
C Subroutine norm...this subroutine normalizes an array of
C                   dimension (n,m).  A search through
C                   the array determines the largest element,rmax,
```

```
C               and then each element of the array is divided
C               by this value, rmax.  If rmax is 0 no division
C               is performed and a warning is written to the
C               screen that the array to be normalized is a
C               zero array.
C
      subroutine norm(rarray,n,m,rnorm)
      double precision rarray(MAXROWS,MAXCOLS), rmax
      double precision rnorm(MAXROWS,MAXCOLS)
      integer i,j,m,n
      logical debug
C  set rmax to be the first element
      rmax = rarray(1,1)
C  search through the array comparing rmax to rarray(j,i)
C  if rarray is bigger then it becomes rmax...
      do 100 i=1,m
           if (debug) print *, 'rarray'
           do 200 j=1,n
                if (debug) print *, i, j, rarray(j,i)
                if (rarray(j,i) .GT. rmax) then
                     rmax = rarray(j,i)
                end if
200        continue
100   continue
C  if the array is a zero array then bypass the normalization and
C  return
      if(rmax .eq. 0) then
        print *, 'rmax is 0--check .dft,.aft,files,'
        print *, '(one of these arrays is a zero array)'
        return
      end if
C now divide rarray(j,i) by rmax to normalize the array
      do 300 i=1,m
           do 400 j=1,n
                rnorm(j,i) = rarray(j,i)/rmax
400        continue
300   continue
      return
      end
C*********************************************************************
C Subroutine normcrl...this subroutine normalizes an array of
C               dimension (n,m).  A search through
C               the array determines the largest element,rmax,
C               and then each element of the array is divided
C               by this value, rmax.  If rmax is 0 no division
C               is performed and a warning is written to the
C               screen that the array to be normalized is a
C               zero array.
C               Note: this is a modification of 'norm' designed
```

```
C               to deal with correlation results which cover a
C               range of -1 to 1.  First the results are normalized
C               to one.  One is added to the array to shift the
C               range to 0 to 2.  The array is then renormalized to
C               one by dividing by 2.0d0 and thus making the range
C               0 to 1 which allows the entire array to be plotted
C               on the same graph.
      subroutine normcrl(rarray,n,m,rnorm)
      double precision rarray(MAXROWS,MAXCOLS), rmax
      double precision rnorm(MAXROWS,MAXCOLS)
      integer i,j,n,m
C  set rmax to be the first element
      rmax = dabs(rarray(1,1))
C  search through the array comparing rmax to |rarray(j,i)|
C  if |rarray| is bigger then it becomes rmax...
      do 100 i=1,m
           do 200 j=1,n
                if (dabs(rarray(j,i)) .GT. rmax) then
                     rmax = dabs(rarray(j,i))
                end if
200        continue
100   continue
C  if the array is a zero array then bypass the normalization and
C  return
      if(rmax .eq. 0) then
        print *, 'rmax is 0--check .crl file,'
        print *, '(the array is a zero array)'
        return
      end if
C now divide rarray(j,i) by rmax to normalize the array
C and add 1.0d0 to shift the range to 0 to 2
      do 300 i=1,m
           do 400 j=1,n
                rnorm(j,i) = rarray(j,i)/rmax+1.0d0
400        continue
C divide by 2.0d0 to renormalize to 1
      do 500 j=1,n
           rnorm(j,i) = rnorm(j,i)/2.0d0
500   continue
300   continue
      return
      end
```

APPENDIX D

This appendix is a source listing of shell scripts plot.prof and plot.stat for a representative sample of the programs written to control the graphic display of the time-intensity profiles, the discrete Fourier transform and correlation results.

plot.prof

```
#! /bin/csh -f
@ rightdig = 0
@ leftdig = 0
set count = "$leftdig$rightdig"
set prefix = $1
set n = $2
set m = $3
set nfile = $4
while ($count <= "$nfile")
    set pltfile = "$prefix.$count.plt"
    #rm $pltfile
    if ($3 == 1) then
    (echo "$pltfile")| ncw.cfile2.i | gr.old $pltfile -p ~/nasa/DOCUMENTS/prms.cw.i1
    endif
    if ($3 == 2) then
    (echo "$pltfile")| ncw.cfile2.i | gr.old $pltfile -p ~/nasa/DOCUMENTS/prms.cw.i2
    endif
    if ($3 == 3) then
    (echo "$pltfile")| ncw.cfile2.i | gr.old $pltfile -p ~/nasa/DOCUMENTS/prms.cw.i3
    endif
    if ($3 == 8) then
    (echo "$pltfile")| ncw.cfile2.i | gr.old $pltfile -p ~/nasa/DOCUMENTS/prms.cw.i8
    endif
    if ($3 == 10) then
    (echo "$pltfile")| ncw.cfile2.i | gr.old $pltfile -p ~/nasa/DOCUMENTS/prms.cw.i10
    endif
    if ( $rightdig == 0 ) then
        @ rightdig = 5
    else
        @ rightdig = 0
        @ leftdig = $leftdig + 1
    endif
    set count = "$leftdig$rightdig"
end
```

plot.stat

```
#! /bin/csh -fx
# $Header$
@ suffixl = 0
@ suffixr = 0
set suffix = "$suffixl$suffixr"
set prefix = $1
@ n = $2
@ m = $3
@ nfile = $4
@ nhalf = $n / 2
@ mnhalf = 0 - $nhalf
while ($suffix <= "$nfile")
      if ($suffix == "00") then
         set dftfile = "$prefix.$suffix.aft"
      if ($3 == 1) then
        (echo "$dftfile")|ncw.cfile.dft| gr.old $dftfile -p ~/nasa/DOCUMENTS/prms.dft1
         set crlfile = "$prefix.$suffix.acr"
        (echo "$crlfile")|ncw.cfile.crl| gr.old $crlfile -p ~/nasa/DOCUMENTS/prms.crl1
      endif
      if ($3 == 2) then
        (echo "$dftfile")|ncw.cfile.dft| gr.old $dftfile -p ~/nasa/DOCUMENTS/prms.dft2
         set crlfile = "$prefix.$suffix.acr"
        (echo "$crlfile")|ncw.cfile.crl| gr.old $crlfile -p ~/nasa/DOCUMENTS/prms.crl2
      endif
      if ($3 == 3) then
        (echo "$dftfile")|ncw.cfile.dft| gr.old $dftfile -p ~/nasa/DOCUMENTS/prms.dft3
         set crlfile = "$prefix.$suffix.acr"
        (echo "$crlfile")|ncw.cfile.crl| gr.old $crlfile -p ~/nasa/DOCUMENTS/prms.crl3
      endif
      if ($3 == 8) then
        (echo "$dftfile")|ncw.cfile.dft| gr.old $dftfile -p ~/nasa/DOCUMENTS/prms.dft8
         set crlfile = "$prefix.$suffix.acr"
        (echo "$crlfile")|ncw.cfile.crl| gr.old $crlfile -p ~/nasa/DOCUMENTS/prms.crl8
      endif
      if ($3 == 10) then
        (echo "$dftfile")|ncw.cfile.dft| gr.old $dftfile -p ~/nasa/DOCUMENTS/prms.dft10
         set crlfile = "$prefix.$suffix.acr"
        (echo "$crlfile")|ncw.cfile.crl| gr.old $crlfile -p ~/nasa/DOCUMENTS/prms.crl10
      endif
      endif
      set dftfile = "$prefix.$suffix.dft"
      if ($3 == 1) then
        (echo "$dftfile")|ncw.cfile.dft| gr.old $dftfile -p ~/nasa/DOCUMENTS/prms.dft1
      set crlfile = "$prefix.$suffix.crl"
        (echo "$crlfile")|ncw.cfile.crl| gr.old $crlfile -p ~/nasa/DOCUMENTS/prms.crl1
      endif
```

```
    if ($3 == 2) then
      (echo "$dftfile")|ncw.cfile.dft| gr.old $dftfile -p ~/nasa/DOCUMENTS/prms.dft2
    set crlfile = "$prefix.$suffix.crl"
      (echo "$crlfile")|ncw.cfile.crl| gr.old $crlfile -p ~/nasa/DOCUMENTS/prms.crl2
    endif
    if ($3 == 3) then
      (echo "$dftfile")|ncw.cfile.dft| gr.old $dftfile -p ~/nasa/DOCUMENTS/prms.dft3
    set crlfile = "$prefix.$suffix.crl"
      (echo "$crlfile")|ncw.cfile.crl| gr.old $crlfile -p ~/nasa/DOCUMENTS/prms.crl3
    endif
    if ($3 == 8) then
      (echo "$dftfile")|ncw.cfile.dft| gr.old $dftfile -p ~/nasa/DOCUMENTS/prms.dft8
    set crlfile = "$prefix.$suffix.crl"
      (echo "$crlfile")|ncw.cfile.crl| gr.old $crlfile -p ~/nasa/DOCUMENTS/prms.crl8
    endif
    if ($3 == 10) then
      (echo "$dftfile")|ncw.cfile.dft| gr.old $dftfile -p ~/nasa/DOCUMENTS/prms.dft10
    set crlfile = "$prefix.$suffix.crl"
      (echo "$crlfile")|ncw.cfile.crl| gr.old $crlfile -p ~/nasa/DOCUMENTS/prms.crl10
    endif
    if ($suffixr == 0) then
       @ suffixr = 5
    else
       @ suffixr = 0
       @ suffixl = $suffixl + 1
    endif
    set suffix = "$suffixl$suffixr"
end
```

VITA

The author was born in Sichuan, China on April 2, 1958. He attended Huazhong University of Science and Technology in Wuhan, China, and received the degree Bachelor of Science in Optical Engineering in January 1982. After graduation, he worked for three years as an assistant physicist at the Atomic and Molecular Labs of Wuhan Institute of Physics, Chinese Academy of Sciences.

The author began his studies at the Oregon Graduate Institute of Science and Technology (formerly Oregon Graduate Center) in January 1985 and received the degree Master of Science in Electrical Engineering in April 1987. He continued towards his Ph.D. at the Oregon Graduate Institute of Science and Technology and completed all requirements for the degree Doctor of Philosophy in Electrical Engineering in August 1990.

The author is married to Yuan Liu and they have a daughter, Carlina Chunlin Yu, aged 1 year.